EXPERIMENTAL INVESTIGATION OF LATERAL TORSIONAL BUCKLING OF GERBER FRAMES

by

Nizar Markiz

Thesis submitted to the Faculty of Graduate and Post Doctoral Studies in partial fulfillment of the requirements for the Master of Applied Science Degree in Civil Engineering under the auspices of the Ottawa-Carleton Institute for Civil Engineering

April 2011

Abstract

The objective of this thesis is to investigate the elastic lateral buckling resistance of Gerber frames based on full scale tests and finite element analyses. Three experiments were undertaken to obtain elastic buckling loads and the buckling modes were recorded. Shell finite element solutions were conducted to predict the elastic lateral buckling resistance of the frames tested. A comparison between the elastic buckling loads obtained from full scale experiments and those predicted by the FEA models provides an assessment of the ability of the finite element analysis model in predicting elastic lateral resistance and buckled mode shapes of Gerber frames. Conclusions and recommendations for future research are provided.

Acknowledgements

I would like to express my gratitude to my supervisor, Dr. Magdi Mohareb, whose expertise, understanding, and patience, added considerably to my graduate experience. I appreciate his vast knowledge and skill in many areas and his assistance in writing reports.

This research would not have been possible without the financial assistance of the National Science and Engineering Research Council (NSERC) and the Steel Structures Education Foundation (SSEF) and express my gratitude to those agencies.

I would also like to thank the Structures Laboratory Technician Mr. Muslim Majeed. The assistance of the Machine Shop Technician Mr. John Perrins and Electronics Specialist Mr. Leo Denner is greatly acknowledged and appreciated in the experimental part of this research.

Very special thanks go to my family for the support they provided me through my entire life and in particular, I must acknowledge my mother, father, brothers and sisters, and my best friend, Ramy Hamza, without whose sacrifice, encouragement and assistance, I would not have finished this thesis.

Table of Contents

CHAPTER 3

Description of Finite Element Model

CHAPTER 4

Comparison of Results

CHAPTER 5

Summary, Conclusions, and Recommendations

List of Tables

Chapter 2

Chapter 3

Chapter 4

Appendix B

Appendix C

Appendix D

Appendix E

List of Figures

Chapter 2

Chapter 3

Chapter 4

Appendix A

Appendix C

List of Symbols

Greek Symbols

α	scaling factor
β	weighting constant
λ_i	critical load combination factor
θ_{FEA}	angle of twist based on FEA
$\bar{\theta}_{exp}$	average angle of twist based on experiments
ν	poisson's ratio
ω_2	moment gradient factor

Latin Symbols

A	cross-sectional area
b	width of a Gerber beam
C_w	warping torsional constant
d	depth of the Gerber beam
E	modulus of elasticity; sum of squares of differences
F	reference in-plane load
F_y	yield strength
G	rigidity modulus
H	frame height
h	section height
i	number of experimental lateral displacement measurements
I_c	moment of inertia about the centroidal axis
I_x	moment of inertia about the strong axis
I_y	moment of inertia about the weak axis
j	number of experimental rotation measurements
J	St. Venant's torsional constant

K	Gerber frame stiffness
K_{IP}	Gerber frame in-plane stiffness
K_{OP}	Gerber frame in-plane stiffness
K_{OPG}	Gerber frame out-of-plane loss in stiffness
L	span of beam
L_b	distance between columns of Gerber frame
L_c	span of cantilever extensions
L_p	distance between column of Gerber frame and point load
L_u	length of unbraced portion of beam
M	bending moment
M_y	yield moment resistance
M_u	ultimate moment
P	applied load
S_x	elastic section modulus about the strong axis
S_y	elastic section modulus about the weak axis
u	in-plane and out-of-plane displacement
u_{FEA}	lateral displacement based on FEA
u_{IP}	in-plane displacement
u_{OP}	out-of plane displacement
$\bar{u}_{exp}$	average lateral displacement based on experiments
t	thickness of flange
w	thickness of web
Z_x	plastic section modulus about the strong axis
Z_y	plastic section modulus about the weak axis

CHAPTER 1

Introduction

1.1 General

This study aims at investigating the lateral torsional buckling resistance of Gerber Frames based on a series of finite element analyses and full-scale experiments. Gerber beams introduce internal hinges in continuous beams to make them statically determinate. The Gerber system consists of a series of simply supported beams extended at their ends by cantilevers in alternate spans and linked by intermediate beams supported on the cantilever ends. The beams are often supported on columns with a square HSS cross-section and less commonly on wide flange columns. The original idea of the Gerber system was to optimize the spans of the cantilever portion to make the maximum negative bending moments at column location nearly equal to the maximum positive moment at mid-span, thus making full usage of the yield flexural resistance of the beam, both at the maximum positive and negative moment sections. Frequently, the top flanges of Gerber beams are connected to the top chord of open web steel joists (OWSJ) which are normally connected to a light gage steel deck. At column locations, it is common to connect the top and bottom chords of OWSJ to Gerber beams.

The Gerber beam system is a common construction method in Canadian warehouses and strip malls. Nevertheless, its lateral buckling behaviour remains relatively unknown. This is due to the fact that a thorough understanding of the lateral buckling behaviour of the Gerber systems is associated with several challenges including:

a) modelling the interaction between the cantilever spans and the backspan,

b) modelling the interaction between the Gerber beam and supporting flexible columns,

c) modelling the distortional buckling behaviour of Gerber system,

d) the quantification of the torsional and lateral restraints provided by the OWSJ to the Gerber system, and

e) the quantification of the partial warping restraint between the cantilever span and the backspan.

Given the above complexities, a reliable determination of the lateral buckling resistance of Gerber systems necessitates the development of elaborate finite element analyses, an impractical option in a design environment. A few design solutions (summarized in Section 1.2.3) were proposed for structures similar to Gerber systems. However, these were based on simplifying assumptions, some of them are conservative but others could lead to un-conservative predictions. Within this context, the present research project was sponsored by the Steel Structures Education Foundation (SSEF) with the ultimate goal of developing design rules for Gerber systems. The study involves numerical and experimental components.

1.2 Literature Review

The following review focuses on experimental studies related to the lateral torsional buckling of steel structures and members (Section 1.2.1), numeric studies (Section 1.2.2), and design methods developed for structural systems with similarities to Gerber systems (Section 1.2.3).

1.2.1 Experimental Investigations on Lateral Torsional Buckling

Vacharajittiphan and Trahair (1973)

Vacharajittiphan and Trahair (1973) investigated the interaction between in plane and out of plane buckling of portal frames. Their investigation focused on elastic lateral buckling and consisted of three components: (1) theoretical, (2) numerical, and (3) experimental.

As part of the theoretical component, the equilibrium equations were developed. The column bases were assumed rigidly fixed. The beam-column joints were assumed fully restrained in the lateral and sway directions and elastically restrained against warping. The method of finite integrals developed in (Brown and Trahair 1968) was used to integrate the equilibrium conditions subject to the boundary conditions.

The experimental investigation consisted of testing a 30" wide x 15" high and a 15" wide x 30" high portal frame. Cross sections for the beams and columns were I-shaped with beam depth d = 0.62", flange width b = 0.28", flange thickness t = 0.06", and web thickness w = 0.05". Material was high strength aluminum with a Modulus of Elasticity E of 8,232 kip. Only the web of the column was welded to the underside of the beam leading to a free warping condition at the top of the column. The column was fixed at its base. A lateral restraint was provided to the beam-column joints. Three vertical loads were applied to the top flange of the beam at mid-span and at both ends. Each frame was subjected to multiple combinations of mid-span and column loads.

A buckling interaction diagram relating the mid-span load versus column loads was generated for each frame. The interaction diagram was based on critical load combinations obtained numerically and experimentally.

The numeric and experimental buckling load combinations agreed within 6%. For the 30" wide x 15" high frame, the mid-span load was observed to be independent of small column loads. When column loads were increased, the mid-span load was found to decrease. In contrast, for the 15" wide x 30" high frame, small column loads were observed to significantly decrease the mid-span load. In the model, when the beam load was assumed to vanish, the predicted mid-span buckling load agreed with the experimental loads. In contrast, when column loads were assumed to vanish, the mid-span buckling load was over-predicted. The mid-span buckling load was over-predicted because of the non conservative assumption of full twisting restraint at both ends of beam.

Kubo and Fukumoto (1988)

Kubo and Fukumoto (1988) studied the interactive behaviour of local and lateral torsional buckling of I-beams in the plastic region. Their study was based on a series of experiments carried out on thin-walled I-beams. The I-beam cross-sections and spans were chosen so that inelastic lateral-torsional buckling takes place. A comparison was conducted between experimental and design capacities.

The experimental investigation consisted of a series of 22 tests on simply supported I-beams with span length between 1.5m and 3.35m. Four cross-sections were extracted from typical members used in industry. The cross-sections were built up using high frequency resistance-seam welding. The cross section dimensions varied as follows: beam depth d = 200mm to 300mm, flange width b = 125mm to 150mm, flange thickness t = 4.17mm to 4.42mm, and web thickness w = 2.92mm to 3.15mm. Material was steel with an average Modulus of Elasticity E of 212 GPa.

Prior the experimental investigation, a series of supplementary tests were undertaken on sections cut out from original members to determine material properties, longitudinal residual stresses, and initial imperfections. A longitudinal residual stress distribution diagram was constructed for two of the cross-sections used. It was observed that seam welding resulted in substantial longitudinal residual stresses. Yield and ultimate material strengths were found to be larger for thinner plates compared to thicker plates. Minor axis initial imperfections were observed to be large for I-beams with fillet welds.

A restraint was provided at end supports of the I-beams to prevent lateral deflection and twisting. No warping restraint was provided at beam ends. A single vertical concentrated load was applied to the top flange of the I-beams at mid-span using a hydraulic tension jack.

A diagram relating the mid-span load versus horizontal and vertical deflections was generated for three specimens with different spans. A second diagram was generated to relate the mid-span load versus longitudinal strains on both surfaces of top flange tips near mid-span and strain reversal.

The experimental and calculated elastic vertical deflections were in good agreement. As the ultimate load was approached, lateral deflections and twist of the cross-section were observed to rapidly increase. All 22 specimens failed by combined local flange and lateral torsional buckling except for five specimens where no local flange buckling was observed prior reaching the ultimate capacity. No web buckling was observed in any of the 22 specimens.

A comparison was conducted between nominal and experimental ultimate capacities of I-beams tested. Nominal ultimate capacities were obtained from the design approach specified by the European Convention for Constructional Steelwork (ECCS 1981). It was observed that the ultimate capacity of I-beams was significantly reduced by local flange buckling.

Nominal ultimate capacities obtained using the effective width approach in AISI Specification (1986) and the Canadian Standard (1984) were compared to experimental ultimate capacity. It was concluded that the effective width concept used in these design approaches provided a reasonable estimate of experimental ultimate capacities.

An interaction equation was proposed and compared to the experimentally obtained ultimate capacities. The equation was found to satisfactorily capture the interaction between local and lateral torsional buckling.

Mottram (1992)

Mottram (1992) experimentally investigated the out of plane buckling of a pultruded I-beam. His investigation focused on linear elastic lateral torsional buckling. The investigation consisted of three components: (1) theoretical, (2) numerical, and (3) experimental.

As part of the theoretical component, a buckling load equation was developed for shear center loading. It was assumed that the I-beam was linearly elastic, clear of initial imperfections, subject to loading acting in the plane of the shear centre, and residual stresses were neglected. The beam was assumed simply supported about the major axis. The I-beam ends were assumed fully restrained in the lateral direction, twisting, and rotation about the minor axis, and elastically restrained against warping.

A relationship relating the mid-span buckling load versus warping parameter of the I-beam was generated. The diagram was based on buckling loads obtained theoretically and numerically. In the case of steel material, it was shown that the ratio of the St Venant rigidity, $G_{xy}J$, to the warping rigidity, $E_{z.yy}I_w/l^2$,should exceed 150 for elastic lateral-torsional buckling to occur.

The method of finite difference (Mottram, 1991) was used to solve the governing fourth-order differential equation in (Timoshenko and Gere, 1961). The buckling load based on the finite difference method was 3-4% less than that calculated theoretically.

The experimental investigation consisted of 35 tests conducted on three simply supported I-beam specimens with a 1.5m span and 50mm extension at each end. Cross section for beams had the following mean dimensions: beam depth d = 101.7 mm, flange width b = 50.9 mm, flange thickness t = 6.38 mm, and web thickness w = 6.59 mm. Material was E-glass reinforced polymer pultruded with a mean Modulus of Elasticity E of 22,500 and 24,200 MPa in the major and minor axes respectively.

A single concentrated vertical load was applied to the top flange of the beam at mid-span. The measured mid-span load was plotted against the lateral displacement. The lateral displacement pattern was decomposed into the first and third buckling mode contributions. The third buckling contribution to the displacement was observed in 20 of the tests. However, as the tests progressed, the amplitude of the third mode decreased and the buckled configuration became predominantly that of the first mode. As the beam gradually lost stability, a theoretical bifurcation in the load versus lateral displacement response was anticipated. It was concluded that dominance of the first mode, without bifurcation, in all 35 tests was due to initial imperfections in geometry, load application, and boundary conditions.

In the theoretical model, full restraint was assumed against warping and lateral displacement at beam ends. In the experiment, only partially fixed conditions to warping and lateral displacement were provided at beam ends. Therefore, the numerically predicted buckling loads obtained were on average 20% higher than experimentally measured buckling loads. Also, the predicted buckling load based on free warping assumption at beam ends was observed to be 50% of the experimentally determined mean buckling load. It was concluded that warping restraints at beam ends significantly increase lateral-torsional buckling capacity of I-beams.

Essa and Kennedy (1993)

Essa and Kennedy (1993) investigated the distortional lateral torsional buckling capacities of cantilever beams of hot-rolled I-shaped steel sections. The investigation consisted of three components: (1) experimental, (2) numerical, and (3) theoretical.

The experimental investigation consisted of 33 full scale tests undertaken on two different I-beam cross-sections. Eleven specimens were used in total to complete the tests. Seven out of the 11 specimens were W360x39 sections and the remaining four were W310x39 sections.

The experimental setup consisted of a simply supported beam either with one or two cantilever extensions. The specimen span length was 9m in total including a 1.22m cantilever. Five loading frames were used to test specimens for different loading configurations. Thrust bearings, rollers, and knife edges were used to apply lateral and torsional restraints either independently or simultaneously. In some tests, open web steel joists (OWSJ) were used as restraints.

A finite element program was used to model the specimens tested. Four-noded plate elements were used to model the web and two-node beam elements were used to model the flanges.

As part of the theoretical component, design equations were recalled from different resources such as: the Structural Stability Research Council (SSRC) guide and the CAN/CSA S16.1 M89. Following the comparison of design equations, a design procedure was proposed. The procedure was then used to obtain the best estimation of lateral torsional buckling capacity of cantilever beams determined experimentally and verified numerically. It was concluded that:

(a) Numerical modeling is reliable for predicting distortional buckling capacity of beams subjected to different loading scenarios and restraints.

(b) OWSJ properly welded to top flange of I-beams provide both lateral and torsional restraint to the top flange which improves its distortional buckling strength.

(c) Behaviour of cantilever beams is dominated by restraint conditions provided.

(d) Effective length factors presented in SSRC guide used to obtain lateral buckling strength of cantilever beams provide inaccurate and unreliable results.

(e) The Canadian Institute for Steel Construction (CISC, 1989) guide predicts non conservative buckling strength results for cantilever beams since it neglects the effect of torsional restraints on such beams.

(f) The proposed design procedure implemented to predict lateral torsional buckling capacity of cantilever beams was found to be in good agreement with numeric and experimental results.

Ghersi et al. (1994)

Ghersi et al. (1994) studied the out of plane buckling modes of double-channel cold-formed beams. Their study focused on inelastic local and lateral torsional buckling. The study consisted of three components: (1) experimental, (2) analytical, and (3) numerical.

The main purpose of the study was to reinvestigate previous experimental analysis of double-channel cold-formed beams to better understand the behaviour of those beams under lateral-torsional buckling.

The experimental investigation consisted of five tests conducted on simply supported double-channel beam specimens with a 3m span. Cross-section dimensions varied between slender, semi-compact, to plastic sections according to the Eurocode 3 classification. Cross section dimensions were: beam depth d = 200 mm, flange width b = 40-100 mm, flange thickness t = 2-5 mm and web thickness w = 2-5 mm. Material was Fe360 steel with a yield strength F_y ranging between 233 and 284 MPa. A system of a displacement-controlled actuator with load-transfer bars was used to apply two vertical loads spaced 1m apart. Lateral torsional buckling was restrained along the 1m central span on each side of the loading bars.

In their analytical predictions, reduction factors were applied to the elastic critical moment equations as per the Eurocode 3 and AISI Specification (1986) in order to account for initial imperfections and decrease in elastic lateral torsional buckling capacity prior to reaching plastic region.

A parametric analysis for the combined effect of local and lateral torsional buckling was undertaken in accordance with the Eurocode 3 provisions. It was found that experimentally obtained critical loads were in agreement within 3 to 11% with those based on code equations.

The numerical analysis was able to predict of the combined instability behaviour of specimens. The conclusions of the study were: 1) as slenderness ratio of cross section increases, the combined effect of local and lateral torsional buckling range increases and 2) ultimate moments provided in Eurocode 3 provide reliable estimates when compared to the experimental test results.

Menken et al. (1994)

Menken et al. (1994) studied the nonlinear interaction between buckling modes. Their study focused on the coupled effect of local and lateral torsional buckling on T-beams. The study consisted of three components: (1) numerical analysis, (2) a pilot model, and (3) experimental investigation.

The main purpose of this study was to investigate the post-buckling behaviour of simply supported T-beams under concentrated transverse loading by using few buckling modes obtained. Towards this goal, a simplified model was developed and compared against numerical analysis and experimental results.

It was concluded that by using the first three buckling modes obtained from numerical analysis, it is possible to successfully describe nonlinear interactions within the post-buckling range.

Razzaq et al. (1995)

Razzaq et al. (1995) studied the lateral torsional buckling of pultruded fibre reinforced plastic (PFRP) channel beams. Their study focused on the overall destabilizing effect of concentrated transverse loadings acting on PFRP C-shaped structural sections. The study consisted of two components: (1) experimental and (2) theoretical. The main purpose of this study was to experimentally investigate the lateral torsional behaviour of PFRP beam sections, develop an elastic buckling expression, and an LRFD design approach.

Because of initial imperfections, beams were observed to undergo both vertical and lateral displacements and twist as soon as the load is applied. Pre-buckling deformations were observed not to diminish the lateral torsional buckling capacity of the beams. An elastic buckling formula was established and used in an LRFD approach for analysis and design purposes. Warping stresses were observed to be significant compared to flexural stresses when loading was applied away from shear center. Two parameters were found to be substantial when determining PFRP buckling loads: (a) the minor axis slenderness ratio and (b) the height of load application relative to the shear center.

Menken et al. (1997)

Menken et al. (1997) investigated the buckling interaction effect between local and lateral torsional buckling in linear elastic plate structures. Towards this goal, finite element software was developed and verified by experimental results. They concluded that for prismatic plate structures, the initial nonlinear post-buckling behaviour can be described in terms of a chosen set of buckling modes.

Roberts and Masri (2003)

Roberts and Masri (2003) studied the effect of shear deformations on overall lateral torsional buckling of pultruded fibre reinforced plastic (PFRP) I-shaped beams. The authors concluded that for I-shaped beams, shear deformations reduces the critical load by 5%, while pre-buckling flexural displacements increases the critical moment by 20%.

Yu and Schafer (2006)

Yu and Schafer (2006) investigated the effect of distortional buckling on cold-formed steel beams of C and Z-shaped cross-sections. They concluded that North American and European codes provide non-conservative predictions for buckling strength of beams. However, Australian and Newzealand design standards (1996) and AISI specification (1994) provide the most reliable buckling predictions.

Liu and Gannon (2009)

Liu and Gannon (2009) investigated the effect of hot-rolled simply supported steel I-beams with reinforced with strengthening plates (i.e., stiffeners), on residual stresses and ultimate buckling capacity of beams. Some of the tests were designed to fail in lateral torsional buckling. A total of 11 four-point-bending tests were conducted. The tests were designed to restrain the steel I-beams at their end supports against lateral deflection and twist. The parameters investigated are: (a) reinforcing patterns (b) span, and (c) load levels prior reinforcing.

It was concluded that for I-beams with long spans, the effect of steel plate reinforcement under pre-loading reduce the lateral-torsional buckling capacity compared to the case of zero preload. However, for I-beams with short spans which fail by yielding, the effect of preloading was found less significant.

1.2.2 Numerical Solutions on Lateral Torsional Buckling

There is a wealth of numerical solutions on lateral torsional buckling in the literature. The large majority of them are devoted to co-linear structures. For a comprehensive and up-to-date literature review, the reader is referred to Erkmen (2006) and Wu (2010). The numerical solutions on Gerber beams isolate the beams from the Gerber frame and disregard the flexibility of the supporting columns (e.g., Essa 2003). To the knowledge of the author, none of the studies has focused on the lateral buckling of Gerber frames as a system. Also, only a few numerical studies were conducted on frames. This includes the study of Vacharajittiphan and Trahair (1973) who focused on the behaviour of portal frames laterally supported at their beam-to-column junctions. Also, the study of Dabbas (2002) and Zinoviev and Mohareb (2004) respectively focused on laterally unsupported T shape and portal frames.

1.2.3 Design Methods for Systems Similar to Gerber Systems

Essa and Kennedy (1994)

Essa and Kennedy (1994) proposed an iterative design method for I-shaped steel beams with a single cantilever extension subject to a concentrated load applied at the cantilever tip. The design method is capable of determining the overall elastic lateral torsional buckling resistance of steel beams with cantilever extensions. The solution is applicable to beams with (a) laterally and torsionally unrestrained backspans and cantilever extensions and (b) full lateral and torsional restraints at the support.

An interaction ratio of the backspan to cantilever span is introduced to account for the effect of the cantilever extension on the lateral buckling resistance of such beams. The overall elastic critical moment is obtained by multiplying the interaction ratio by the difference of the backspan and cantilever segments critical moments and adding the result to the cantilever segment critical moment.

Essa and Kennedy (1995)

In a subsequent study, Essa and Kennedy (1995) studied the effect of lateral and torsional restraints on the lateral torsional buckling resistance of cantilever-suspended-span beams. A step-by-step design procedure was proposed based on the following assumptions: (a) doubly symmetric cantilever extensions, (b) cantilever span is 1/4 to 1/6 of the backspan, (c) presence of open web steel joists (OWSJ) which provide lateral and torsional restraints at the top flange, and (d) columns are spaced evenly. Various lateral restraint configurations and loading patterns were analyzed in an attempt to provide an accurate design procedure. The design method is valid for beams with single and double cantilever extensions. It also accounts for the lateral and torsional restraint provided by OWSJ. All solutions were developed for the case where the Gerber beam is fully restrained laterally and torsionally at column locations. However, the proposed method has the following design limitations: (a) solutions were developed by smearing the torsional restraint provided by OWSJ, (b) the rigid connection between the supporting columns and Gerber beam was neglected, and (c) the flexibility of the supporting columns supporting the Gerber beams was neglected.

Rongoe (1996)

Rongoe (1996) analyzed bracing effectiveness and provided design guidelines for lateral and torsional bracings in cantilever-suspended-span construction. The design document also presented two methods for determining the lateral torsional buckling resistance of I-shaped steel beams. The methods were based on Essa and Kennedy (1995) and Yura (1995).

The design document compares Essa and Kennedy new method to traditional methods in terms of unbraced length values and effective length factors for the cantilever segments. The second method, which is proposed by Yura, is based on the AISC LRFD approach. The Gerber beam is assumed to be analyzed in two separate segments, the backspan and cantilever segments. All solutions were developed for the case where the Gerber beam is assumed to have continuous restraint at either the top or bottom flanges. However, the proposed method neglects warping continuity between the backspan and cantilever segments.

The author concluded that traditional code-based methods of analysis lead to either overly conservative or non-conservative buckling capacity for I-beams with cantilever extensions. The Essa and Kennedy (1995) design approach was adapted and recommended for design.

1.3 Scope of Thesis

Among all the studies surveyed, only the study of Vacharajittiphan and Trahair (1973) has focused on the experimental investigation of lateral torsional buckling on plane frames. The frames investigated were laterally supported at the beam to column junction. For the Gerber system, Essa and Kennedy (1994, 1995) have simplified the problem by neglecting the interaction between the columns and beams and conducting their experimental investigation only for beams with overhangs. Various loading patterns were investigated in their study. A numerical analysis was conducted and the reliability of the numerical predictions was assessed through comparisons against experimental results. However, the flexibility of column supports for beams was neglected, both in the experiments and the finite element model. Another difference between the simplified beam representation in Essa and Kennedy (1993) and that based on a complete representation of the Gerber frames is the fact that the welds between the column supports and Gerber beams are able to transfer moments from the beam to the column, the result of which is a different moment distribution in the backspan, leading to different buckling resistances under both representations. Within this context, the present study contributes to the experimental database by providing a more realistic representation of the Gerber system by testing and analyzing the whole beam-column Gerber assembly.

CHAPTER 2

Description of Experimental Investigation

2.1 General

The experimental investigation on lateral buckling resistance of Gerber frames in this thesis is part of a larger study which focuses on the effect of two parameters: 1) gravity load combinations (i.e., tip loading, mid-span loading, and combinations thereof). This parameter is the focus of the present thesis, and 2) the effect of various OWSJ lateral and torsional support configurations on the buckling resistance of Gerber frames, which is outside the scope of the thesis.

A limited experimental database of full-scale tests on laterally unsupported Gerber frames subject to various gravity load combinations is developed. Section 2.2 describes the ancillary tests conducted to obtain the stress versus strain relationship curves. Section 2.3 presents key aspects for the design of experiment while Section 2.4 provides the various experimental details including fabrication details, method of load application, and instrumentation used.

2.2 Ancillary Tests

A total of six longitudinal tension coupons (two from each test specimen) were tested to determine the stress versus strain relationship curve of the steel material. The tension coupons were cut from the tips of cantilever extensions of each specimen and dimensioned according to ASTM E8 (2004) specifications. First, rough cuts ranging between 2 to 3 inches away from the perimeter of the actual tension coupons were completed in an effort not to introduce any residual stresses. The coupons were tested in a 600 kN capacity Galdabini universal machine. The machine was programmed to pause for one minute at pre-selected strain values in order to capture static stress values. A total of four longitudinal and transverse strain gages were mounted on the central region of each tension coupons. One longitudinal and one transverse strain gages were mounted on one side of the coupon, while the remaining two strain gages were mounted the same way on the opposite side. By averaging the strain values obtained from both sides, possible errors arising from initial misalignment and eccentricity with respect to the machine loading grip were minimized. A 50mm gage length extensometer was also mounted on the central region of the tension coupons for the longitudinal strain measurements. While strain gages yield reliable results in the initial stage, the extensometer provide reliable readings in the post-yield range. Following yield, readings from all four longitudinal and transverse strain gages were discarded. Table 2.1 provides a summary of results obtained from the six coupons.

Table 2.1 Material Properties

Material Properties	Specimen 1		Specimen 2		Specimen 3	
	Left	Right	Left	Right	Left	Right
Young's Modulus (MPa)	205,463	217,838	204,190	213,832	209,814	214,024
Average	211,651		209,011		210,860	
Poisson's Ratio	0.297	0.306	0.288	N/A	0.291	0.305
Average	0.302		0.288		0.298	
Yield Strength (MPa)	413	412	348	348	345	342
Average	412.5		348		343.5	
Ultimate Stress (MPa)	> 431		> 394		> 387	
Rupture Strain	0.278	0.193	0.262	0.258	0.221	0.208
Average	0.236		0.260		0.215	

All Young's Modulus values in Table 2.1 were calculated based on manually recorded strain values obtained from longitudinal strain gages in the elastic region and their corresponding stress values. Strain values based on extensometer readings were automatically recorded by using a computerized data acquisition. However, extensometer strain values recorded in the elastic region were found unreliable in calculating Young's Modulus and were discarded. For all test specimens, Poisson's ratios were calculated based on manually recorded strain values obtained from longitudinal and transverse strain gages in the elastic region. For Specimen 2 Right, both transverse strain gages recorded faulty strain values due to the early detachment of the strain gages. Therefore, no reliable data was available to calculate the Poisson's ratio for this particular specimen. For all specimens, yield strength values were extracted from the stress versus engineering stress relationship. The lowest static value in the yielding plateau was selected as the yield strength. Since the ultimate strength was not recorded in all three tests, the maximum static stress recorded was selected as the reference point. Rupture strain values were calculated based on the measurements of Demec points before and after the test. Two Demec points were dinted in the test specimen along the gauge length. The distance between the Demec points was measured before and after the tests. The stress versus engineering stress relationship curves are presented in Figures A.1- A.6 of *Appendix A*.

2.3 Design of Experiment

2.3.1 Frame Dimensions

The geometries of the specimens were selected to be as representative as possible to the geometry of Gerber frames in practice while remaining within the spatial and testing constraints of the structural laboratory at the University of Ottawa. The specimen geometry is schematically presented in Fig. 2.1. The measured dimensions for all three specimens as built are provided in Table 2.2. As expected, there are slight variations in the cross-dimensions of each specimen. No stiffeners were provided at the beam-to-column junction.

2.3.2 Test Specimens Dimensions

The cross-sectional dimensions for all three specimens were measured and provided in Tables B.1 to B.4. The cross-sectional properties based on the dimensions measured are provided in Tables B.5 through B.8. The nominal properties as provided in the handbook of steel construction are also provided for comparison. There are slight differences between the tabulated properties (Column 4 in Tables B.5 through B.8) and those calculated based on the measured dimensions (Column 3). These differences are due to: a) the presence of fillets in HSS sections and in W-shape sections at their flange to web junctions and b) the difference between the nominal and measured dimensions.

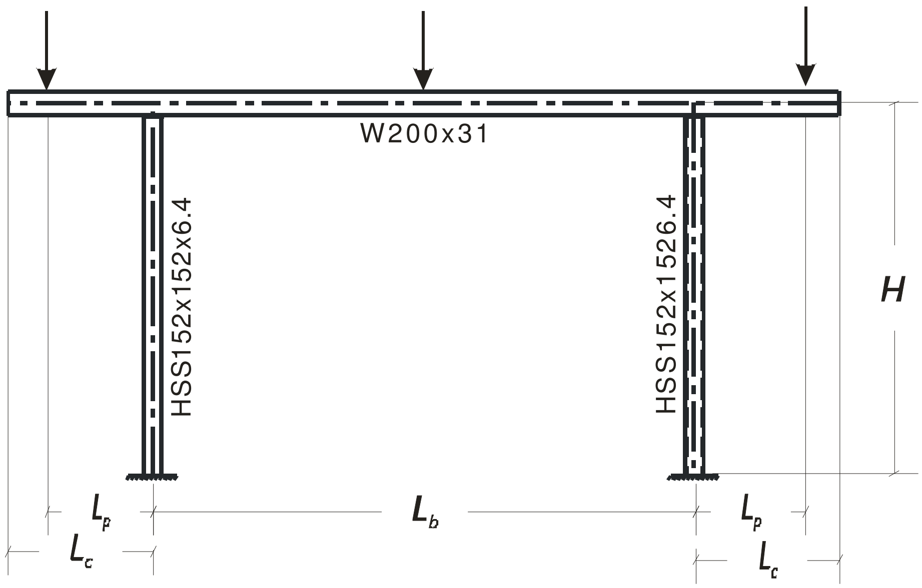

Figure 2.1-Geometry of Gerber Frame and Typical Loading Configuration

Table 2.2 Measured Dimensions of Frame Geometry (m)

Specimen No.	Middle Span (L_b)	Cantilever Extension (L_c)		Location of tip load relative to column centreline (L_p)		Column Height (H)	
		Left	Right	Left	Right	Left	Right
1	4.56	1.50	1.52	N/A	N/A	3.12	3.09
2	4.58	1.52	1.52	1.37	1.39	3.12	3.09
3	4.58	1.52	1.52	1.45	1.45	3.12	3.09

2.3.3 Selection of Cross-Sections

The frame consists of a W200x31 beam supported by two columns with an HSS152x152x6.4 cross-section (Fig. 2.1) with the following nominal cross-sectional dimensions; cross-section depth d = 210 mm, flange width b = 134 mm, flange thickness t = 10.2 mm, and web thickness w = 6.4 mm. The measured dimensions are given in Table 2.3 and the corresponding sectional properties are presented in *Appendix B*. The chosen beam cross-section was selected to meet Class 1 requirements (according to CAN/CSA S16-09 classification rules) in order to minimize the tendency of the specimen to undergo cross-section distortions during the tests.

Table 2.3 Measured Cross-Sectional Dimensions (mm)

Specimen No.	Flange Width (b)	Flange Thickness (t)	Section Height (d)	Web Thickness (w)
1	132.9	10.1	210.9	6.5
2	131.9	10.2	212.8	7.5
3	131.7	10.0	212.6	7.0

2.3.4 Nominal Material Properties

All materials were chosen to match the most common steel grades in the Canadian market. For the beam specimens, material used is hot-rolled 350W steel with specified minimum yield strength of 350MPa. For column specimens, material used is hot-rolled ASTM A500 Grade C steel with a yield strength of 345MPa (Handbook of Steel Construction, p. 4-100). All members had a nominal modulus of Elasticity, E, is 200,000MPa.

2.3.5 Target Modes of Failure

The frame dimensions and cross-sections were chosen so that the Gerber frame specimen is expected to undergo elastic lateral torsional buckling when no lateral bracings are provided. When the frame is laterally braced through open web steel joists (OWSJ) (in the subsequent stage of the research), frame dimensions are such that inelastic lateral torsional buckling is expected to occur. This was ensured by conducting two types of analyses for each load configuration: a) an elastic buckling finite element analysis, which predicted the elastic buckling resistance for each loading configuration, and b) Based on the buckling resistance determined in (a) A linearly elastic analysis was conducted for each specimen, and maximum bending moments predicted within the frame was ensured to be less than 67% of the yield moment of the cross-section, in order to allow for the presence of residual stresses. The details of both types' analyses will be provided under Chapter 3.

2.3.6 Preliminary Finite Element Analyses

A series of elastic buckling finite element analyses based on shell analysis conducted on the frame nominal geometries. The details and specifics of the FEA model are similar to those described in Chapter 3. The analyses were based on nominal dimensions as provided in Section

2.3.3 and nominal properties of steel (E=200,000 MPa, ν=0.3). Column height was taken as 3m, the middle span was 4.5m, and distance from centreline to cantilever tip was 1.2m.

The ratio α of the mid-span load αP to tip load P was varied within the range $(0 \le \alpha \le \infty)$ and an interaction diagram was developed (Fig. 2.2). Different values of α represent different loading distributions between the middle and cantilever spans. The resulting buckling load combinations for each loading ratio α as predicted by ABAQUS are provided in Table 2.4.

Table 2.4 Mid-span versus Tip Predicted Buckling Loads (kN)

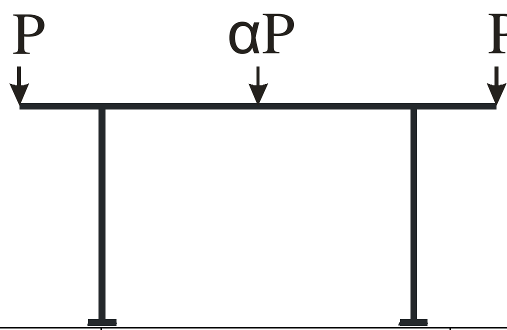

α	$P_{centre} = \alpha P$	$P_{tip} = P$
0	**0.0**	**46.8**
1	**46.8**	**46.8**
1.2	56.2	46.8
1.5	70.2	46.8
1.8	83.7	46.5
2	87.6	43.8
3	82.8	27.6
4	79.2	19.8
5	77.5	15.5
10	73.0	7.3
∞	**69.5**	**0.0**

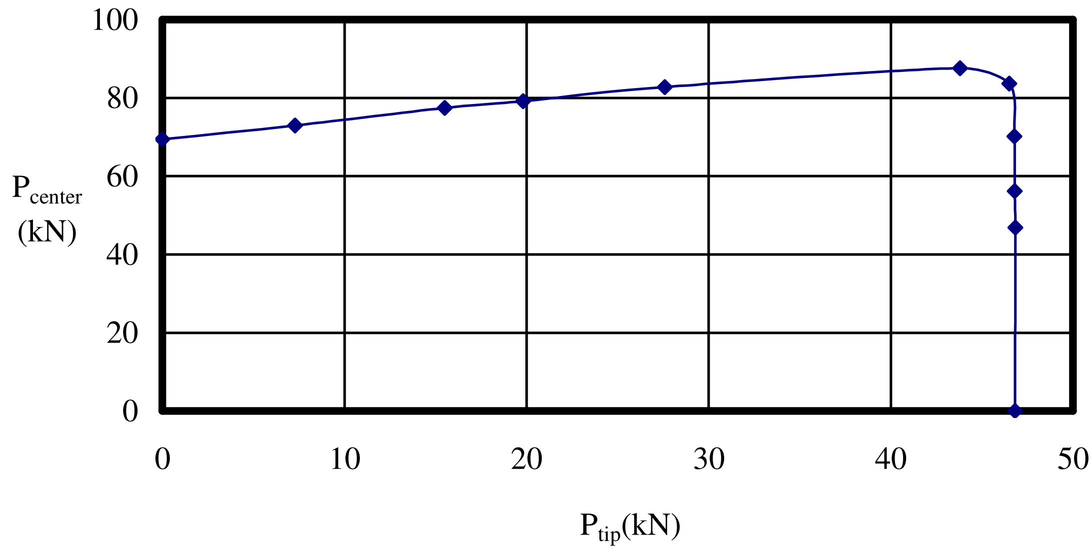

Figure 2.2-Mid-span Load versus Tip Load Interaction Diagram

2.3.7 Selection of Load Combinations to be tested

Three of the load configurations in Table 2.4 were tested. These are (1) single mid-span load $\alpha \to \infty$, (2) cantilever tip loads $\alpha = 0$, and (3) one combination of mid-span and cantilever tip loads $\alpha = 1$. The value $\alpha \to \infty$ simulates the limiting condition where the middle span is subject to maximum loading while the cantilever loading is negligible. The value $\alpha = 0$ corresponds to the other limiting loading condition where cantilever load is maximal while middle span load is negligible. Real loading conditions lie in between the above two limiting conditions. The combination $\alpha = 1$ is intended to represent a more representative loading case lying in between the limiting ones $\alpha \to \infty$ and $\alpha = 0$. A schematic for the experimental setup for each specimen is provided in Figures 2.3 through 2.5.

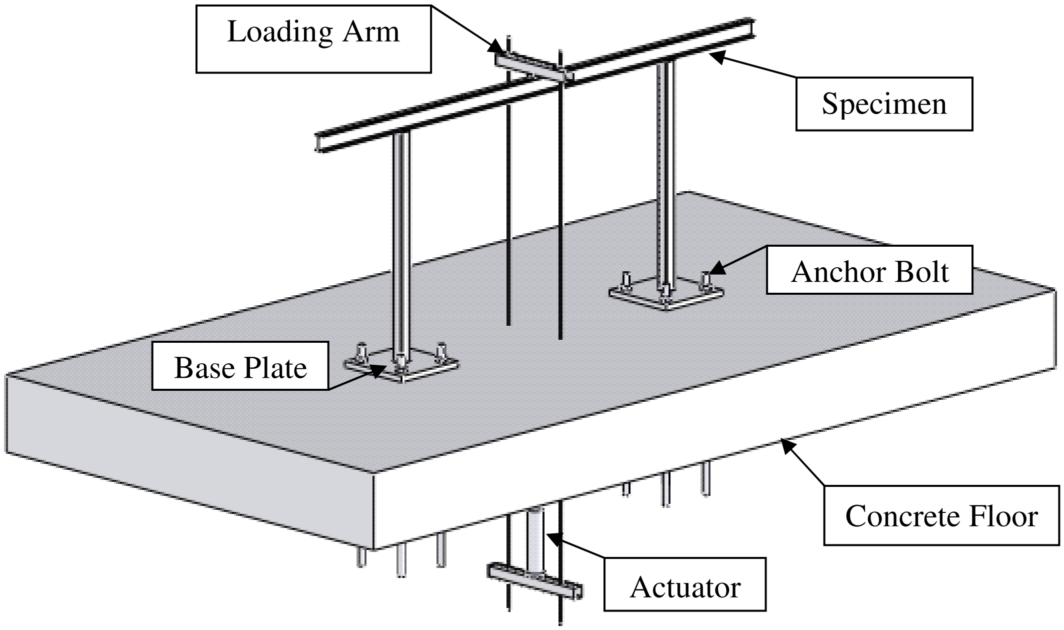

Figure 2.3-Specimen 1-Schematic of Experimental Setup

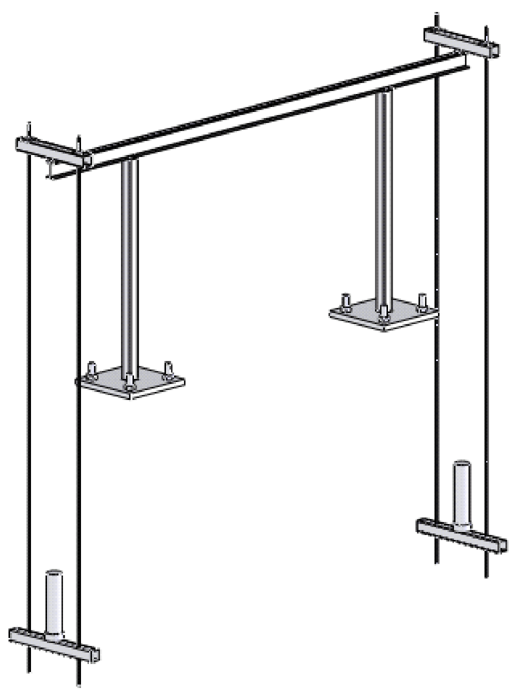

Figure 2.4-Specimen 2-Schematic of Experimental Setup (strong floor removed for clarity)

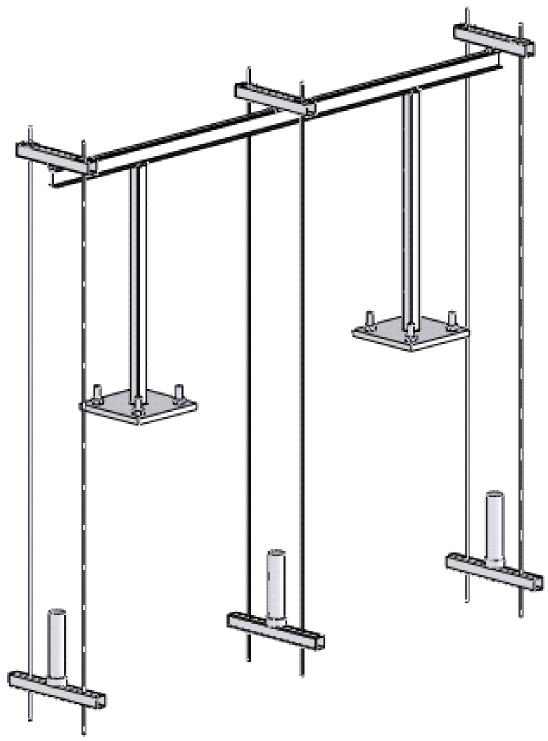

Figure 2.5-Specimen 3-Schematic of Experimental Setup (strong floor removed for clarity)

2.4 Specimen Geometry and Material Properties

2.4.1 Specimen Fabrication and Details

The experimental investigation was undertaken at the University of Ottawa structural laboratory. The test setup is illustrated in Fig. 2.6. The base of both columns were welded all around using a 6mm fillet weld to a 1,219x1,219x76.2 mm base plate with a nominal yield strength of 300MPa. Each base plate was anchored to the strong concrete floor (900mm deep) through four 70mm diameter anchor rods to prevent potential uplift on the tension sides. Figure 2.7 shows the column base detail.

Figure 2.6-Specimen 1-Overall view

Figure 2.7-Column-Base Plate-Strong Floor Connection

The top of the column was welded all around to the underside of a 152.4x152.4x12.7mm cap through 6mm fillet all around to the top of the column. The top of the plate was also welded all around through a 6mm fillet weld to the underside of bottom flange of the beam (Fig. 2.8).

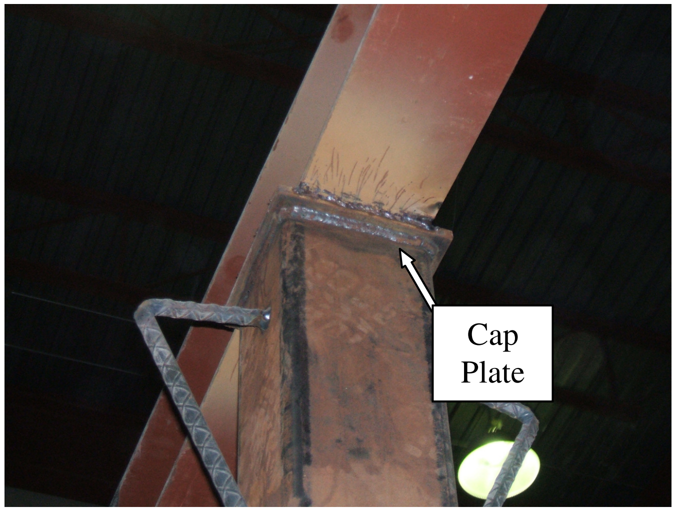

Figure 2.8-Cap Plate Detail (looking up)

2.4.2 Load Application

The loading detail and arrangement is illustrated in Fig. 2.9(a), in which the frame is loaded at mid-span. Loading details were designed to apply a vertical point load slightly above the top flange (which simulates loads normally transferred from OWSJ) while allowing twisting of the beam cross-section. The loading details consist of:

1. A hydraulic actuator mounted on the underside of the strong floor is shown in Figure 2.9(d). The actuator consists of a cylinder with a collapsed height of 247mm and a stroke distance of 156mm. The maximum capacity is 101kN. The stroke is manually controlled by regulating the fluid flow rate to the actuator.

2. The actuator is mounted on the lower cross-beam (Fig. 2.9(d)). The cross-beam has an HSS127x127x4.8mm cross-section. The centerline of the actuator coincides with the vertical axis of symmetry of the cross-beam.

3. Two threaded steel rods with a 25.4mm diameter and nominal yield strength of 414MPa pass through two drilled holes in the bottom cross-beams (Fig. 2.9(b)). A 152.4x152.4x12.7mm bearing plate was provided underneath the cross-beam to prevent local yielding the cross-beam when the specimen is loaded (Fig. 2.10). Two sets of nuts are provided at the bottom and top of the cross-beam to ensure the rod is snug tight against the cross-beam.

4. The two steel rods also pass through holes in the top cross-beams. Similar to the bottom cross-beam, a top cross-beam with an HSS152.4x152.4x12.7mm is provided. A bearing plate is provided on top of the cross-beam to prevent local yielding and the assembly is brought to a snug tight position through two sets of nuts.

5. The underside of the top cross beam was welded to 127x76.2x50.8mm grooved cold-formed steel plate. The angle of the grooved cold-formed steel plate was machined at 130° as shown in Figure 2.9(c) to allow relative rotation between the top cross-beam and the specimen cross-section.

6. The grooved steel plate was placed in contact to the heel of the angle (Fig. 2.9(c)). L38x38x6.4mm. The toes of the steel angle were tack welded at four corners to the top of the beam (Fig. 2.9(c)). The heel of the angle acted as a pivot point to the applied load. The loading detail adopted was intended to simulate the load transferred from OWSJ while providing neither lateral nor torsional restraint to the top of the beam. This is consistent with the objective of this study in which the effect of lateral and torsional restraints provided by OWSJ is conservatively omitted.

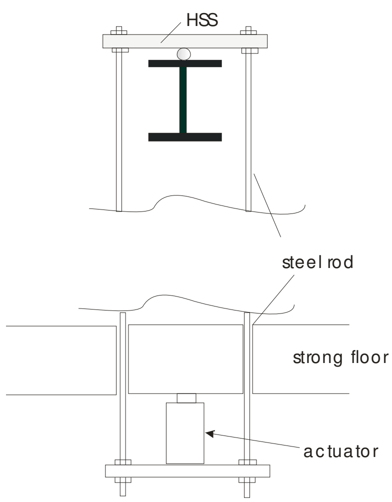

(a) Loading Concept and Arrangement


(b) Upper Loading Arm(for loading details; see figure c)

(c) Upper Loading Arm, Grooved Plate, Angle, Top Flange of Beam

(d) Actuator Underneath Strong Concrete Floor

Figure 2.9-Loading Details

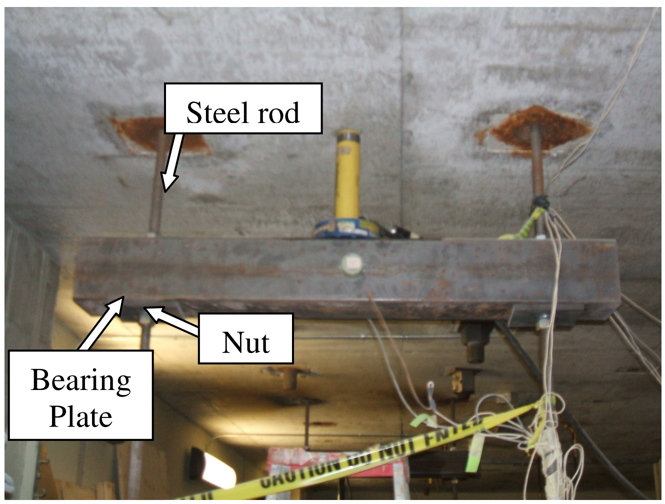

Figure 2.10-Lower Cross-Beam Detail

Throughout the test, the angle of rotation of both cross-beams was monitored. For tests involving more than one loading, a system of needle valves with a maximum capacity of 10,000psi was used to simultaneous control the stroke of all actuators involved. These valves were essentially functioning as one-way flow controllers. They were manually controlled to regulate the hydraulic fluid pumped through hydraulic hoses to actuators. Figure 2.11 shows the system of valves. Pressure gages with a maximum capacity of 10,000psi were installed at each valve to monitor hydraulic fluid pressure throughout the test (Fig. 2.11).

When two or three loads were applied simultaneously, only one valve at a time was opened to control the stroke of one actuator at a time. The valve was fully opened and hydraulic oil was manually pumped. When the stroke desired was reached, the valve was then shut and the other valve was opened to control the stroke of the other actuator. The process was repeated until the loads at all actuators were nearly equal to their target values. The pressure gages were used to assist in controlling pressure build up in the valve system. Due to the elongation of the steel rods during testing, the system of nuts was tightened periodically as the test progressed. Tightening of the nuts has resulted in maintaining the cross-beams nearly horizontal throughout the entire experiment.

Figure 2.11-System of Needle Valve Couplers

2.4.3 Instrumentation

The instrumentation used in the experiment include 17 horizontal linear variable differential transducers (LVDT) to measure lateral displacements of Gerber beam (Fig. 2.12) relative to a fixed frame of reference, seven single-axis rotation meters (clinometers), three load cells, and six vertical LVDTs. For Specimen 1, one LVDT with a displacement range of 25mm was calibrated and used to measure vertical displacements of Gerber beam at mid-span (Fig. 2.13). For Specimens 2 and 3, six LVDTs were calibrated and used to measure vertical displacements at mid-span and cantilever tips. Two LVDTs were used per location in order to provide redundancy in the measurements. The instrumentation locations and calibration data are provided in *Appendix C*.

Figure 2.12-Typical Horizontal LVDTs

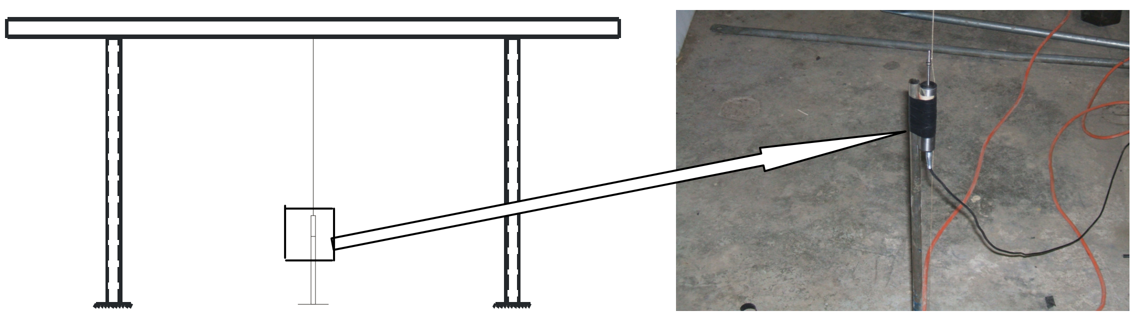

Figure 2.13-Typical Vertical LVDT located at Gerber Frame Mid-span

Actuator loads were measured using calibrated load cells. Load cells were placed underneath the actuators as shown in Fig. 2.10(d). Clinometers were mounted on each of cross-beams (Fig. 2.14) involved in a given test in order to monitor their angle of rotation.

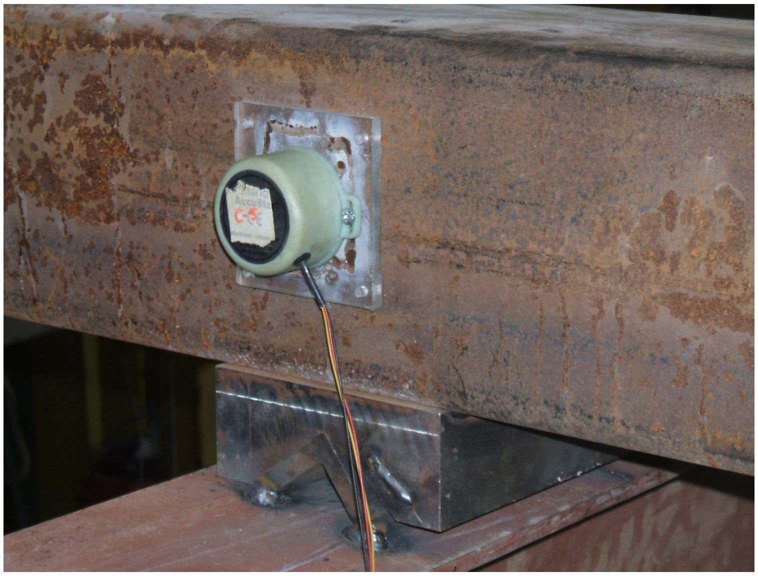

Figure 2.14-Clinometer Mounted on Upper Cross-Beam

Seven single-axis clinometers with an angle range of 90° but calibrated for a smaller angle range of 5° were used to monitor the angle of twist of cross-beams and Gerber beam (Fig. 2.15).

Figure 2.15-Clinometer Mounted on Gerber Beam Web at Mid-span

A computerized data acquisition equipped with 40 channels was used to electronically record data throughout the test at 5kN intervals. In order to avoid dynamic effects and obtain reliable readings, it was essential to record data 2-3 minutes following application of load strokes at the manual hydraulic pump. The tests were stopped when one of the following three criteria was attained: (a) elastic lateral torsional buckling of Gerber beam as determined from the load versus angle of twist is attained, (b) the inability of the specimen to carry additional loads based on load cell readings (indicating that the buckled state has been reached), or (c) when the side of the grooved cold-formed steel plate was observed to come into contact with one of the legs of the angle (implying an excessive angle of twist of the specimen, a characteristic of buckling). The experimental results will be discussed in detail in Chapter 4.

CHAPTER 3

Description of Finite Element Model

3.1 Lateral Buckling Behaviour of Frames

3.1.1 Behavior of a Frame without Imperfections

An elastic plane structure with no lateral imperfections and subjected to a reference in-plane loads $\{F\}$ is expected to undergo in-plane displacements and rotations $\{u_{IP}\}$ given by:

$$[K_{IP}]\{u_{IP}\} = \{F\} \qquad (3.1)$$

where $[K_{IP}]$ is the in-plane stiffness matrix. As the applied loads are increased, the corresponding displacements, strains, and stresses are assumed to proportionally increase when in-plane second order effects are negligible, i.e.,

$$[K_{IP}]\lambda_i\{u_{IP}\} = \lambda_i\{F\} \qquad (3.2)$$

For a frame without imperfections under in-plane loads (Fig. 3.1.c), no out-of-plane displacements are expected to take place (i.e., $\{u_{OP}\} = \{0\}$) within this stage of the response. The initial of out-of-plane stiffness is assumed to be characterized by matrix $[K_{OP}]$. The presence of compressive stresses induced by the reference loads $\{F\}$ in the pre-buckled stage cause an out-of-plane loss in stiffness characterized by matrix $[K_{OPG}]$. Once the applied loads attain a certain critical load combination λ_i, the in-plane stresses determined in Eq. 3.2 cause an entire loss of the stiffness characterized by $\lambda_i[K_{OPG}]$ such that,

$$\{[K_{OP}] - \lambda_i[K_{OPG}]\}\{u_{OP}\}_i = \{0\} \qquad (3.3)$$

As a result, the structure acquires a tendency to undergo sudden lateral displacements and twist $\{u_{OP}\}_i$. The magnitude λ_i of the applied loads at which such a sudden deformation pattern is of prime design importance and is given by the eigen-value problem:

$$\left\|[K_{OP}] - \lambda_i[K_{OPG}]\right\| = 0 \qquad (3.4)$$

When matrix $[K_{OP}]-\lambda_i[K_{OPG}]$ is singular, the magnitude of the buckling displacements is indeterminate. Specifically, it can be shown that if a vector $\{u_{OP}\}_i$ satisfies equation 3.4, vector $\alpha\{u_{OP}\}_i$ will satisfy Eq. 3.4, α, being any scalar.

3.1.2 Effect of Imperfections

Real frames (such as the ones tested in the present study) have initial minor lateral imperfections prior loading (Fig. 3.1.d). As a result, when subject to in-plane loading $\{P\}$, the structure undergoes in-plane and out-of-plane displacements simultaneously denoted as $\{u\}$. Conceptually, the response of such a structure with imperfections can be characterized by: a) measuring the initial geometric out-of-straightness, and b) conducting a geometrically nonlinear FEA analysis based on the initially imperfect structure. This leads to the nonlinear problem:

$$[K(u)]\{u\}=\{P\} \qquad (3.5)$$

Unlike a perfect structure, the given problem is not an eigen-value problem. It is solved incrementally and results in a non-linear displacement vs. load relationship. Figure 3.1 schematically shows the load vs. deformation relationship between a frame without imperfections and that of a frame with imperfection. It is observed that:

a) An imperfect frame will approach the buckling load from below, and
b) Due to initial imperfections, lateral displacements take place early on in the load deformation response for an imperfect frame.

This contrasts to the case of a perfect frame, in which no lateral displacement takes place prior attaining the critical load. In the present study, no attempt was made to measure the initial imperfections. Therefore, the nonlinear solution such that the one characterized by Eq. 3.5 was not conducted. Instead, the eigen-value analysis characterized by Eq. 3.3 was performed and an upper bound for the predicted buckling load combinations and mode shapes were determined.

The analysis consisted of two steps. Firstly, a linearly elastic pre-buckling analysis was conducted. The analysis was aimed at providing the stresses and strains in the beams before the member undergoes buckling, and thus the out-of-plane loss of stability matrix $[K_{OPG}]$. Secondly, a linearly elastic finite element buckling analysis was undertaken. The analysis provides the load level at which a perfectly straight structure is expected to undergo lateral buckling. It also provides the associated expected buckling mode. The details of the buckling finite element analysis used are described in Section 3.2 while a description of the analysis procedures is provided in Section 3.3. The results based on the FEA model described in this chapter will be presented in Chapter 4 along with a comparison with experimental results.

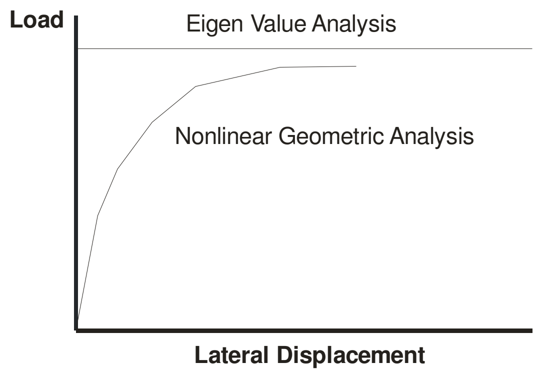

(a) Load vs. Lateral Displacement

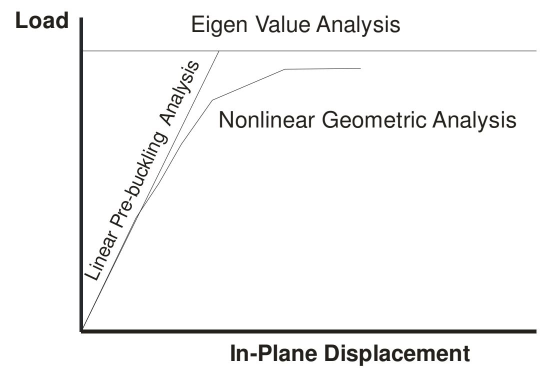

(b) Load vs. In-Plane Displacement

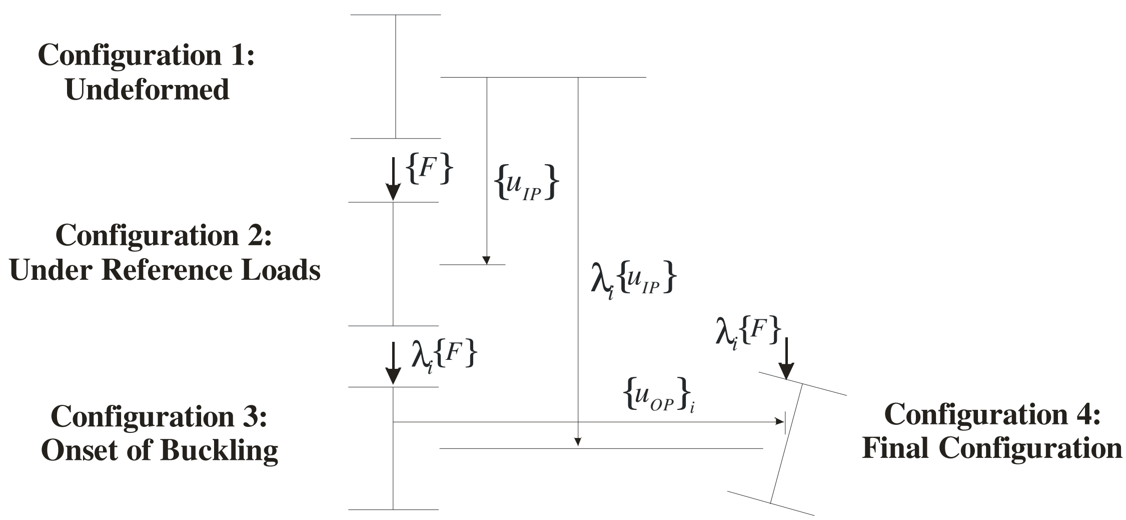

(c) Beam Cross-Section without Imperfections

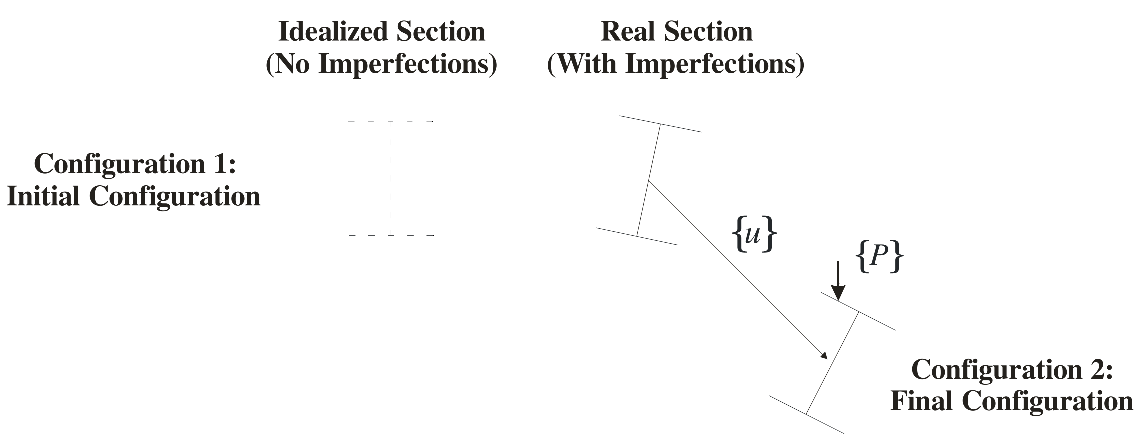

(d) Beam Cross-Section with Imperfections

Figure 3.1-Stages of Deformation

3.2 Details of Finite Element Model

3.2.1 Finite Element Program

The finite element analysis program, ABAQUS, was used to model the specimens described in Chapter 2. ABAQUS was selected since it is equipped with buckling analysis features. The program features a shell element S4R, which is reliable in modeling shell finite element, and an elastic eigen-value buckling procedure based on either the subspace eigen-solver or a linear perturbation procedure to obtain elastic buckling loads.

3.2.2 Shell Element

The Gerber frame structure was modeled using S4R shell elements. The S4R is a quadrilateral, four-noded, doubly curved stress/displacement shell element with reduced integration. This element is known for its reliability in modeling and predicting the buckling strength of similar frame structures. It prevents the occurrence of shear locking which is a typical malfunction in fully integrated elements. The S4R element internally uses three displacement components and two independent components of the normal vector to the shell surface at each node totalling five degrees of freedom per node. Linear interpolation is involved for each of the independent degrees of freedom. Externally, three translational components and three rotations totalling six degrees of freedom per node are readily made available to the user.

3.2.3 Material Properties

Steel material is assumed elastic, with an average Modulus of Elasticity, E, and an average Poisson's Ratio, ν. The values used in the model are those presented in Table 2.1.

3.2.4 Finite Element Mesh

As illustrated in Figure 3.2, six shell elements were used to model each flange, eight elements were taken across web height, and six shell elements were used to model each of the four faces of steel columns. Table 3.1 presents the total number of shell elements for each specimen. Further mesh refinements were observed not to result in any noticeable changes in predicted buckling loads. The element size and aspect ratio were selected based on an earlier study by

Dabbas (2002). According to Hibbit et al. (2006), elements with a nearly square shape give the best results. In this model, a finite element aspect ratio nearly equal to unity was targeted.

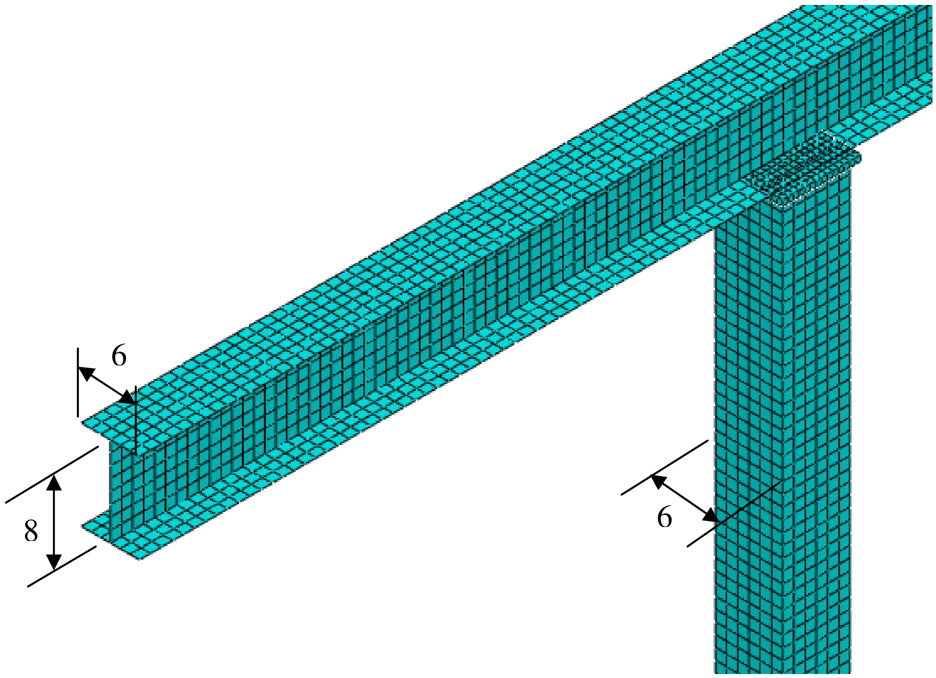

Figure 3.2-Finite Element Mesh

Table 3.1 Total Number of Shell Elements

Specimen No.	Cantilever Extension		Mid-span
	Left	Right	
1	1,354	1,373	3,333
2	1,386	1,383	3,331
3	1,385	1,385	3,635

3.2.5 Boundary Conditions

The beam cross-section is modeled without the inclusion of fillet welds for simplicity. This approximation is expected to lead to a minor underestimation of the elastic buckling resistance. Two 6"x6"x¼" steel columns cap plates were modeled using C3D8R solid element, a linearly interpolated brick stress/displacement solid element with reduced integration and hourglass control. The cap plate translational and rotational degrees of freedom were coupled to those of the column top by using the "TIE" feature in ABAQUS. The "TIE" feature couples the degrees of freedom of a pair of surfaces so that the translational and rotational motions as well as all other active degrees of freedom are equal. Steel columns were assigned full fixity conditions at their bases to simulate a rigid connection at the column-base plate interface. Fixation of columns is modeled by restraining the six degrees of freedom for all nodes at the column base. In order for the column top end to undergo rigid body displacements and rotations under imposed loads, all six degrees of freedom of the column top end and the bottom flange of the beam were coupled using the "TIE" feature.

3.2.6 Load Application

The three loading configurations investigated were applied to the beam top flange through a grooved plate and an L-shaped angle as illustrated in Section 2.4.2 of Chapter 2. A 152.4x152.4x38.1mm solid plate with an assumed Modulus of Elasticity, E =200,000MPa which approximately simulates the L-shaped angle welded to top flange of beam was modeled using C3D8R elements. The solid plate translational and rotational degrees of freedom were coupled to those of the beam top flange using the "TIE" feature in ABAQUS. The central node on the solid plate at 38.1mm above beam top flange is selected for the application of single point load at the desired locations.

3.3 Analysis Procedures

3.3.1 Pre-Buckling Analysis

The pre-buckling analysis is implicitly done by ABAQUS prior performing an eigen-value buckling analysis. This is a necessary step to determine the destabilizing matrix $\left[K_{OPG}\right]$. This step is done at the shell analysis level. In order to obtain the bending moments, shearing force, and normal force diagrams, a stand-alone structural analysis program, SAP2000, was used for this purpose. This yielded the linearly elastic load vs. displacement relationship prior buckling (Fig. 3.1.b).

3.3.2 Buckling Analysis

The buckling analysis is conducted by ABAQUS to solve Eq. 3.3 to yield the eigen-values λ_i and corresponding eigen-vectors $\left\{u_{OP}\right\}_i$. This was performed by using the subspace eigen-solver to extract the first few eigen-modes.

CHAPTER 4

Comparison of Results

4.1 Introduction

This chapter aims at providing a detailed discussion of experimental and FEA results. Section 4.2 provides a comparison of the experimental and FEA predicted pre-buckling displacements. Section 4.3 presents the experimental loads versus buckling displacements. Section 4.4 provides a comparison of experimental and FEA predicted buckling loads while Section 4.5 presents a comparison of the experimental buckling deformations and the FEA predicted buckling modes. Since the FEA is based on an assumed elastic analysis and thus should be valid only if the Gerber frames tested buckle elastically, Section 4.6 shows that the buckling behaviour is indeed elastic. Section 4.7 uses the experimental and FEA results to determine the effective length for cantilever segments and provides a comparison with other methods in the literature while Section 4.8 provides a discussion of possible optimum locations for torsional and translational braces based on the three specimens tested and analyzed.

4.2 Load vs. Vertical Displacements

The applied load as measured by the load cell versus vertical displacement of the specimens as measured by the LVDTs is plotted for each specimen. For Specimen 1 which was subjected to a single mid-span loading, the applied load was plotted versus the mid-span vertical displacement as presented in Fig. 4.1. For Specimens 2 and 3 which were subjected to cantilever tip loads and mid-span and cantilever tip loads respectively, the applied load was plotted versus the cantilever tip vertical displacement as presented in Figs. 4.2 to 4.8. On the figures, the load versus displacement relationships, as predicted by a pre-buckling linear elastic analysis, are overlaid for comparison. Also shown on the figures is the buckling load for each specimen as predicted by a shell finite element elastic buckling analysis based on ABAQUS. The raw experimental measurements are provided in *Appendix D* and experimental results are presented in *Appendix E.*

As illustrated in Figures 4.1 to 4.8, the pre-buckling load versus vertical displacement relationships based on a linear elastic analysis are observed to be in good agreement with the experimental measurements in the initial part of the response. An exception is observed in Figure 4.5, in which the experimental results show a milder slope than that of the elastic analysis. The discrepancy could be attributed to a combination of two possible factors: 1) The magnitude of the displacement is significantly smaller than other vertical displacement and thus the LVDTs which were calibrated for a significantly larger range are not expected to yield readings as accurate as those for other cases where the displacements are large, and/or 2) A possible calibration error for the LVDT.

As the load is increased, the experimental load versus displacement relationships tend to have a milder slope, possibly due to the effect of initial imperfections being amplified as the load approaches the buckling capacity.

In Specimen 1, the peak experimental buckling load of 63.5kN was found lower than that predicted by the eigen-value analysis (71.3kN). For Specimen 2, the peak experimental buckling load of 54.3kN was found slightly higher than that predicted by the eigen-value analysis (53.8kN). For Specimen 3, the peak experimental buckling load of 55.1kN was found significantly lower than that predicted by the eigen-value analysis (66.4kN). This could be attributed in part due to the presence of initial imperfections in the system. Another possible reason for the discrepancy is the fact that the finite element formulation in ABAQUS does not account for pre-buckling deformation effects. The effect of initial imperfections could be investigated in a geometrically nonlinear finite element analysis while that of pre-buckling deformation necessitates the development of solutions beyond those available in commercial programs.

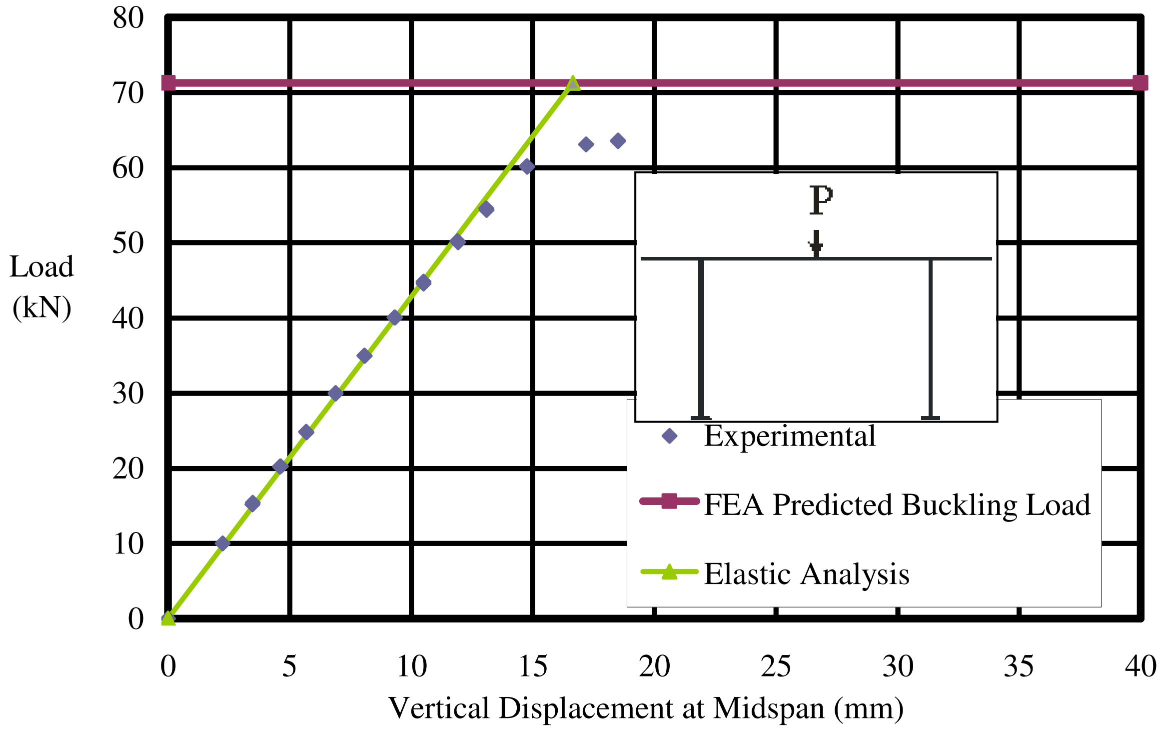

Figure 4.1-Specimen 1-Mid-span Load versus Mid-span Vertical Displacement

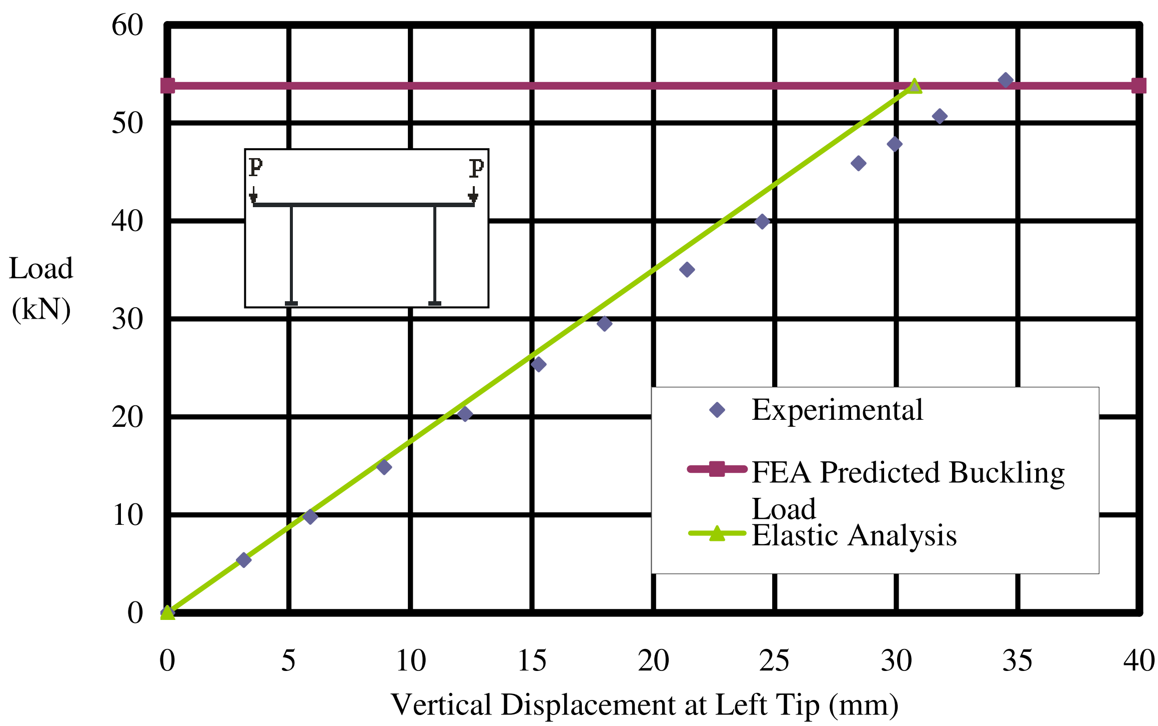

Figure 4.2-Specimen 2-Left Tip Load versus Left Tip Vertical Displacement

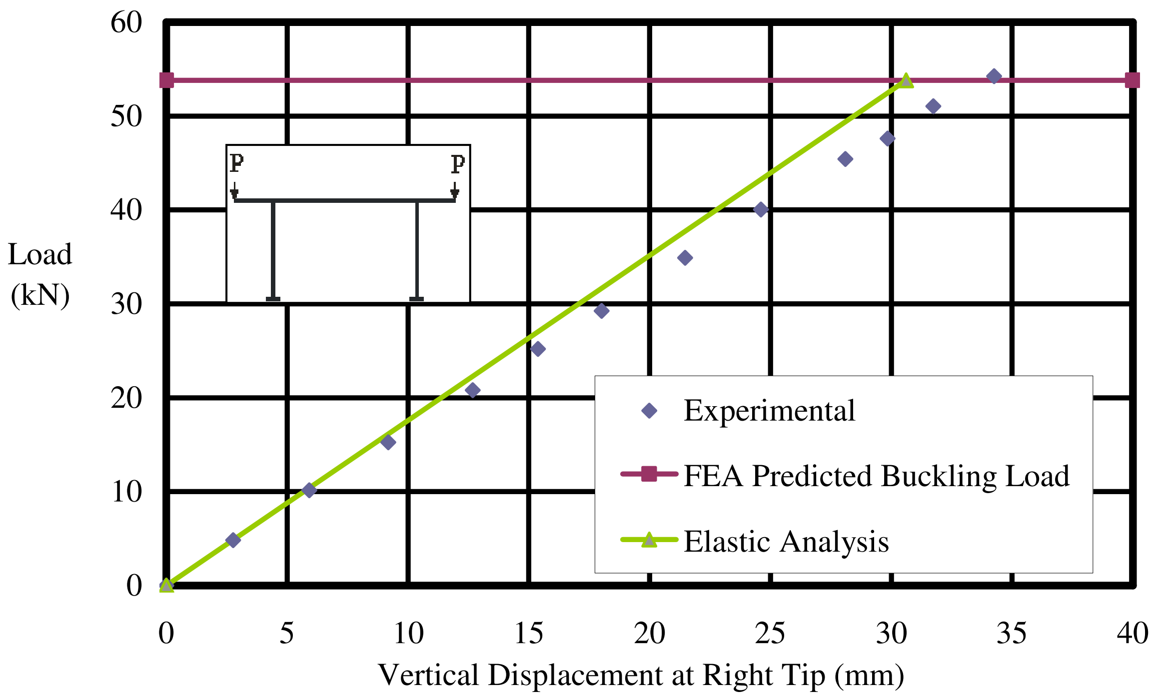

Figure 4.3-Specimen 2-Right Tip Load versus Right Tip Vertical Displacement

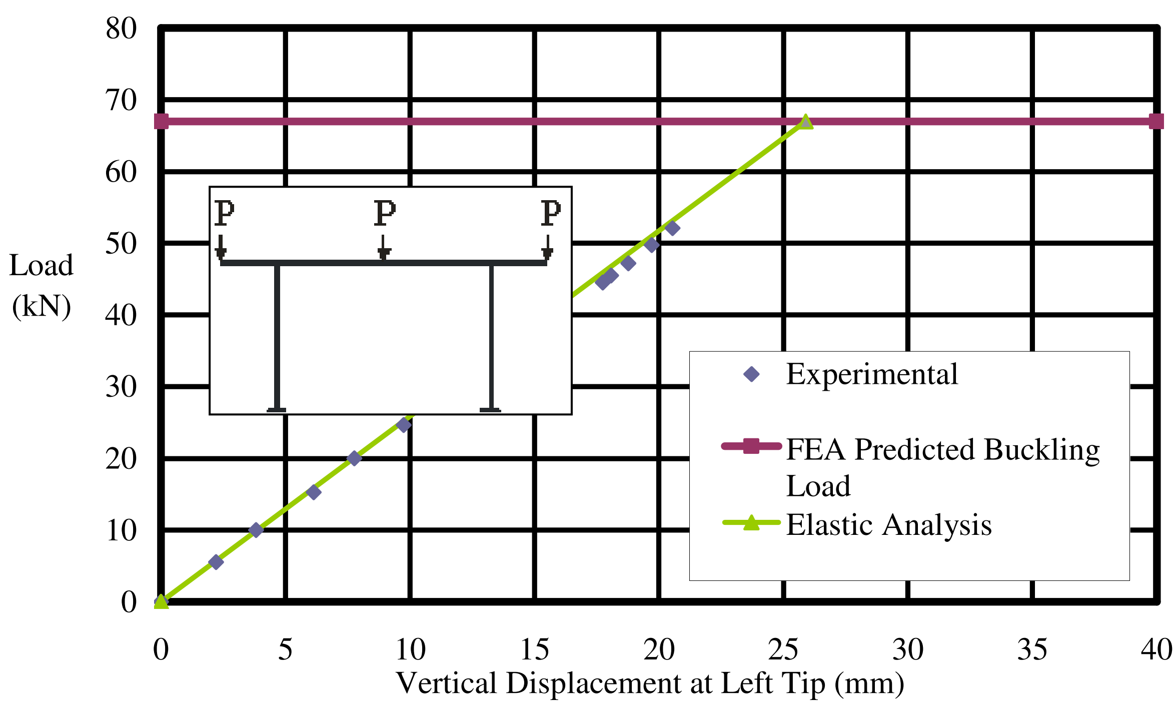

Figure 4.4-Specimen 3-Left Tip Load versus Left Tip Vertical Displacement

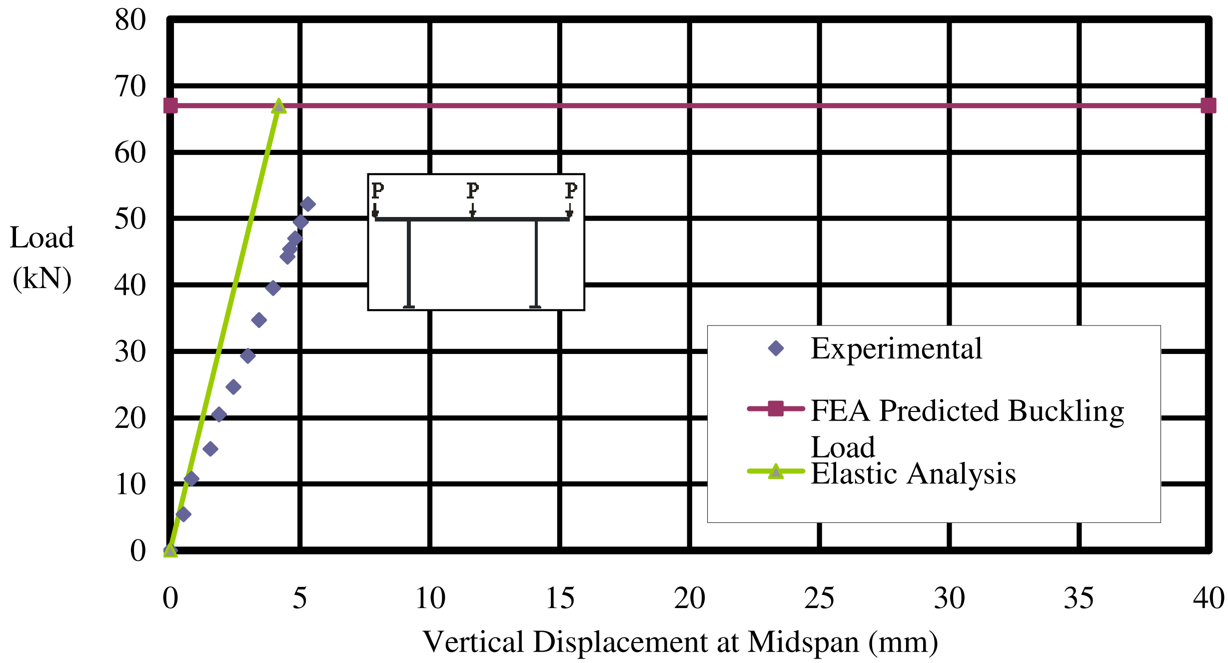

Figure 4.5-Specimen 3-Mid-span Load versus Mid-span Vertical Displacement

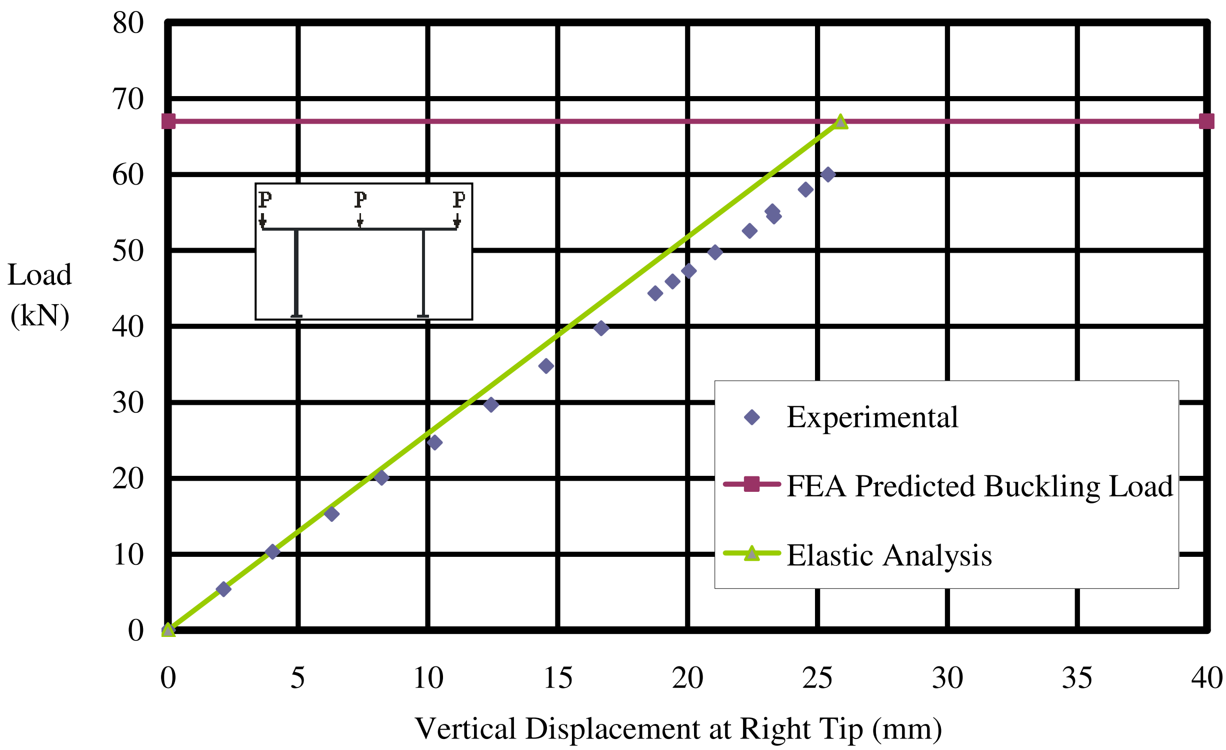

Figure 4.6-Specimen 3-Right Tip Load versus Right Tip Vertical Displacement

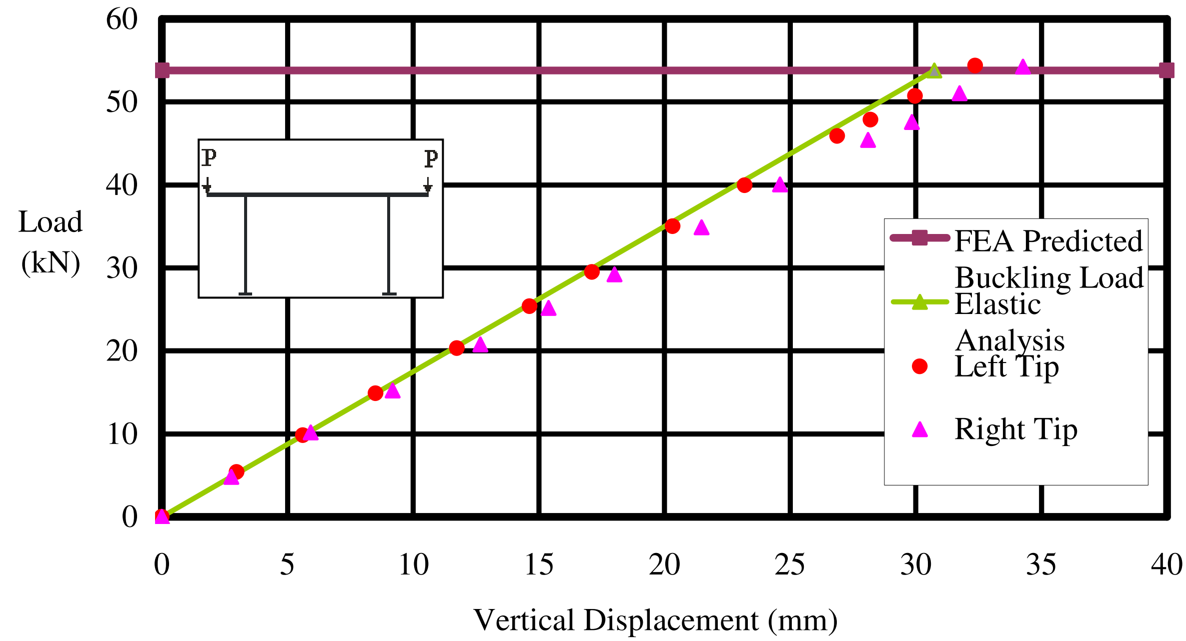

Figure 4.7-Specimen 2-Load versus Vertical Displacement

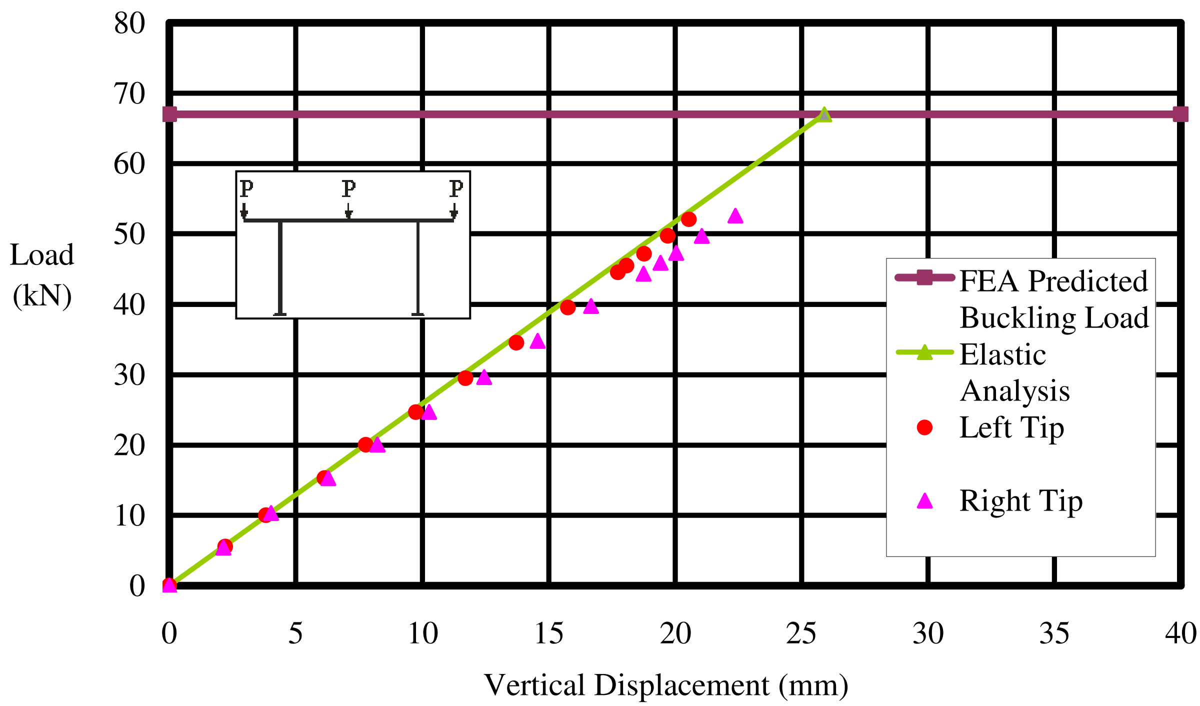

Figure 4.8-Specimen 3-Load versus Vertical Displacement

4.3 Load vs. Buckling Displacements

While the previous section has focused on the load versus *pre-buckling* displacement (i.e., vertical displacement), the present section focuses on the load vs. *buckling* displacements (i.e., web mid-height lateral displacement and angle of twist).

The experimental load versus the lateral displacement at web mid-height is plotted in Fig. 4.9. Also, the experimental load versus angle of twist is provided in Fig. 4.10. Since the transducers were mounted near the top and bottom flanges, the mid-height displacement was determined by interpolation while the angle of twist was obtained by dividing the relative lateral displacement by the vertical distance between the transducers. For Specimen 2, similar curves are provided in Figures 4.11 and 4.12 while Figures 4.13 and 4.14 provide the load vs. buckling displacements for Specimen 3.

For Specimen 1, Figs. 4.9 and 4.10 indicate a gradual buckling behaviour, in which the specimen gradually undergoes lateral displacement and twist as the load is increased. This contrasts with the behaviour of Specimen 2 as depicted in Figs. 4.11 and 4.12 which exhibit a sharp increase in the lateral displacement and twist once the peak load is attained. For Specimen 3, Figs. 4.13 and 4.14 indicate that only the left tip exhibited lateral displacement and twist while the right tip exhibited relatively minor buckling deformations. Similar to Specimen 2, the buckling behaviour of Specimen 3 is observed to be sudden as evident by the large lateral displacement and angle of twist attained after the peak load of 55kN was reached. After buckling was attained, the right tip load was increased to 60kN in attempt to force the right cantilever to buckle laterally. However, the right cantilever did not exhibit any sign of buckling up to a load of 60kN.

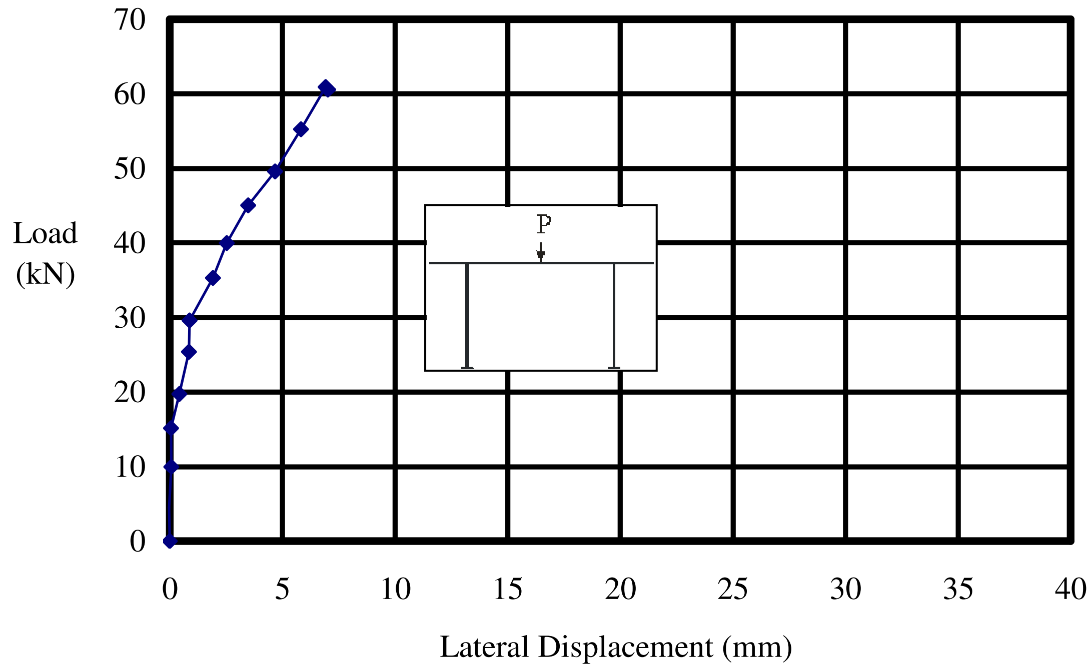

Figure 4.9-Specimen 1-Mid-span Load versus Mid-span Lateral Displacement at Web Mid-Height

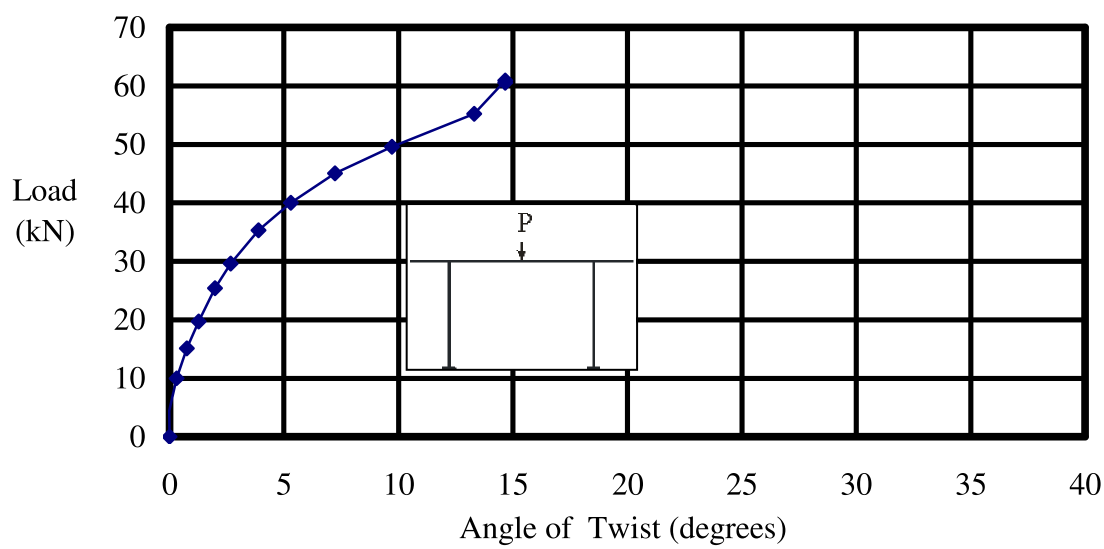

Figure 4.10-Specimen 1-Mid-span Load versus Mid-span Angle of Twist at Web Mid-Height

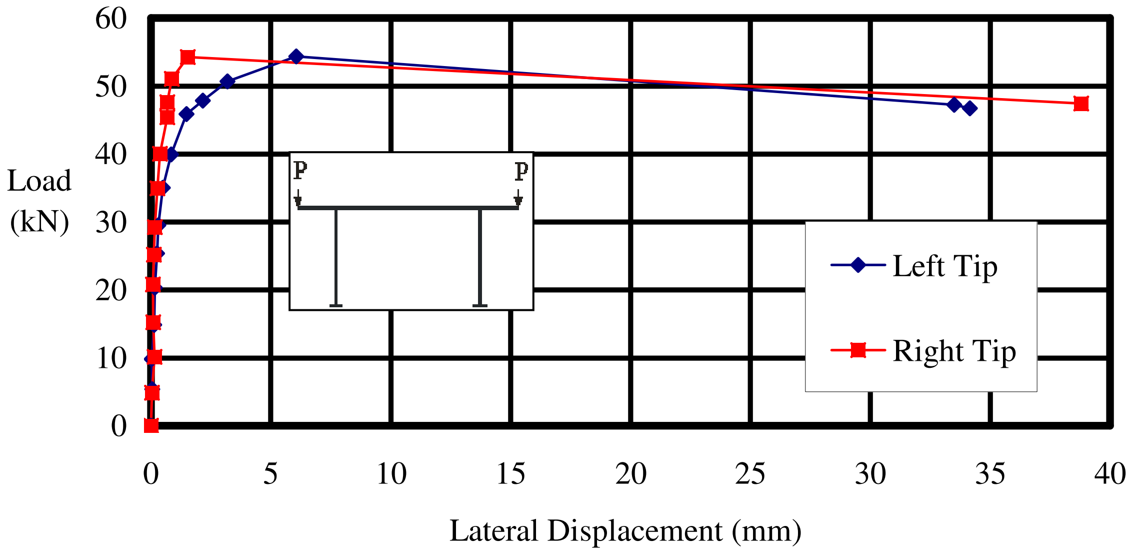

Figure 4.11-Specimen 2-Load versus Lateral Displacement at Web Mid-Height

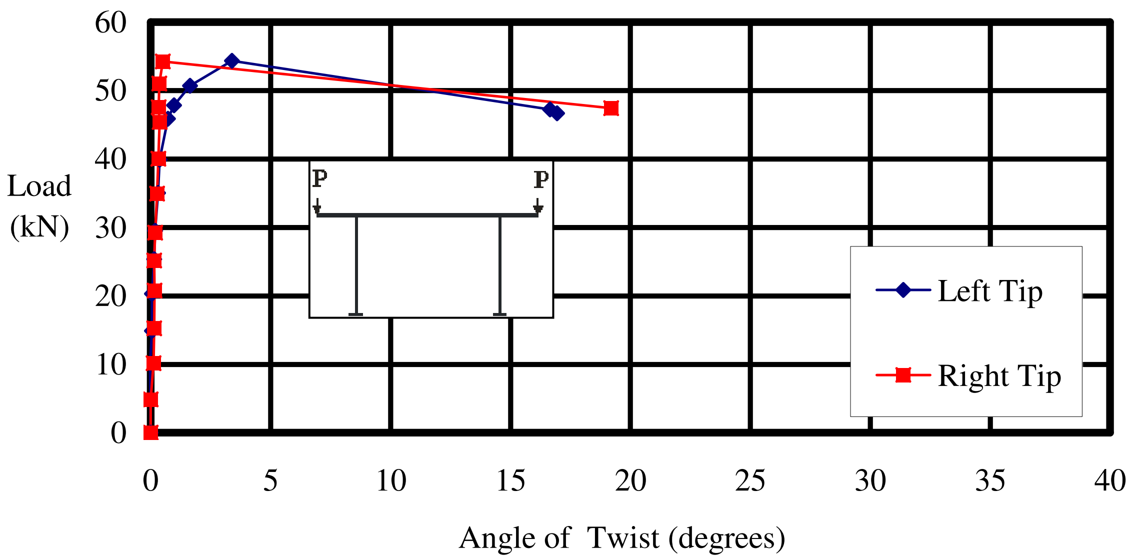

Figure 4.12-Specimen 2-Load versus Angle of Twist at Web Mid-Height

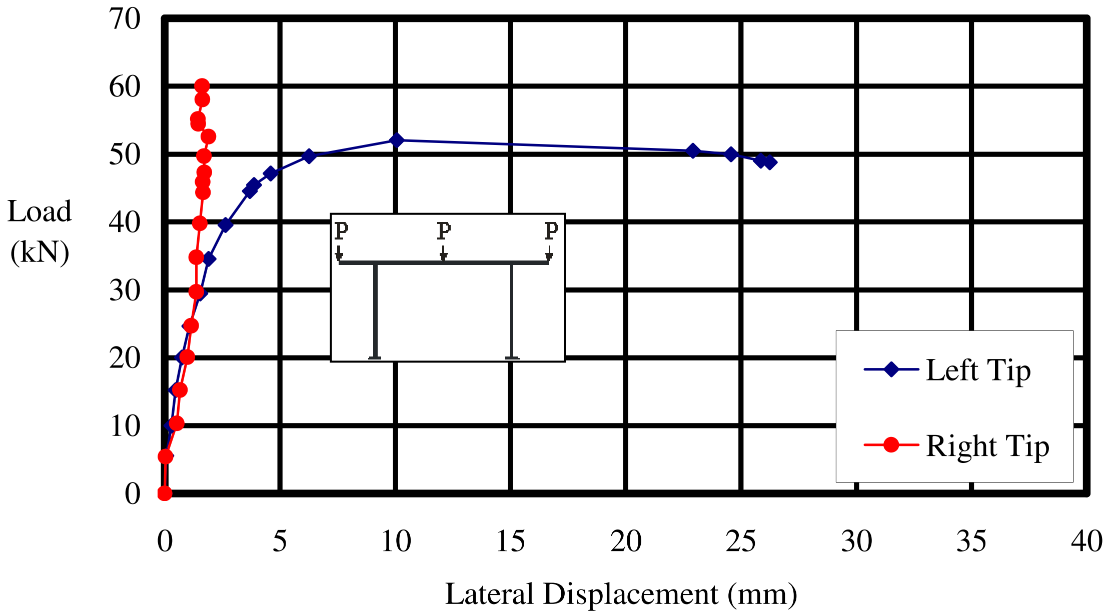

Figure 4.13-Specimen 3-Load versus Lateral Displacement at Web Mid-Height

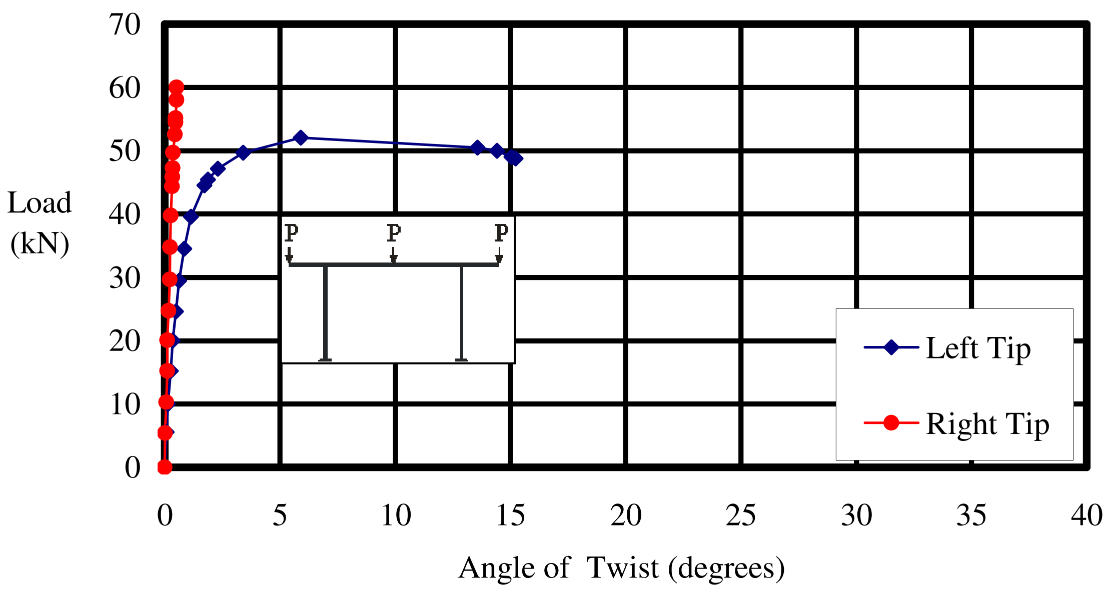

Figure 4.14-Specimen 3-Load versus Angle of Twist at Web Mid-Height

4.4 *Buckling Loads*

Table 4.1 presents a comparison between buckling loads as predicted by the FEA and experimental loads. The buckling loads based on the first two buckling modes are provided. In general, only the first buckling load is of importance in predicting the buckling capacity of the system. Therefore, the experimental loads were compared to the buckling loads based on Mode 1. The predicted to experimental ratios are 1.123, 0.991, and1.216 with an average predicted to experimental buckling ratio of 1.110. The difference between the FEA buckling predictions and the experimental results could be attributed to two factors: a) the presence of imperfections which were neither measured nor captured in the FEA eigen-value model, and b) the buckling analysis formulation in commercial programs such as ABAQUS neglect the effect of pre-buckling deformations.

The proximity of the first and second buckling loads is for Specimens 2 and 3 has implications on the buckled configurations. These will be discussed in the following section.

Table 4.1 Comparison between Predicted and Experimental Loads (kN)

Load	Pattern 1 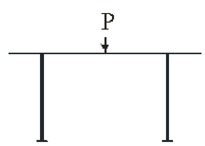	Pattern 2 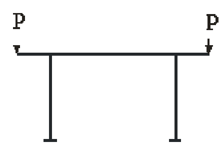	Pattern 3 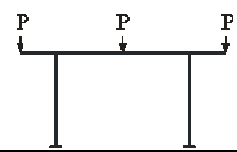
Predicted-Mode 1	71.3	53.8	66.4
Predicted-Mode 2	311.7	54.6	67.0
Experimental	63.5	54.3	55.1
Predicted Mode 1 /Experimental	1.123	0.991	1.216

4.5 *Buckling Modes*

4.5.1 Evolution of Experimental Buckling Deformations

The mid-height lateral displacement as measured by the displacement transducers versus the horizontal coordinates measured from the left tip of the specimens at several loading stages are plotted in Figures 4.15, 4.18, and 4.21. The angle of twist as measured from clinometers and as calculated from the differential lateral displacements at the top and bottom transducers and as measured from clinometers are also provided in Figures 4.16, 4.19, and 4.22 and Figures 4.17, 4.20 and 4.23 respectively.

For Specimen 1, Fig 4.15 provides the lateral displacement progression of the as the applied loads were increased. Readings were recorded at 5kN intervals. Figs. 4.16 and 4.17 show a reasonable agreement between the angle of twist as measured by the clinometers a that calculated from the lateral displacement readings. Figures 4.15 through 4.17 show a gradual progression of the buckling deformations, consistent with a gradual buckling behaviour. All buckling deformations are observed to exhibit essentially a symmetric buckling mode.

For Specimen 2, Fig 4.18 provides the lateral displacement progression of the buckling configuration while Figs. 4.19 and 4.20 provide a comparison between the angles of twist as measured based on the clinometers to those calculated based on the lateral displacement transducers. Again, all readings were taken at 5.0 kN intervals Figures 4.18-4.20 indicate a skew symmetric buckling modes. Unlike Specimen 1, there is a significant jump in the measured buckling deformation, characteristic of a sudden buckling behaviour. In Fig. 4.20, the angle of twist curve was plotted only for the left portion of the specimen. This is due to the fact that the clinometers for Specimen 2 were mounted only for the left half of the specimen

For Specimen 3, the progression of the lateral displacement at mid-height is presented in Fig. 4.21. It is observed that the lateral displacement curve exhibit a sudden jump when the load was increased from 52.3 kN to 52.5kN, indicating sudden buckling.

While significant buckling deformation took place at the left tip, very little deformation was observed at the left tip and buckling mode was asymmetric. Again, Figs 4.22 and 4.23 provide a comparison for the angle of twist as determined from the lateral transducers to those measured by clinometers. Reasonable agreement is observed for the left tip angles of twist. For the right tip angles of twist, reasonable agreement is obtained up to a load level of 52.4 kN. After this reading, clinometers provide a reading of 5-6 degree range while the angle of twist provided by the lateral displacement sensors essentially vanish. The later set of readings is consistent with the photo taken for the specimen at the end of the test (Fig. 4.24(f)), which shows essentially no twist. Thus, it is believed that the right clinometer provided erroneous readings. Thus, their measurements will be discarded from the following discussion.

One point of interest in Figs. 4.15 through 4.23 is the fact that, in all three specimens, the columns (marked by dotted red lines in the Figures) are observed to undergo lateral movement and bending throughout buckling. This suggests that a proper modelling of the buckling behaviour of Gerber systems, either experimentally or numerically, necessitates the investigation of the Gerber system as a whole (including the columns and the Gerber beams), in order to account for the effect of the column flexibility on the overall buckling resistance and behaviour of the system. This effect is modelled in the present study and contrasts with previous investigations by various researchers as discussed in Chapter 1.

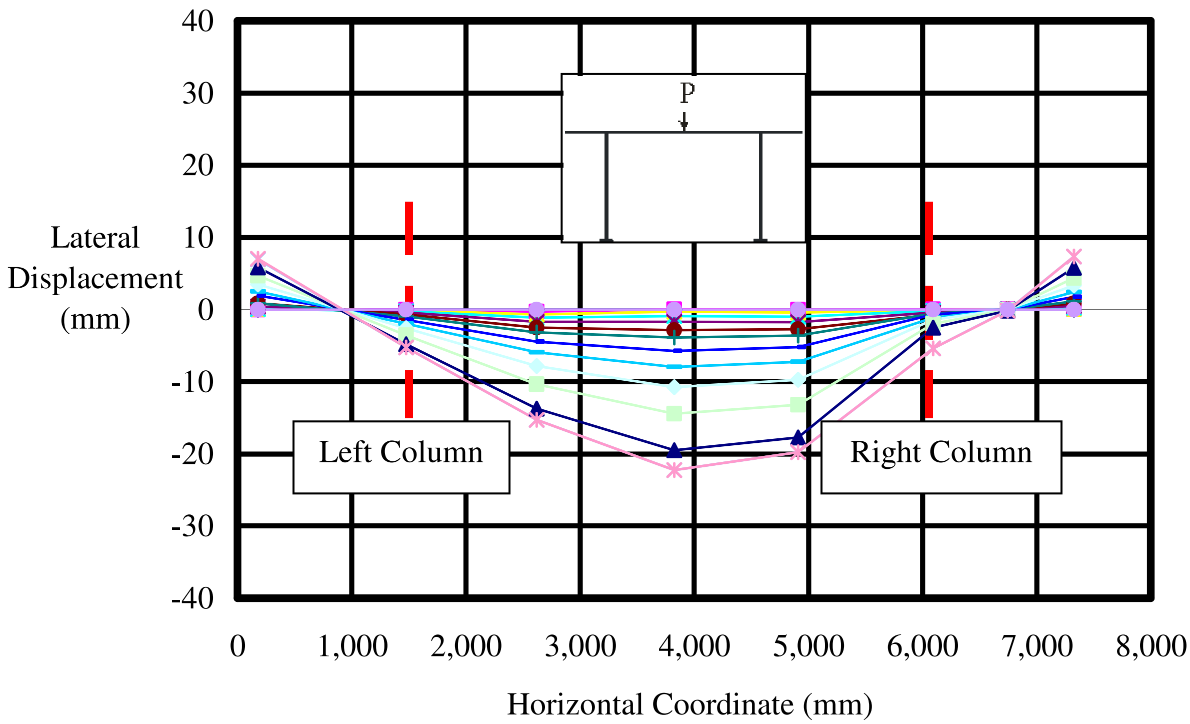

Figure 4.15-Specimen 1-Lateral Displacements (mm) at Web Mid-Height versus Horizontal Coordinate (mm) at various Loading Levels (kN)

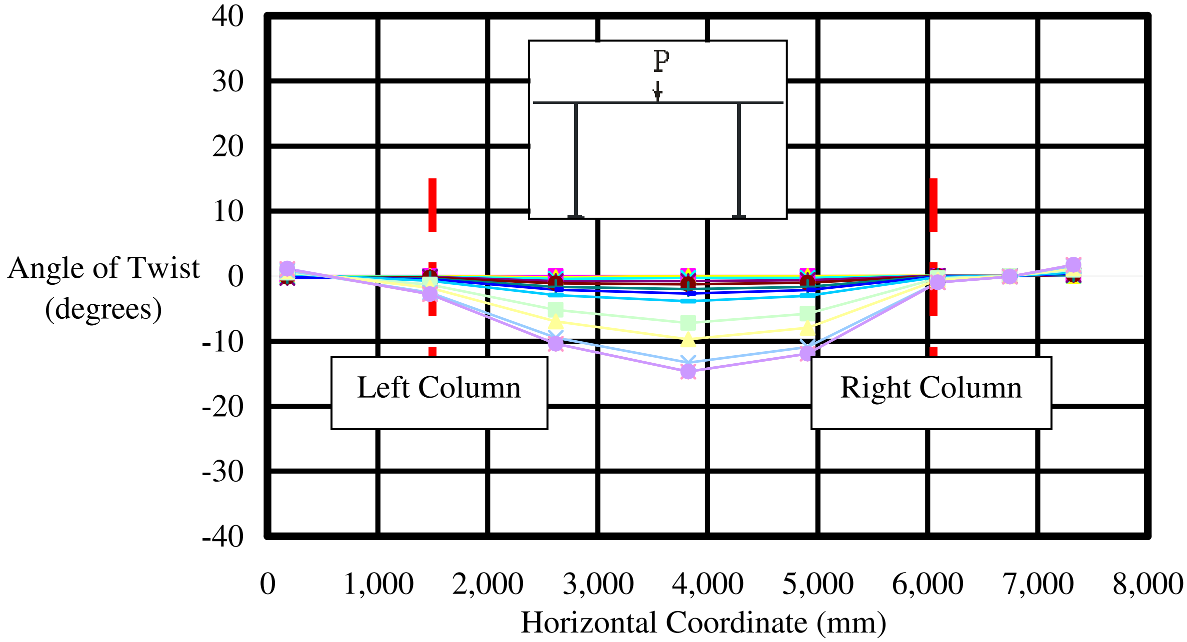

Figure 4.16-Specimen 1-Angle of Twist (degrees) versus Horizontal Coordinate (mm) based on Horizontal Transducer Readings at various Loading Levels (kN)

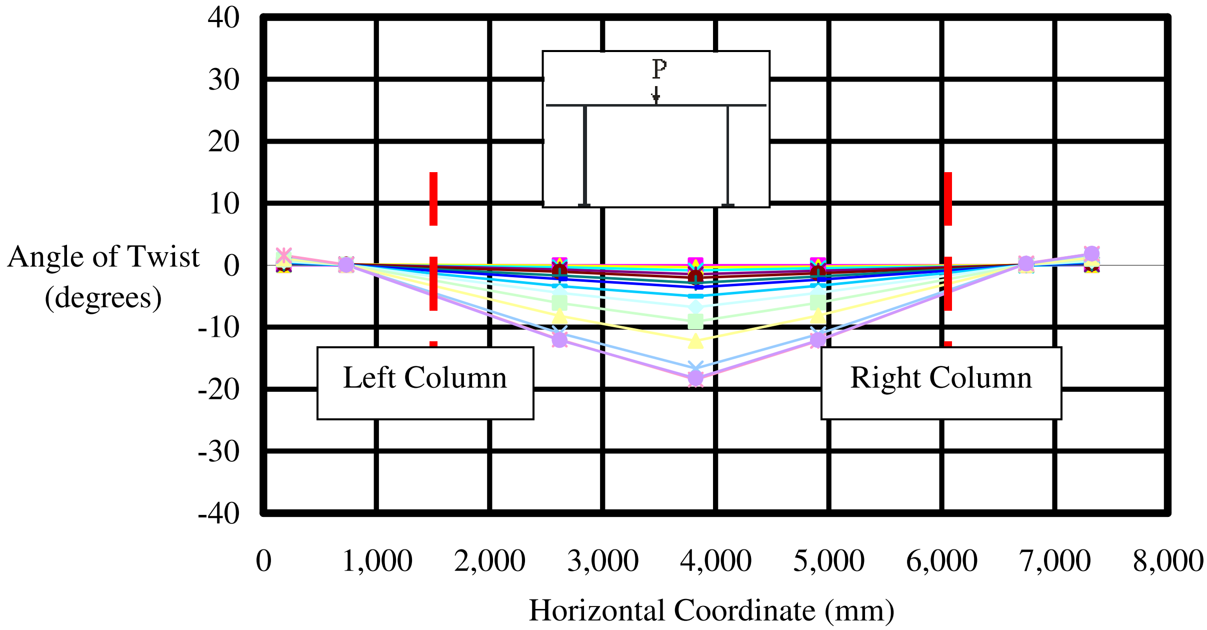

Figure 4.17-Specimen 1-Angle of Twist (degrees) versus Horizontal Coordinate (mm) based on Clinometer Readings at various Loading Levels (kN)

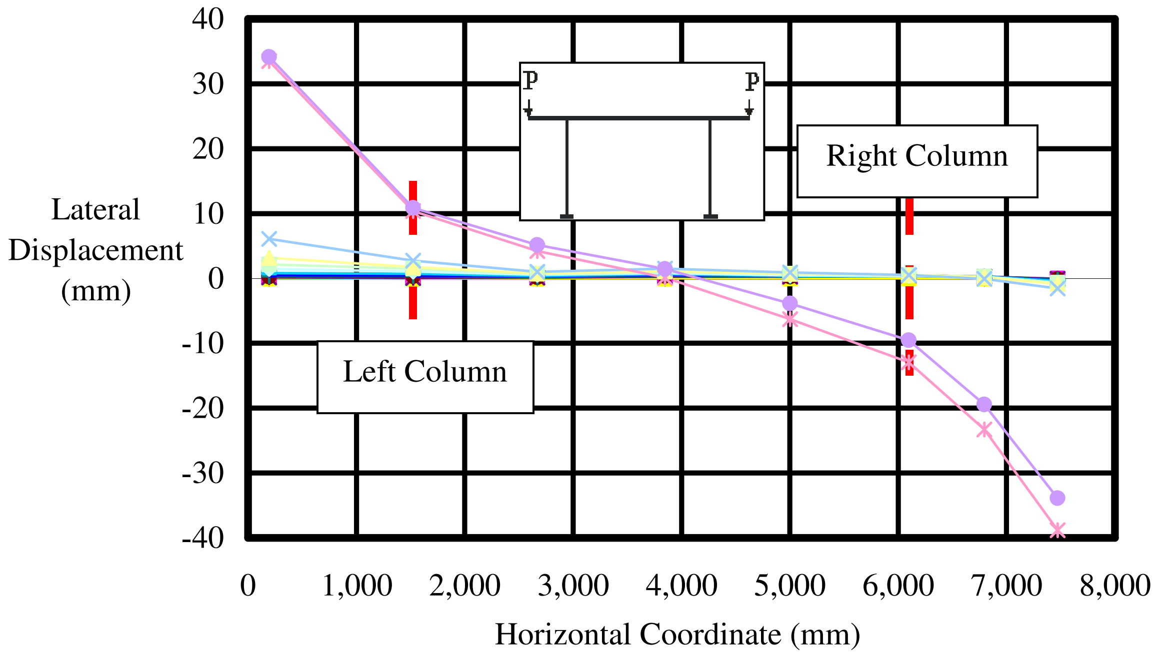

Figure 4.18-Specimen 2-Lateral Displacements (mm) at Web Mid-Height versus Horizontal Coordinate (mm) at various Loading Levels (kN)

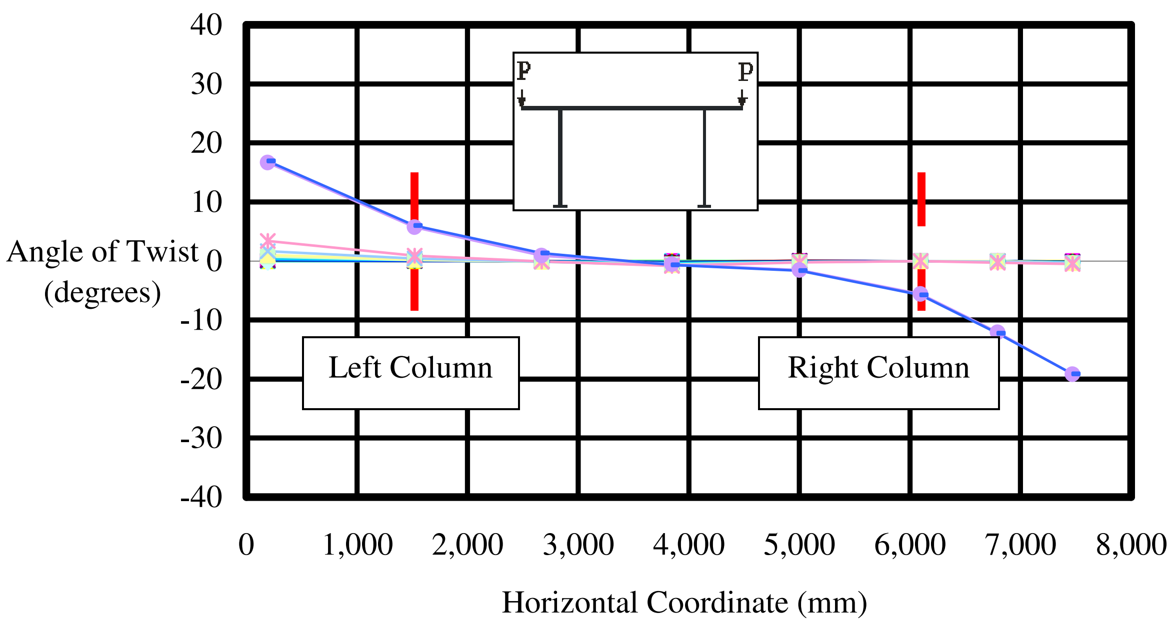

Figure 4.19 Specimen 2-Angle of Twist (degrees) versus Horizontal Coordinate (mm) based on Horizontal Transducer Readings at various Loading Levels (kN)

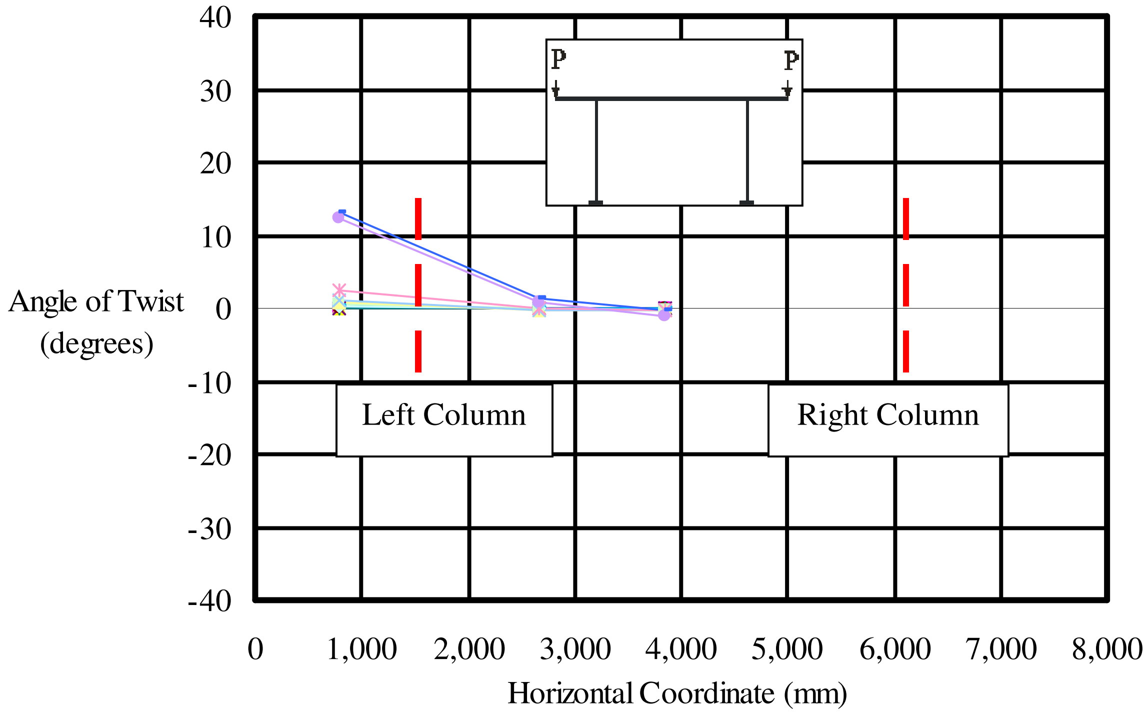

Figure 4.20-Specimen 2-Angle of Twist (degrees) versus Horizontal Coordinate (mm) based on Clinometer Readings at various Loading Levels (kN)

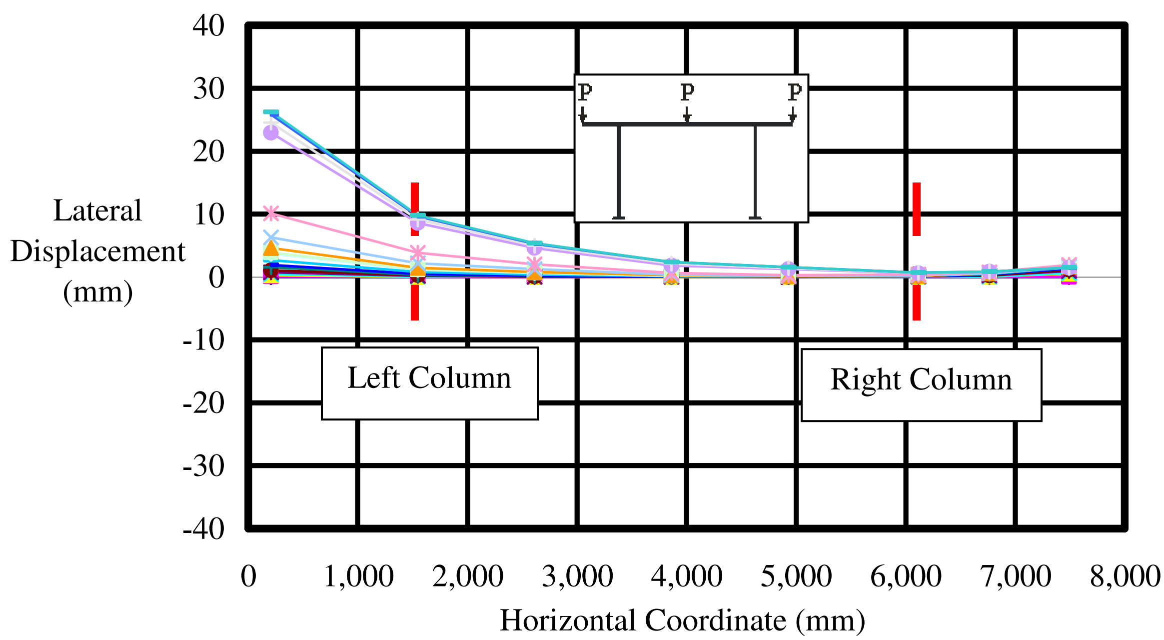

Figure 4.21-Specimen 3-Lateral Displacements (mm) at Web Mid-Height versus Horizontal Coordinate (mm) at various Loading Levels (kN)

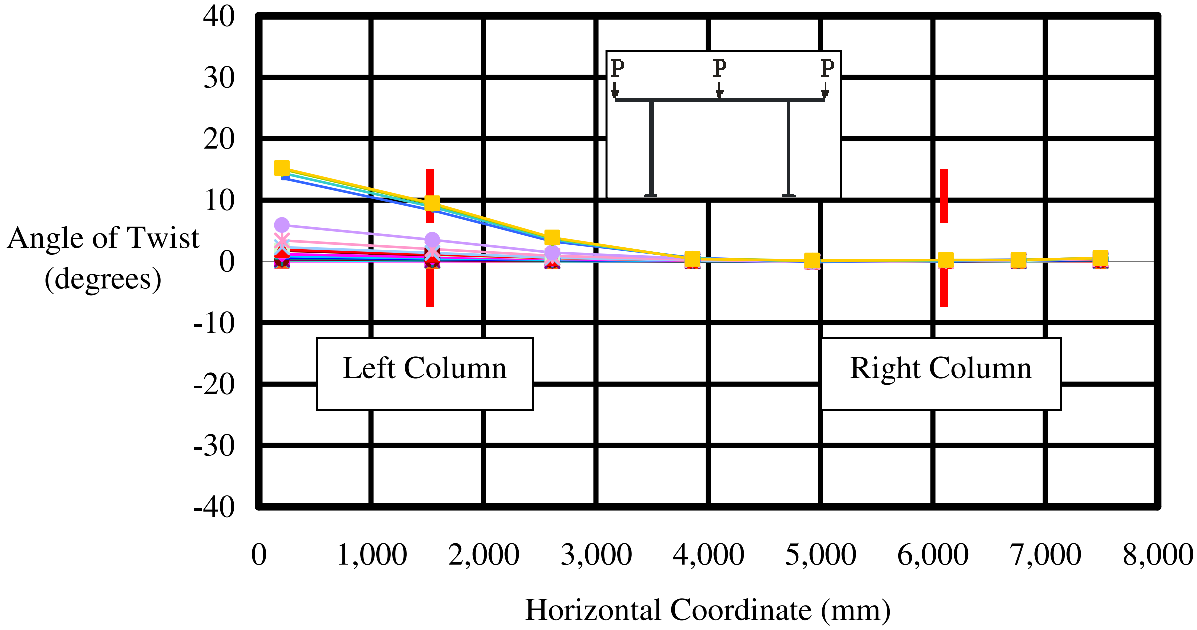

Figure 4.22-Specimen 3-Angle of Twist (degrees) versus Horizontal Coordinate (mm) based on Horizontal Transducer Readings at various Loading Levels (kN)

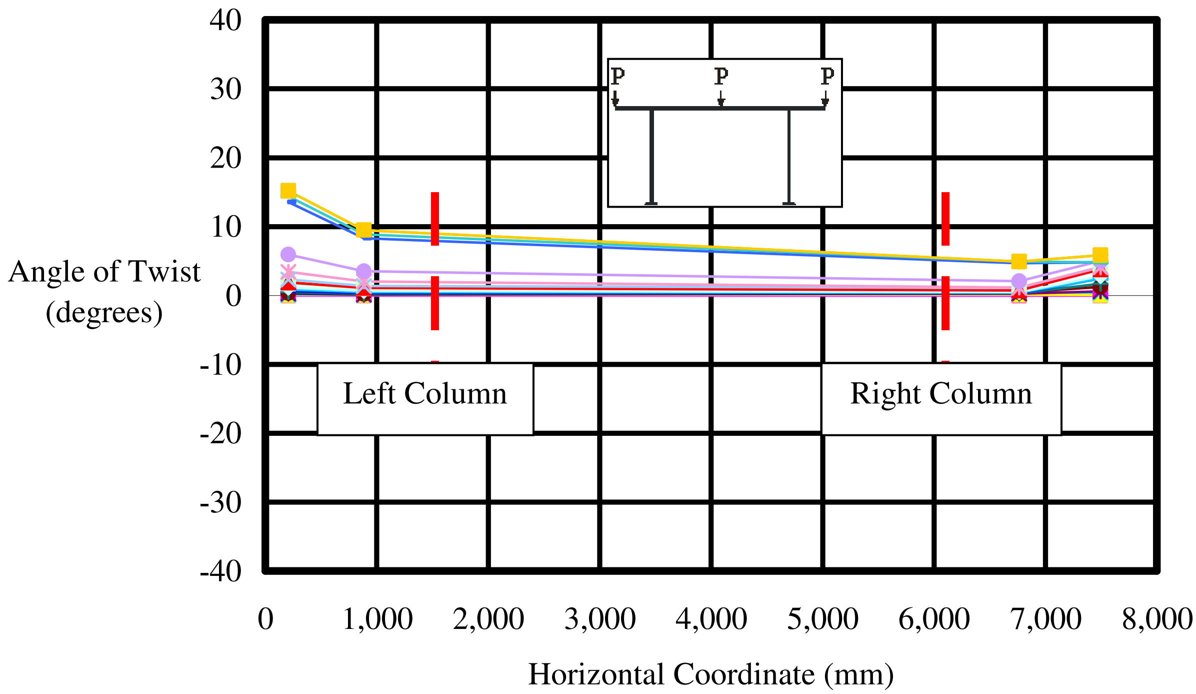

Figure 4.23-Specimen 3-Angle of Twist (Degrees) versus Horizontal Coordinate (mm) based on Clinometer Readings at various Loading Levels (kN)

4.5.2 Final Experimental vs. Predicted Buckling Modes

Figures 4.24 provides photos of the final buckled configurations for all three test specimens while Fig. 4.25 the FEA predicted first two buckling mode shapes for each specimen. For Specimen 1, the final experimental configuration and first FEA predicted buckling mode are essentially symmetric.

It is well accepted that, as the applied loading approaches the critical magnitude, an initially imperfect specimen tends to assume the shape of the first mode, while the deformations based on higher modes tend to dampen out. This is particularly the case when the buckling load based on the first mode is significantly lower than those based on subsequent modes. For specimen 1, the FEA predicted second buckling mode corresponds to a buckling load of 311.7 kN which is significantly larger than that of the FEA predicted first buckling load of 71.3kN. As expected, both the final experimental configuration and the first buckling mode show a similar deformation patterns and the contribution of the second mode is essentially non-existent.

For Specimens 2 and 3, the first two buckling loads are found to be very close with less than 1kN difference in both cases. Unlike Specimen 1, where the first two buckling loads are equal, the final experimental configuration may assume a pattern according to the first mode, the second mode, or more generally, according to any linear combination of the first two modes. For both specimens, the first eigen-mode corresponds to a nearly skew symmetric buckling mode while the second eigen-mode corresponds to a nearly symmetric one. The experimentally observed buckled shape for Specimen 2 is nearly skew symmetric, i.e., it deformed according to the first mode. In contrast, the experimentally observed buckled configuration for Specimen 3 is asymmetric, i.e., it was a linear combination of the first and second FEA predicted buckling mode. For this particular specimen, the variability within material and geometric properties could have resulted in the two first loads being essentially equal, with the possibility of the buckling modes taking any linear combination of the two modes, resulting in the asymmetric mode obtained.

It is noted that the buckling modes are not entirely symmetric or skew-symmetric due to the fact that the frame geometry is not perfectly symmetric (i.e., the cantilever portions have slightly different spans.

(a) Buckling Configuration (b) Loading Arm at Mid-span

Specimen 1 (Buckling Load = 63.5kN)

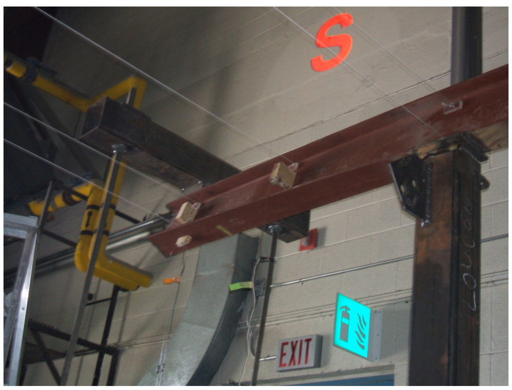

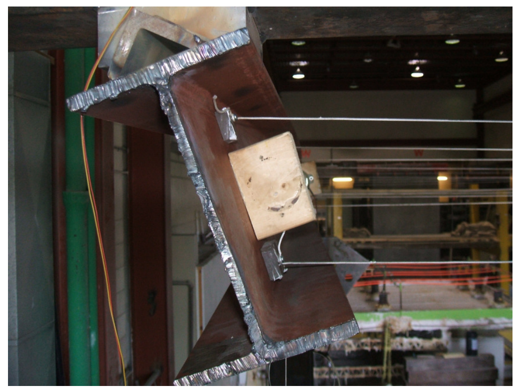

(c) Buckling Configuration (d) Left Tip-Side View

Specimen 2 (Buckling Load = 54.3kN)

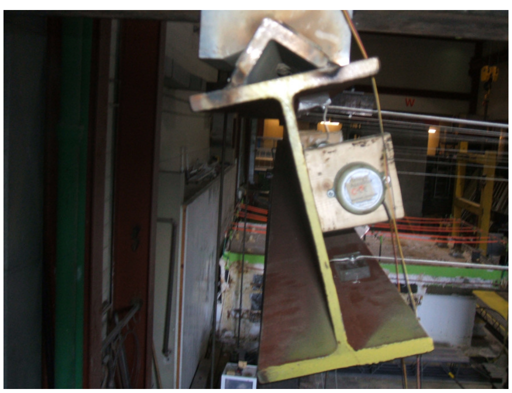

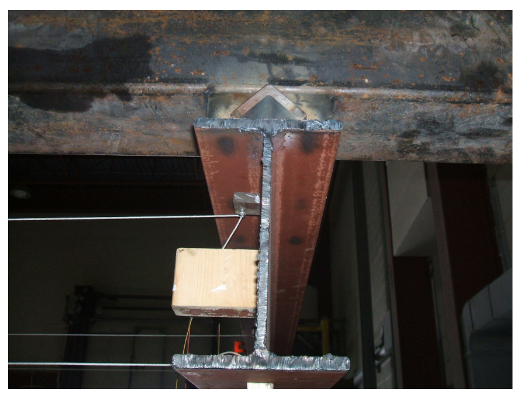

(e) Left Tip (f) Right Tip

Specimen 3 (Buckling Load = 55.1kN)

Figure 4.24-Final Experimental Buckling Mode Shapes

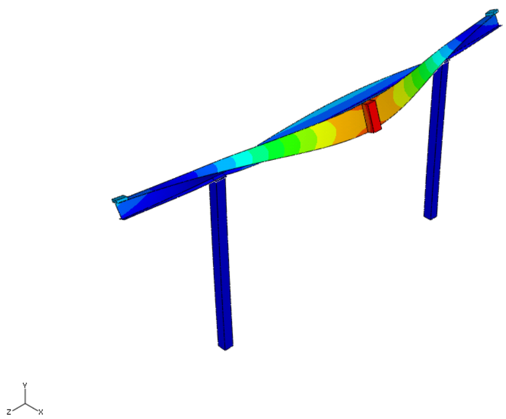

(a) Specimen 1-Mode 1
(Buckling Load = 71.3kN)

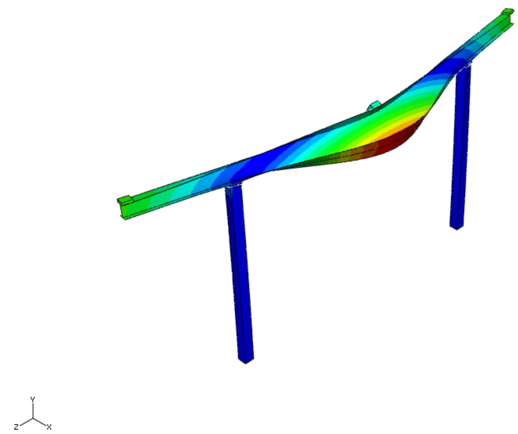

(b) Specimen 1-Mode 2
(Buckling Load = 311.7kN)

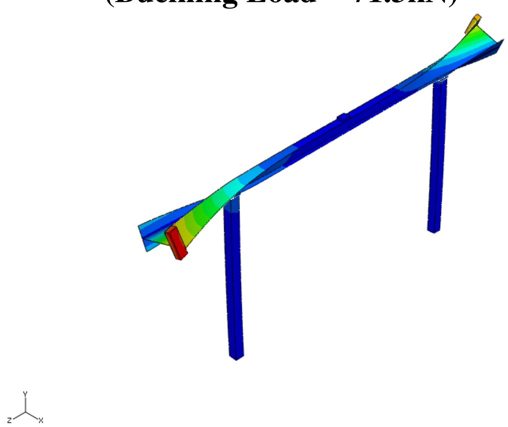

(c) Specimen 2-Mode 1
(Buckling Load = 53.8kN)

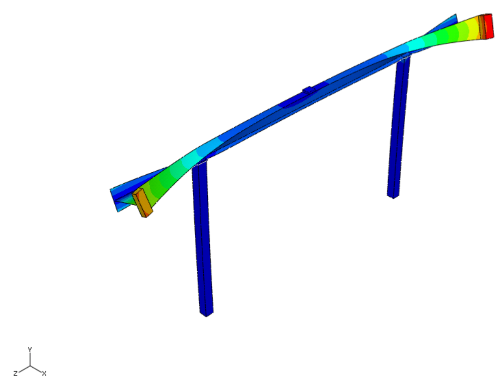

(d) Specimen 2-Mode 2
(Buckling Load = 54.6kN)

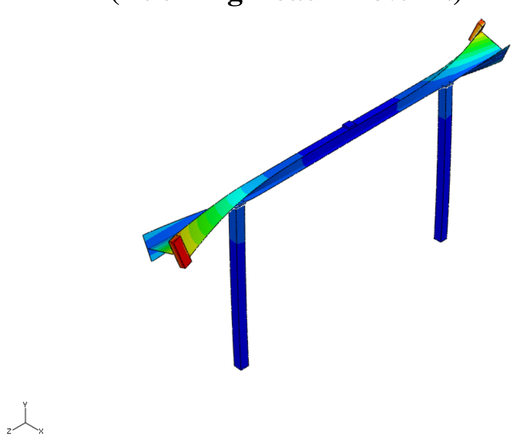

(f) Specimen 3-Mode 1
(Buckling Load = 66.4kN)

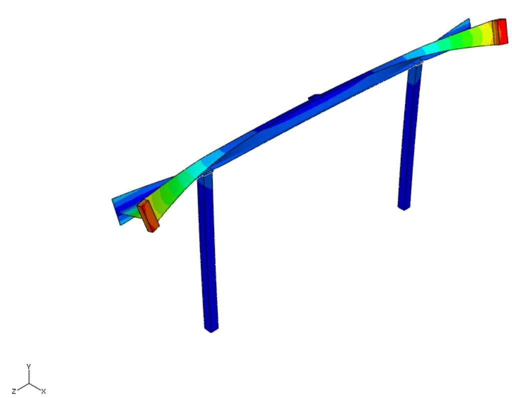

(g) Specimen 3-Mode 2
(Buckling Load = 67.0kN)

Figure 4.25-Predicted Buckling Mode Shapes

4.5.3 Extraction of FEA Buckling Modes

Buckling modes results were obtained from ABAQUS by extracting the lateral displacement at the Gerber beam top and bottom junctions' nodes. In order to obtain lateral displacements at web mid-height, the top and bottom displacements were averaged. For the angle of twist values, the difference between the top and bottom displacements was obtained and divided by the Gerber beam cross-section height.

4.5.4 Predicted Buckling Eigen-Modes Results

In this section, the normalized buckling mode curves are provided. For Specimen 1, the first and second eigen-modes are symmetric as shown in Fig. 4.26. When comparing lateral displacements, it is observed that the second eigen-mode cantilever tip displacements are larger than those of the first eigen-mode. However, when comparing the angle of twist, the first eigen-mode is observed to have larger rotations than the second-eigen mode. For Specimens 2 and 3, the first eigen-mode is skew symmetric while the second is symmetric as illustrated in Figs 4.27 and 4.28 respectively. Lateral displacements at the cantilever tips are nearly equal. When comparing the angle of twist values, it is observed that the second eigen-mode left cantilever tip rotations are slightly higher than those of the first eigen-mode. However, rotations at the right tip are nearly equal for the two modes.

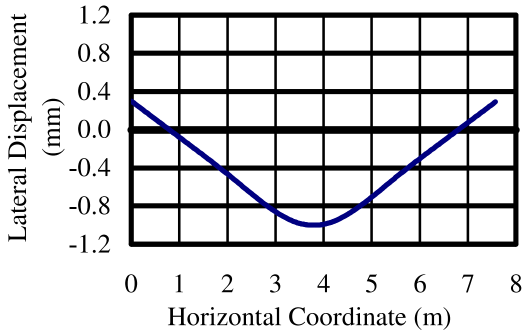

(a) Mode 1-Lateral Displacement

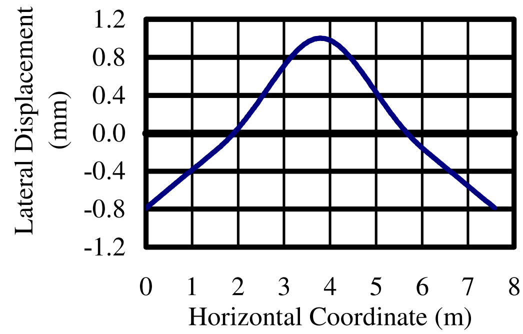

(b) Mode 2-Lateral Displacement

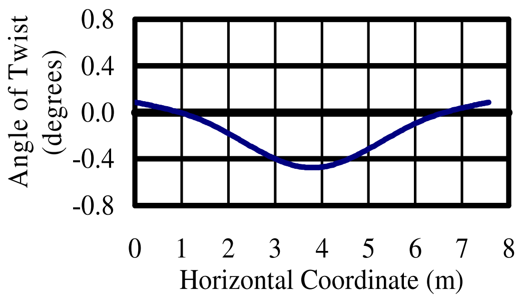

(c) Mode 1-Angle of Twist

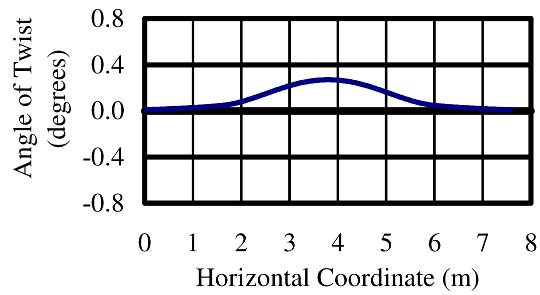

(d) Mode 2-Angle of Twist

Figure 4.26-Specimen 1-FEA Predicted Buckling Modes at Web Mid- Height

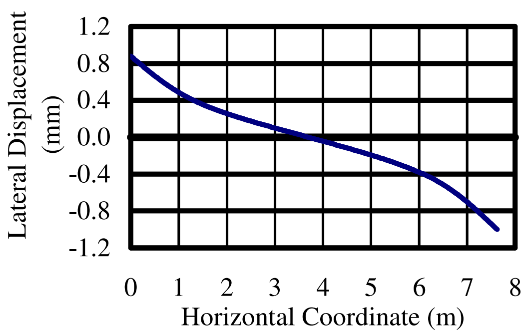

(a) Mode 1-Lateral Displacement

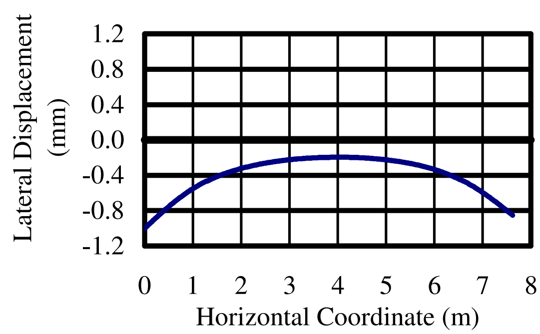

(b) Mode 2-Lateral Displacement

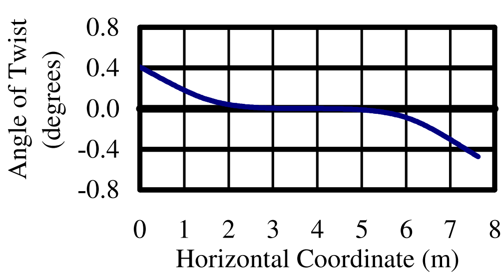

(c) Mode 1-Angle of Twist

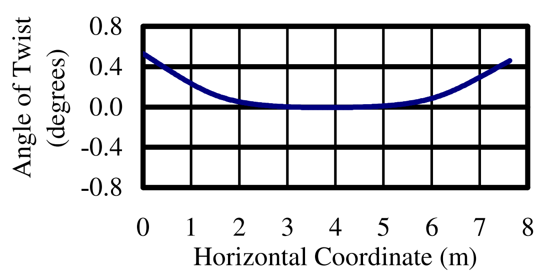

(d) Mode 2-Angle of Twist

Figure 4.27-Specimen 2-FEA Predicted Buckling Modes at Web Mid-Height

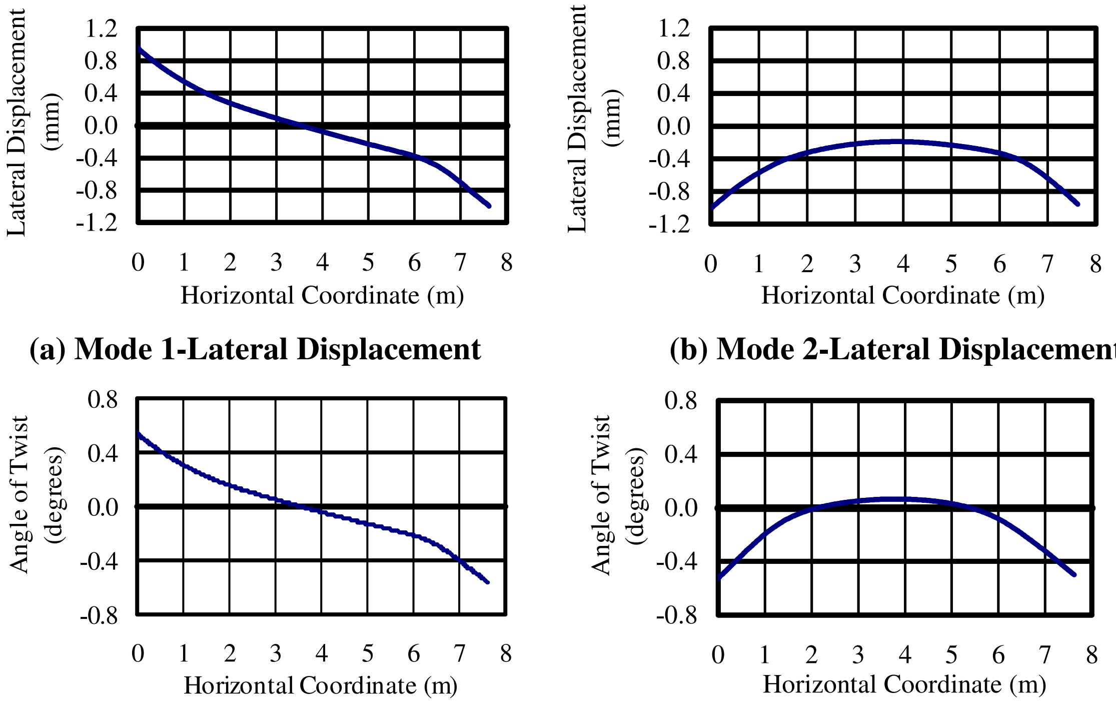

(a) **Mode 1-Lateral Displacement**

(b) **Mode 2-Lateral Displacement**

(c) **Mode 1-Angle of Twist**

(d) **Mode 2-Angle of Twist**

Figure 4.28-Specimen 3-FEA Predicted Buckling Modes at Web Mid-Height

4.5.5 Comparison of Experimental and Predicted Eigen-Modes

An error minimization procedure was used for the curve-fitting of the FEA predicted eigen-modes to the experimentally measured buckled deformations. The procedure is based on a applying a scaling factor a_1 to the FEA predicted buckling lateral displacements u_{FEA} and angles of twist θ_{FEA} based on the first buckling mode. The sum E of the squares of differences between the experimental and FEA predicted displacements and angles of twist was then minimized to obtain the magnitude of a_1 factor that results into the best fit with the experimental data. The following minimization scheme was adopted:

$$E = \sum_{i=1}^{n}\left[\frac{u_{exp,i} - a_1\left(u_{FEA_i}\right)}{\bar{u}_{exp}}\right]^2 + \beta\sum_{j=1}^{m}\left[\frac{\theta_{exp,j} - a_1\left(\theta_{FEA_j}\right)}{\bar{\theta}_{exp}}\right]^2 = min \qquad (4.1)$$

where $i = 1...n$ are the number of experimental lateral displacement measurements, and $j = 1...m$ are the number of experimental rotation measurements, $u_{exp,i}$ and $\theta_{exp,j}$ are the experimentally measured lateral displacement and angle of twist at the i^{th} location, respectively, a_1 is a scaling factor to be applied to the FEA predicted eigenvector displacement and rotation values, $u_{FEA,i}$ and $\theta_{FEA,j}$ are the predicted lateral displacement and angle of twist at j^{th} location, respectively. Factor β is a weighting constant. When it takes a large value, it places more emphasis on providing an accurate fit for the angle of twist measurements. Conversely, when β is small, it places more emphasis on providing an accurate fit for the lateral displacement measurements. It is noted that the bracketed terms in Eq. 4.1 have been normalized with respect to the average lateral displacement $\bar{u}_{exp}$ and average angle of twist $\bar{\theta}_{exp}$;

$$\bar{u}_{exp} = \frac{1}{n}\sum_{i=1}^{n} u_{exp,i}, \bar{\theta}_{exp} = \frac{1}{m}\sum_{j=1}^{m} \theta_{exp,j} \qquad (4.2)$$

For Specimen 3, two scaling factors a_1, a_2 were applied to the first and second eigen-modes, respectively such that;

$$E = \sum_{i=1}^{n}\left[\frac{u_{exp,i} - a_1\left(u_{FEA_i}\right) - a_2\left(u_{FEA_i}\right)}{\bar{u}_{exp}}\right]^2 + \beta\sum_{j=1}^{m}\left[\frac{\theta_{exp,j} - a_1\left(\theta_{FEA_j}\right) - a_2\left(\theta_{FEA_i}\right)}{\bar{\theta}_{exp}}\right]^2 = min \quad (4.3)$$

The experimental buckling deformations towards the end of the tests and FEA predicted buckling eigen-modes are overlaid for comparison in Figs. 4.29 to 4.34. The experimental buckling deformations shown are those corresponding to the load levels of 63.5, 54.3, and 55.1 kN for Specimens 1 through 3, respectively.

For all three specimens, the predicted lateral displacements and angles of twist based the eigen-modes provided a very good representation of the measured buckled configuration near the end of the tests.

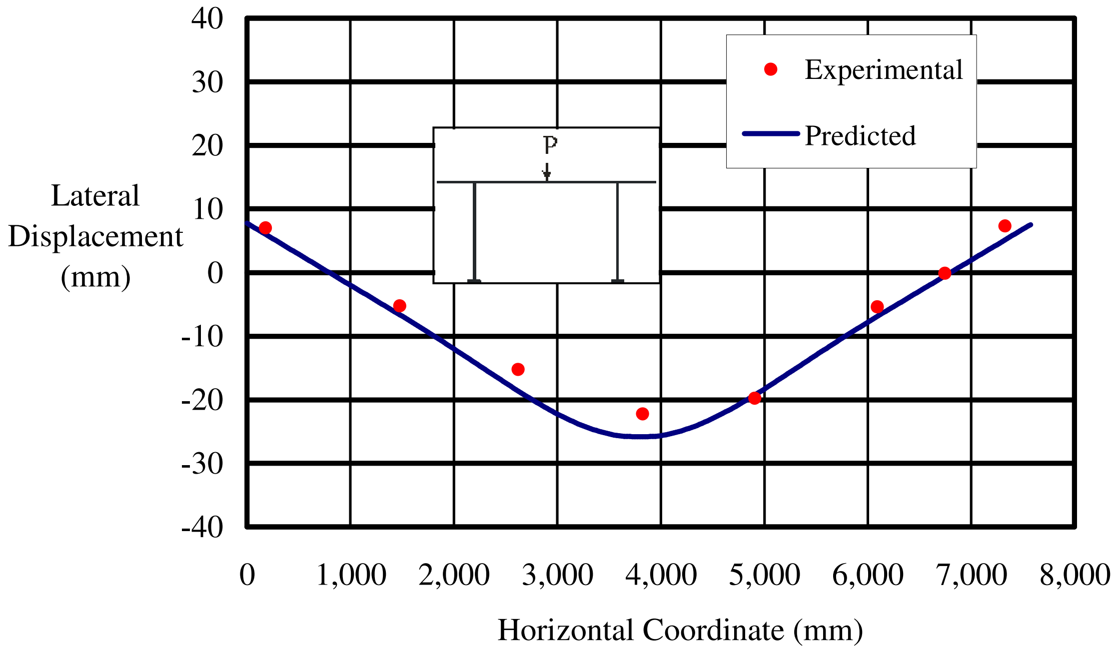

Figure 4.29-Specimen 1-Buckling Configuration Based on Lateral Displacement at Web Mid-Height

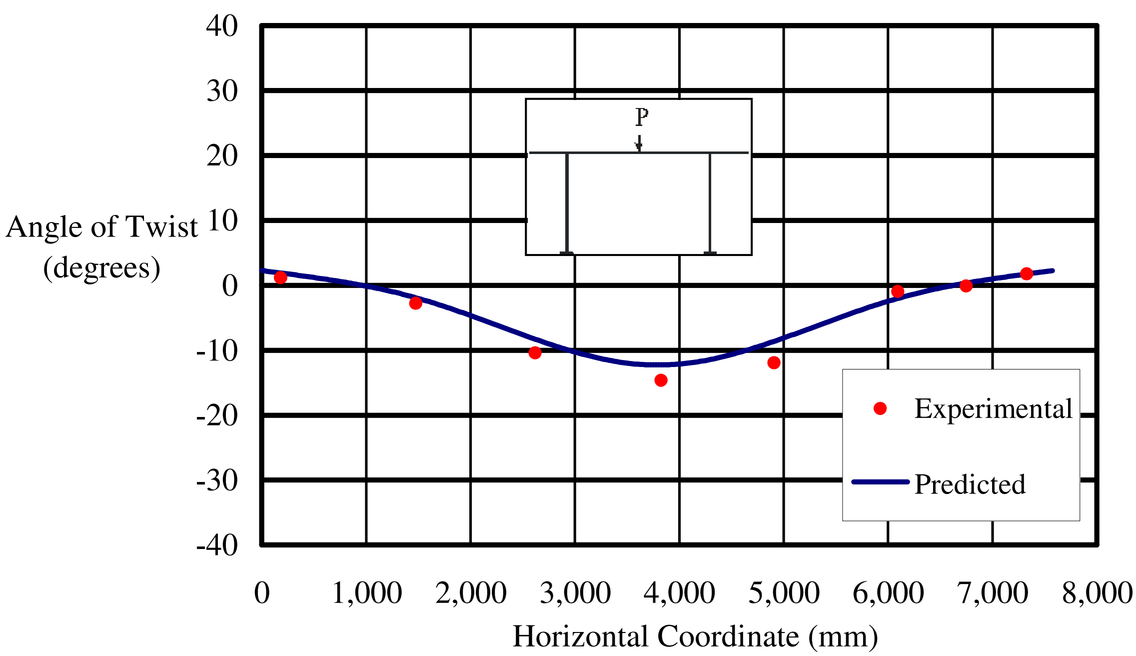

Figure 4.30-Specimen 1-Buckling Configuration Based on Angle of Twist at Web Mid-Height

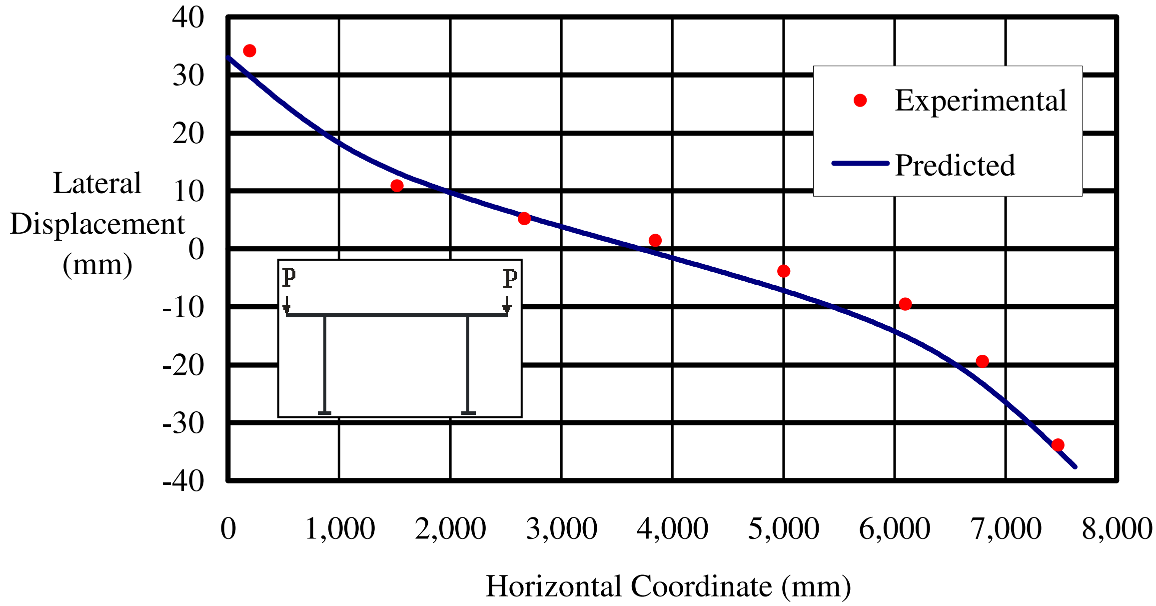

Figure 4.31-Specimen 2-Buckling Configuration Based on Lateral Displacement at Web Mid-Height

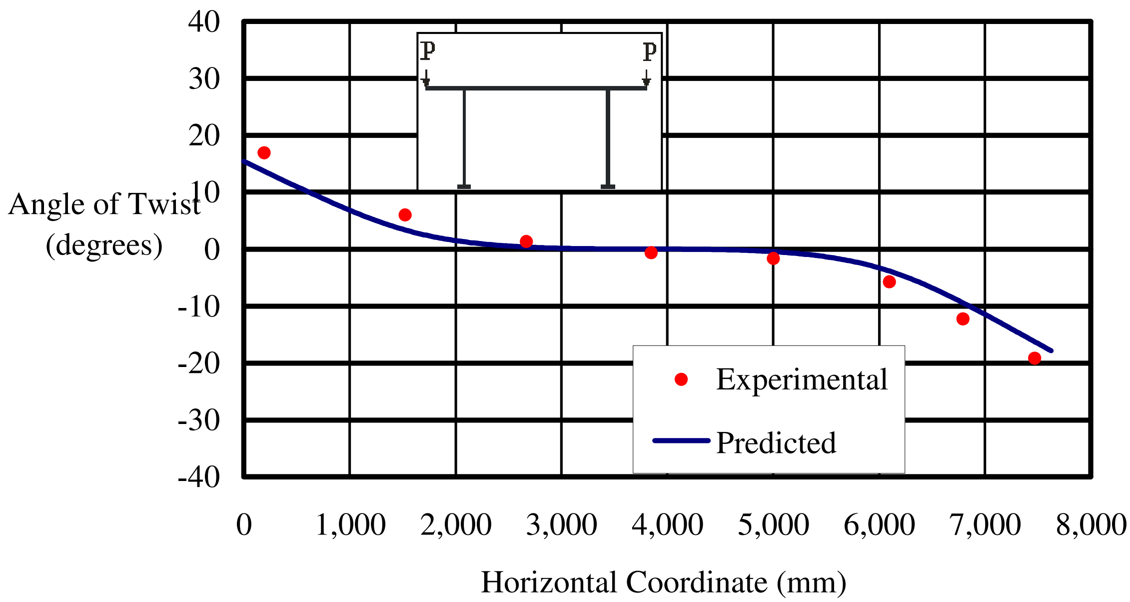

Figure 4.32-Specimen 2-Buckling Configuration Based on Angle of Twist at Web Mid-Height

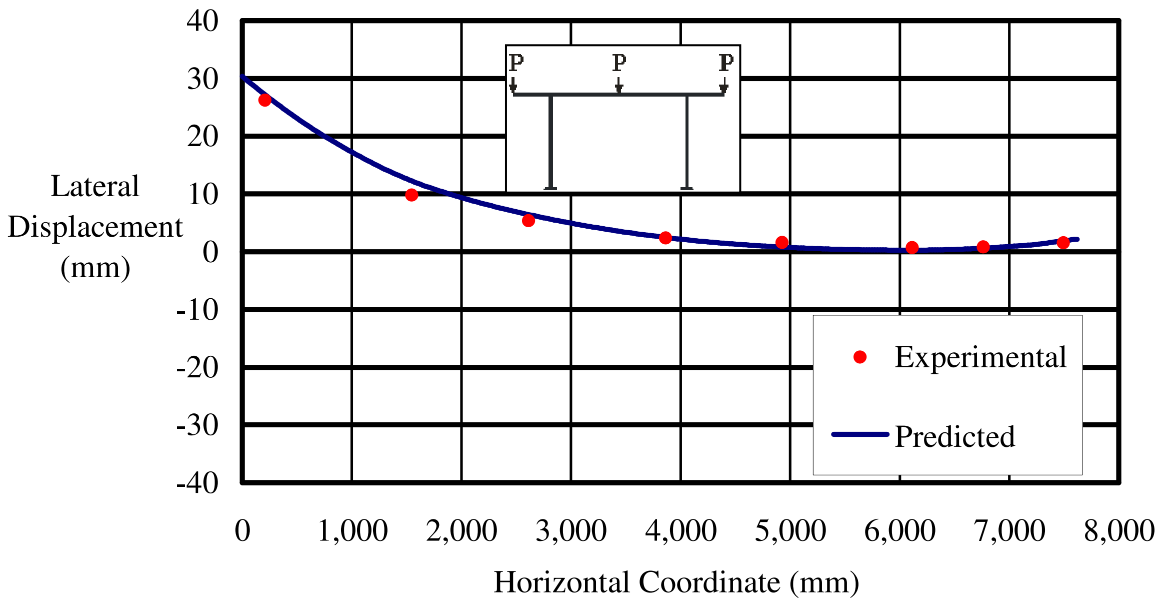

Figure 4.33-Specimen 3-Buckling Configuration Based on Lateral Displacement at Web Mid-Height

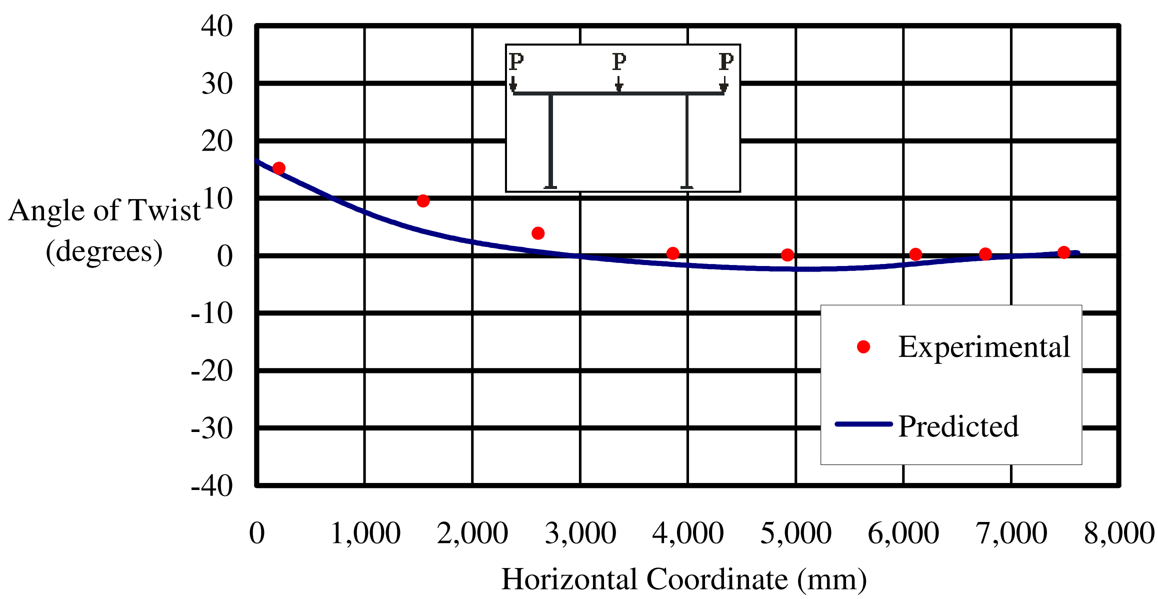

Figure 4.34-Specimen 3-Buckling Configuration Based on Angle of Twist at Web Mid-Height

4.6 Elastic Buckling Assessment

The FEA buckling analyses conducted in the previous sections are based on an assumed material response, and thus are expected to yield reliable predictions only when the frames tested buckle elastically prior attaining the yielding. Within this context, this section aims at assessing whether any yielding has been initiated under the load levels applied prior buckling.

The bending moment and normal force diagrams for the three specimens are shown in Figs. 4.35 to 4.37. A comparison between the maximum internal forces at the critical moment section the section yield moment resistance M_y and axial moment resistance N_y are provided in Table 4.2. Two comparisons are provided, one based on the experimentally measured buckling load (leading to the internal force combination $\left(N_{exp}, M_{exp}\right)$) and the other one based on the FEA predicted buckling load (leading to the internal force combination (N_{FEA}, M_{FEA}). The interaction coefficients $N_{exp}/N_y + M_{exp}/M_y$ and $N_{FEA}/N_y + M_{FEA}/M_y$ at the location of maximum moments provide an indication of the proximity of the stresses induced to the yield strength. For Specimen 1, the maximum bending moment and axial force values were obtained at mid-span (as represented by the red arrows in Fig. 4.35). However, for Specimens 2 and 3, the maximum bending moments were obtained at the column face nearest to the cantilever tip (as represented by the red arrows in Figs. 4.36 and 3.37). The corresponding normal forces at this section vanish in both specimens.

The residual stresses for wide flange sections are conservatively assumed as $0.30\,F_y$ =115 MPa (Galambos and Ketter 1959) for a specified minimum yield strength of 350 MPa. Accordingly, interaction coefficients of 0.70 or lower are thought of to indicate an elastic response prior buckling. More accurate predictions for the residual stresses of a W200x31 section were recently predicted by a thermo-mechanical analysis in (Nowzartash and Mohareb 2011) and resulted in a tip longitudinal stress of 78 MPa. This suggests that the section remains elastic up to a yield strength of $\left(F_y - 78\right)MPa$. For a nominal yield strength of $350MPa$, this suggests that, for the section of interest, a interaction ratio of 0.78 or lower guarantees an elastic response. Based on the interaction ratios computed in Table 4.2, all three specimens are judged to have buckled elastically since their corresponding interaction ratios are less than 0.78. This signifies that the elastic buckling analysis conducted in the present study is applicable in predicting the capacity of the Gerber frames tested.

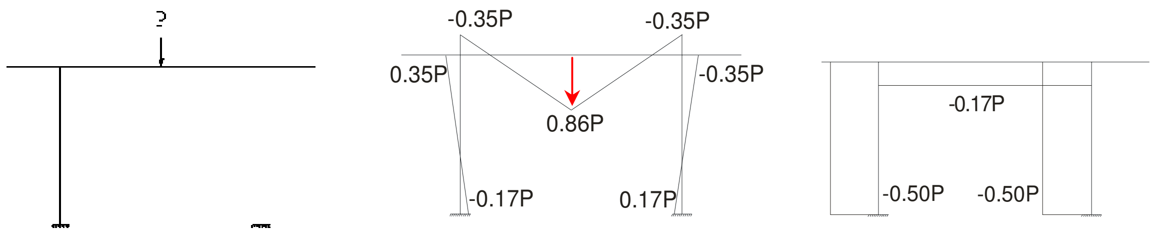

(a) Load (b) Bending Moment (c) Axial Force

Figure 4.35-Specimen 1-Load, Bending Moment, and Axial Force Diagrams

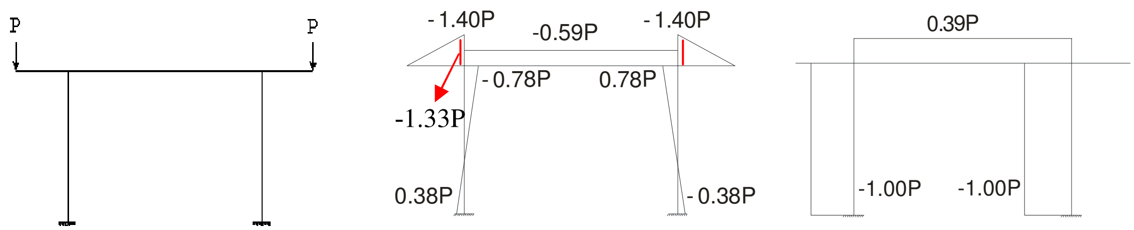

(a) Load (b) Bending Moment (c) Axial Force

Figure 4.36-Specimen 2-Load, Bending Moment, and Axial Force Diagrams

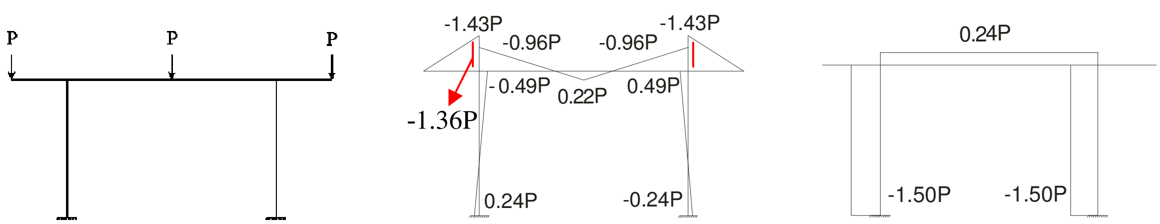

(a) Load (b) Bending Moment (c) Axial Force

Figure 4.37-Specimen 3-Load, Bending Moment, and Axial Force Diagrams

Table 4.2 Comparison between Maximum Forces and Yield Resistances (kNm)

	Specimen		
	1	2	3
Yield Moment M_y (kNm)	102.6	105.7	102.9
Axial yield resistance N_y (kN)	1,373	1,447	1,393
Maximum Moment based on experimental loads M_{exp} (kNm)	$0.86P$ =54.6	$1.33P$ =72.2	$1.36P$ =74.7
Corresponding normal force N_{exp} (kN)	10.8	0	0
$N_{exp}/N_y + M_{exp}/M_y$	0.540	0.683	0.726
Maximum Moment based on FEA predicted buckling loads M_{FEA} (kNm)	61.3	71.6	90.8
Corresponding normal force N_{FEA} (kN)	12.1	0	0
$N_{FEA}/N_y + M_{FEA}/M_y$	0.606	0.677	0.882

4.7 Effective Length for Cantilever Segments

Clause 13.6 in the newest Canadian Standards (CAN-CSA S16-09) provides an expression for the elastic buckling moment M_u for a cantilever as follows:

$$M_u = \frac{\omega_2 \pi}{L_u} \sqrt{E I_y G J + \left(\frac{\pi E}{L_u} \right)^2 I_y C_w} \qquad (4.4)$$

where E is the Modulus of Elasticity, I_y is the moment of inertia about the y-y axis, G is the Modulus of Rigidity, J is the St. Venant's torsion constant, and C_w is the warping torsional constant. In Eq. 4.4, ω_2 is a moment gradient factor taken as unity for cantilevers.

The effective length L_u is known to depend on the boundary conditions, load configuration, and point of applications of the loads relative to the shear centre. Various codes and design aids take the approach of specifying L_u for various boundary conditions. Once the effective length L_u is known, the elastic buckling moment resistance M_u can be determined from Eq. 4.4. For a cantilever of span L, Clause 13.6 of the code specifies an effective length $L_u = 1.2L$ times the cantilever span. When the load is applied to the top flange as is the case in the specimens tested, Clause 13.6 specifies an increase of the effective length by 20%. Thus, for the cantilever segment subject to top flange loading, the effective length, the Canadian standards suggest the use of $L_u = 1.44L$. This compares with the Gerber design guidelines (AISC 1989) which recommends $L_u = 1.5L$ and contrasts with Kirby and Nethercot (1987) who suggest the use of $L_u = 7.5L$ when the top flange at the root and tip locations of a cantilever segment are laterally unsupported.

One of the outcomes of the present investigation is the experimental and numerical determination of the critical moments M_u for the cantilever segments in Specimens 2 and 3. These are obtained by multiplying the buckling load obtained by the distance from the point of load application of the cantilever to the nearest column face. In Figs. 34.6 and 34.7, the corresponding moments are $M_u = 1.33P = 72.2kNm$ and $M_u = 1.36P = 74.7kNm$, respectively. Knowing M_u, the effective length L_u can be determined. The computed effective length factors (L_u / L) are summarized in Table 4.3.

The effective length factors of 2.21 and 2.57 obtained from the present experimental study are larger than the value 1.44 implied in the Canadian code and 1.5 provided in (AISC 1989). This is due to the fact that the lateral, torsional, and warping restraints at the cantilever roots in the Gerber system are only partial while the provisions in CAN-CSA S16 (2009) and (AISC 1989) are intended with cantilevers with full fixity conditions at the root. On the other hand, the effective lengths computed based on the present experimental study are significantly smaller than that proposed by Kirby and Nethercot (1987), indicating the overly conservative nature of their solution.

Table 4.3 Comparison of Effective Lengths (L_u / L) for Cantilever Segments

Specimen No.	Based on Experiments	Based on FEA
2	2.57	2.59
3	2.21	1.93

Helwig and Yura (1995) have proposed an expression for the critical moment of cantilevers in which the warping contribution were neglected, i.e.,

$$M_u = \frac{\pi}{L}\sqrt{EI_y GJ} \tag{4.5}$$

The critical moments as computed based on Eq. 4.5 are summarized in Table 4.4. The experimental moments are provided for comparison. It is observed that the Helwig and Yura formula grossly overestimates the buckling resistance of cantilever segments and are judged not suitable for the design of Gerber beams.

Table 4.4 Comparison of Critical Moments (kNm) for Cantilever Segments

Specimen No.	Based on Experiments	Based on Helwig and Yura
2	72.2	212.8
3	74.7	189.5

4.8 Lateral and Torsional Bracing

In all three test specimens (Figs 4.15 to 4.23), columns were observed to move laterally as the frames buckled. This suggests that the presence of lateral support at column tops are expected to improve the buckling resistance of Gerber frames.

For Specimen 1, the maximum lateral displacements as shown in Fig. 4.15 were observed to take place at mid-span and cantilever tips. The maximum angles of twist were observed in Fig. 4.16 to occur at mid-span. This suggests that lateral bracing would be effective at tip locations; while torsional bracing are expected to be effective at mid-span location.

For Specimens 2 and 3, the maximum lateral displacements as shown in Figs. 4.18 and 4.21 and maximum angles of twist as shown in Figs. 4.19 and 4.22 were observed to take place at cantilever tip locations. The predicted loads for buckling modes 1 and 2 were very close. In order to increase the buckling resistance of the Gerber system in these two cases, one would need to suppress both modes. Thus, the lateral and torsional bracing are expected to be effective at the tips.

In current design practice, Gerber beams are generally detailed to be torsionaly restrained at column locations primarily. The above experimental observations of the buckled configuration suggest that providing torsional braces at mid-span and cantilever tips could be more effective measures in increasing the buckling resistance of Gerber frames. Further experimental and finite element investigations on the effect of the location of braces are needed to confirm the validity of this proposition.

CHAPTER 5

Summary, Conclusions, and Recommendations

5.1 Summary and Conclusions

1) An experimental investigation was conducted on the lateral buckling analysis of laterally unsupported Gerber frames. Also, a finite element model was developed for the prediction of the elastic buckling resistance of the system. The finite element predictions of the buckling resistance and mode shapes agreed well with the experimental results.

2) Based on the bending moments and axial forces corresponding to the buckling loads, all test specimens experienced elastic lateral torsional buckling, i.e., they underwent buckling prior yielding takes place in the material.

3) Specimen 1, subject to a single mid-span load, exhibited a gradual lateral torsional deformation pattern as the load was increased. In contrast, Specimens 2 and 3, with tip loads, exhibited a sudden lateral torsional deformation response once the buckling load was reached.

4) Based on lateral displacement and rotation measurements, the columns were observed to undergo lateral displacements and bending. This signifies that the whole frames underwent buckling. The buckled configurations as predicted by finite element confirm this observation. This suggests that the isolation of the beam from the rest of the structure would not result in a reliable prediction of the buckling response.

5) The FEA and experimental results suggest that the buckling modes can be symmetric (such as Specimen 1) or skew symmetric (Specimen 2), depending on the load configurations. In some cases (Specimens 2 and 3), the symmetric and skew symmetric modes correspond to nearly equal buckling loads. In such cases, any linear combination of modes can take place (Specimen 3), resulting in an asymmetric response.

6) Present solutions for designing cantilever segments and Gerber systems show a large discrepancy in estimating the critical moments. The effective length factor for such structures varies from 1.44 to 7.5. Within this context, the present experimental study provided in effective length ranging from 2.1-2.6. This suggests that the lower bound of 1.44 is un-conservative while the upper bound of 7.5 is overly conservative. The un-conservative solution based on an effective length of 1.44 is a result of the fact that the underlying method assumes full warping, torsional, and lateral restraints at the cantilever root, which contrasts with the Gerber frame situation.

7) The solution proposed by Yura and Helwig (2005) was found to provide grossly un-conservative predictions of the elastic moments of the Gerber frames tested.

5.2 Recommendations for Future Research

1) Given the scarcity of experimental investigations on lateral-torsional buckling of frames, it is recommended to conduct further experiments. Attention should be given to the effect of lateral and torsional restraints provided by open web steel joists.

2) The FEA model developed has the potential to reliably model other Gerber frame configurations, loading patterns, and lateral and torsional restraints. The expansion of the experimental and numeric databases of solutions is an important step towards developing rational design rules for Gerber frames.

3) The measured and FEA buckled configurations suggest that bracing at mid-span and cantilever tips locations could be an effective method to increase the capacity of Gerber beams. This hypothesis needs to be verified through additional tests and FEA.

APPENDIX A

Ancillary Tests-Stress vs. Strain Relationships

Contents

As discussed in Chapter 3, this appendix provides the stress vs. strain relationships as obtained from the six tension coupons tested. Two coupons were taken from the web of each Specimen, one from the left cantilever web and another one from the right cantilever web. Results are provided in Figs. A.1 and A.2 for Specimen 1, Figs. A.3 and A.4 for Specimen 2, and Figs. A.5 and A.6 for Specimen 3.

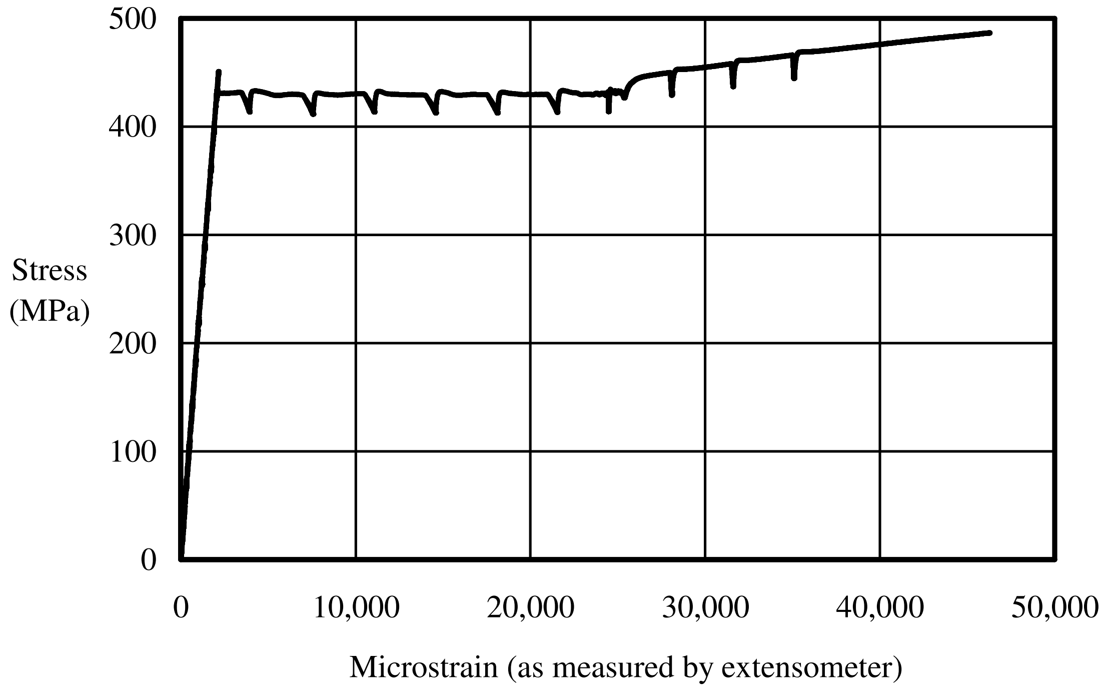

Figure A.1-Specimen 1 Left-Stress vs. Engineering Strain Curve of Coupon Test

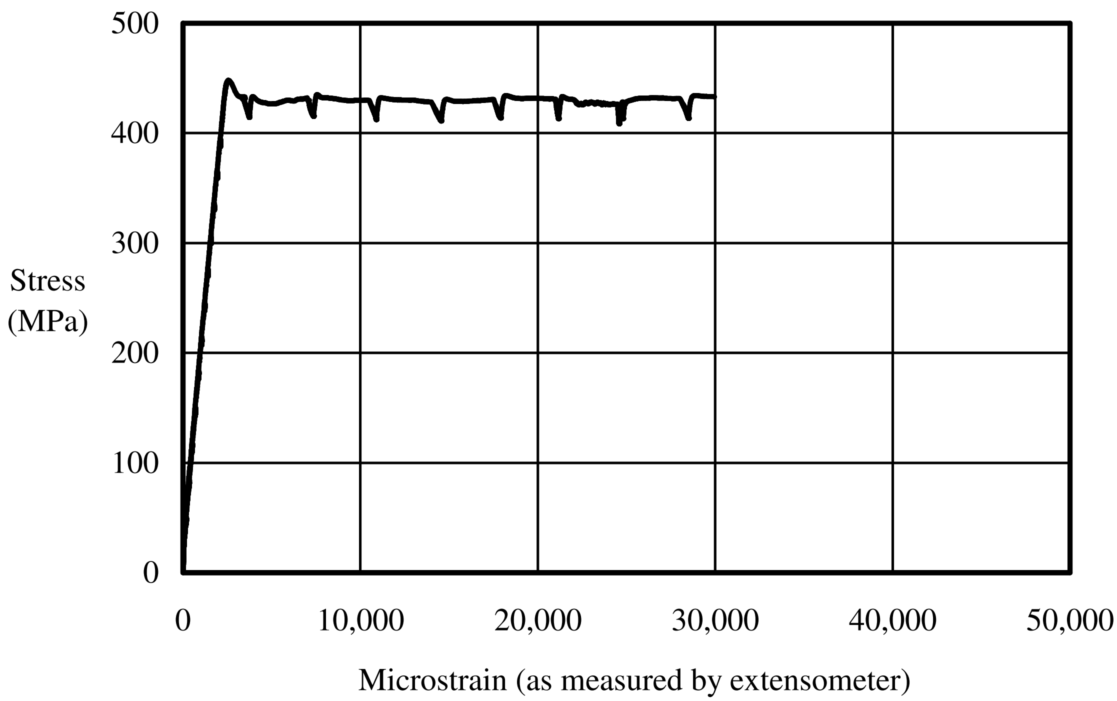

Figure A.2-Specimen 1 Right-Stress vs. Engineering Strain Curve of Coupon Test

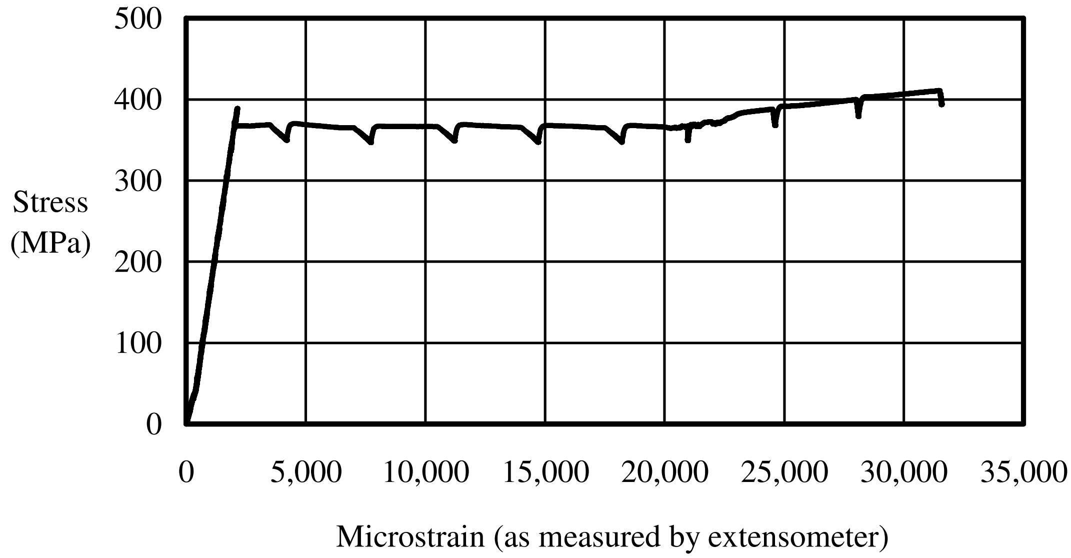

Figure A.3-Specimen 2 Left-Stress vs. Engineering Strain Curve of Coupon Test

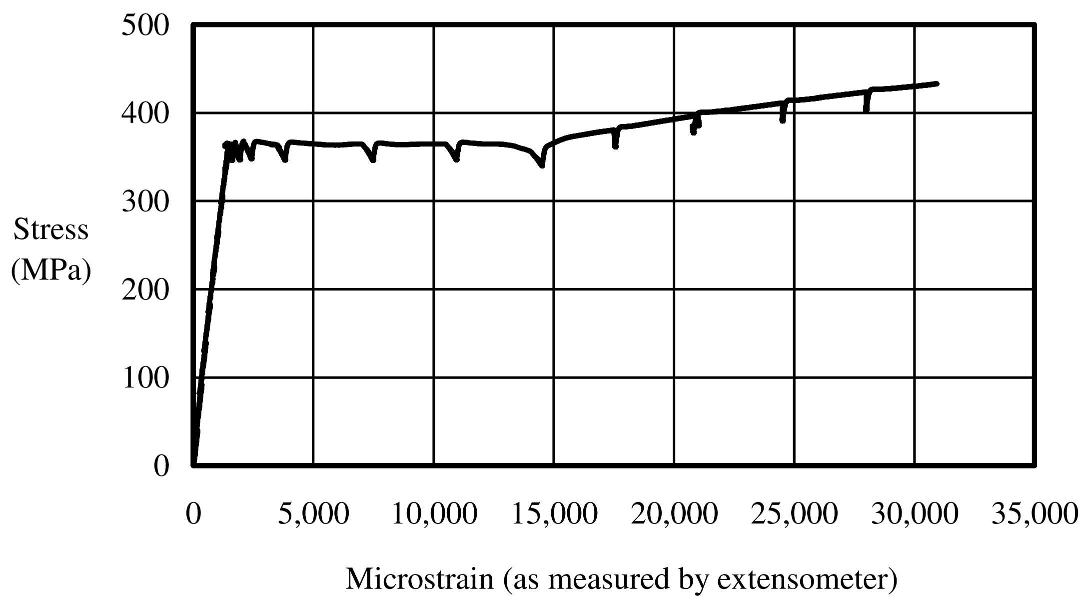

Figure A.4-Specimen 2 Right-Stress vs. Engineering Strain Curve of Coupon Test

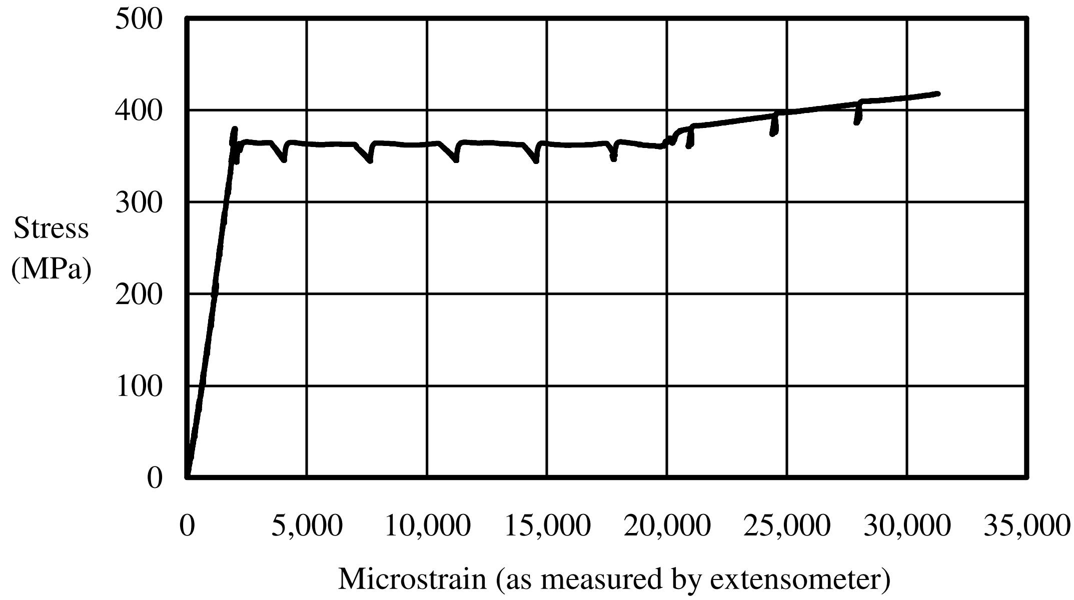

Figure A.5-Specimen 3 Left-Stress vs. Engineering Strain Curve of Coupon Test

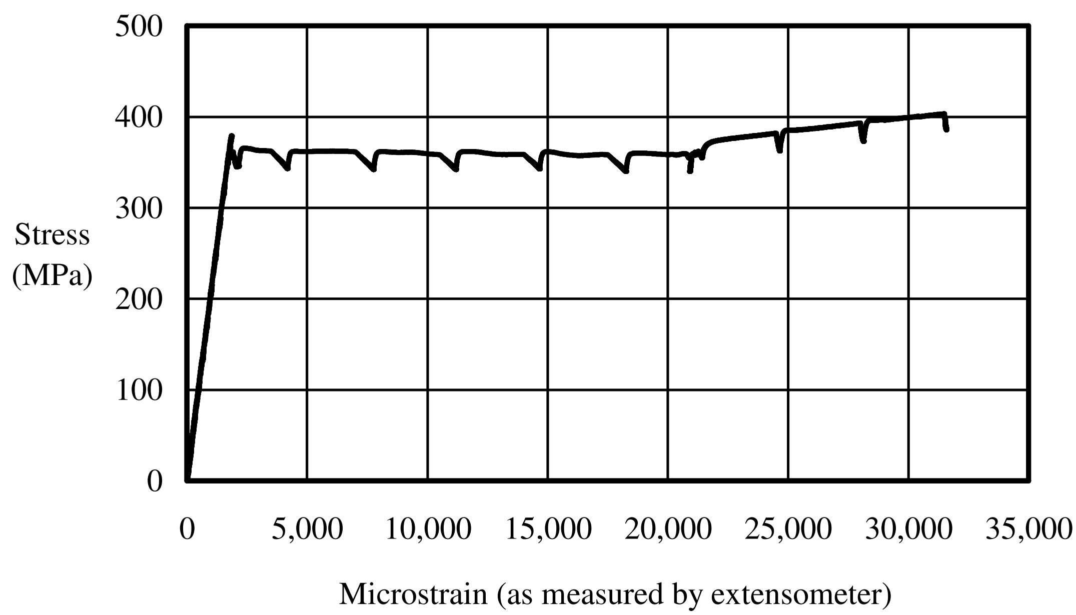

Figure A.6-Specimen 3 Right-Stress vs. Engineering Strain Curve of Coupon Test

APPENDIX B

Cross-Sectional Properties

Contents

- Tables B.1, B.2, and B.3 present the measured cross-sectional dimensions for Specimens 1, 2, and 3 respectively followed by sample calculations for Specimen 1. Table B.4 presents the measured cross-sectional dimensions for the HSS columns.

- Calculated versus nominal cross-sectional properties for Specimens 1, 2, and 3 are provided in Tables B.5-B.7 respectively. For HSS columns, the calculated versus nominal cross-sectional properties are provided in Tables B.8.

Table B.1 Specimen 1-Measured Cross-Sectional Dimensions (mm)

Measurement No.	Flange Width (b)	Flange Thickness (t)	Section Height (d)	Web Thickness (w)
1	132.9	10.0	210.0	6.3
2	132.8	10.2	210.0	6.4
3	132.7	10.3	210.5	6.5
4	132.7	9.7	210.5	6.5
5	132.6	9.8	213.0	6.5
6	132.7	10.2	212.5	6.4
7	133.2	10.2	210.5	6.6
8	133.3	10.1	211.0	6.5
9	133.2	10.1	211.0	6.5
10	133.4	10.1	210.0	6.4
AVERAGE	132.9	10.1	210.9	6.5
Tabulated Values	134.0	10.2	210.0	6.4
Percentage Difference	0.82%	0.91%	-0.43%	-1.56%

Table B.2 Specimen 2-Measured Cross-Sectional Dimensions (mm)

Measurement No.	Flange Width (b)	Flange Thickness (t)	Section Height (d)	Web Thickness (w)
1	131.4	9.8	212.5	7.4
2	131.7	10.2	212.5	7.3
3	132.0	9.8	213.5	7.6
4	131.8	10.3	212.5	7.4
5	132.0	9.8	212.5	7.5
6	132.0	10.7	213.0	7.4
7	131.9	10.6	213.5	7.4
8	131.9	10.2	212.0	7.5
9	132.0	10.2	213.0	7.6
10	132.0	10.4	212.5	7.5
AVERAGE	131.9	10.2	212.8	7.5
Tabulated Values	134.0	10.2	210.0	6.4
Percentage Difference	1.57%	0%	-1.32%	-17.18%

Table B.3 Specimen 3-Measured Cross-Sectional Dimensions (mm)

Measurement No.	Flange Width (b)	Flange Thickness (t)	Section Height (d)	Web Thickness (w)
1	131.5	9.8	211.5	7.0
2	131.8	10.0	213.0	7.0
3	131.8	9.8	212.5	7.0
4	131.7	10.0	212.0	6.9
5	131.7	9.9	213.0	7.2
6	131.6	10.1	212.5	7.0
7	131.7	10.1	212.5	7.0
8	131.8	10.0	213.0	7.0
9	131.7	10.0	213.0	7.1
10	132.0	10.0	212.5	7.2
AVERAGE	131.7	10.0	212.6	7.0
Tabulated Values	134.0	10.2	210.0	6.4
Percentage Difference	1.72%	1.96%	-0.29%	-9.38%

Table B.4 HSS Columns Measured Cross-Sectional Dimensions (mm)

Measurement No.	Column Width (b)	Column Thickness (t)
1	152.0	6.35
2	152.0	6.35
3	152.0	6.22
AVERAGE	152.0	6.31
Tabulated Values	152.0	6.35
Percentage Difference	0%	0.63%

Sample calculations for cross-sectional properties of Specimen 1:

The cross-sectional area is:

$$A = 2bt + w(d - 2t)$$
$$A = 2 \times 132.9 \times 10.1 + 6.5(210.9 - 2 \times 10.1)$$
$$A = 3924 mm^2$$

The elastic section modulus is:

$$S_x = \frac{1}{6d}\left[bd^3 - (b - w)(d - 2t)^3\right]$$
$$S_x = \frac{1}{6 \times 210.9}\left[132.9 \times 210.9^3 - (132.9 - 6.5)(210.9 - 2 \times 10.1)^3\right]$$
$$S_x = 293 \times 10^3 mm^3$$

The plastic section modulus is:

$$Z_x = \frac{1}{4}\left[bd^2 - (b - w)(d - 2t)^2\right]$$
$$Z_x = \frac{1}{4}\left[132.9 \times 210.9^2 - (132.9 - 6.5)(210.9 - 2 \times 10.1)^2\right]$$
$$Z_x = 329 \times 10^3 mm^3$$

The Moment of Inertia about the x-x axis is:

$$I_x = \frac{1}{12}\left[bd^3 - (b - w)(d - 2t)^3\right]$$
$$I_x = \frac{1}{12}\left[132.9 \times 210.9^3 - (132.9 - 6.5)(210.9 - 2 \times 10.1)^3\right]$$
$$I_x = 30.8 \times 10^6 mm^4$$

The Moment of Inertia about the y-y axis is:

$$I_y = \frac{1}{12}\left[2tb^3 + (d - 2t)w^3\right]$$
$$I_y = \frac{1}{12}\left[2 \times 10.1 \times 132.9^3 + (210.9 - 2 \times 10.1)6.5^3\right]$$
$$I_x = 3.96 \times 10^6 mm^4$$

The St. Venant's torsion constant is:

$$J = \frac{1}{3}\left[2bt^3 + hw^3\right]$$

$$J = \frac{1}{3}\left[2 \times 132.9 \times 10.1^3 + (210.9 - 10.1)6.5^3\right]$$

$$J = 110 \times 10^3 \, mm^3$$

The Warping Torsional Constant is:

$$C_w = \frac{h^2 I_y}{4} = \frac{(210.9 - 10.1)^2 \times 3.96 \times 10^6}{4} = 39.9 \times 10^9 \, mm^6$$

Table B.5 Specimen 1-Calculated versus Nominal Cross-Sectional Properties

1	2	3	4	5
Sectional Property	Calculated based on tabulated dimensions	Calculated based on measured dimensions	Tabulated	Percentage difference between tabulated and measured values
A (mm^2)	3,947	3,924	4,000	1.90%
S_x (mm^3)	295 x 10^3	293 x 10^3	299 x 10^3	2.01%
Z_x (mm^3)	331 x 10^3	329 x 10^3	335 x 10^3	1.79%
I_x (mm^4)	30.9 x 10^6	30.8 x 10^6	31.4 x 10^6	1.91%
I_y (mm^4)	4.09 x 10^6	3.96 x 10^6	4.10 x 10^6	3.41%
J (mm^3)	113 x 10^3	110 x 10^3	119 x 10^3	7.56%
C_w (mm^6)	40.8 x 10^9	39.9 x 10^9	40.9 x 10^9	2.44%

Table B.6 Specimen 2-Calculated versus Nominal Cross-Sectional Properties

1	2	3	4	5
Sectional Property	Calculated based on tabulated dimensions	Calculated based on measured dimensions	Tabulated	Percentage difference between tabulated and measured values
A (mm^2)	3,947	4,134	4,000	3.35%
S_x (mm^3)	295 x 10^3	302 x 10^3	299 x 10^3	1.00%
Z_x (mm^3)	331 x 10^3	342 x 10^3	335 x 10^3	2.09%
I_x (mm^4)	30.9 x 10^6	32.1 x 10^6	31.4 x 10^6	2.23%
I_y (mm^4)	4.09 x 10^6	3.91 x 10^6	4.10 x 10^6	4.63%
J (mm^3)	113 x 10^3	122 x 10^3	119 x 10^3	2.52%
C_w (mm^6)	40.8 x 10^9	40.1 x 10^9	40.9 x 10^9	1.96%

Table B.7 Specimen 3-Calculated versus Nominal Cross-Sectional Properties

1	2	3	4	5
Sectional Property	Calculated based on tabulated dimensions	Calculated based on measured dimensions	Tabulated	Percentage difference between tabulated and measured values
A (mm^2)	3,947	3,979	4,000	0.53%
S_x (mm^3)	295 x 10^3	294 x 10^3	299 x 10^3	1.67%
Z_x (mm^3)	331 x 10^3	332 x 10^3	335 x 10^3	0.90%
I_x (mm^4)	30.9 x 10^6	31.2 x 10^6	31.4 x 10^6	0.64%
I_y (mm^4)	4.09 x 10^6	3.81 x 10^6	4.10 x 10^6	7.07%
J (mm^3)	113 x 10^3	111 x 10^3	119 x 10^3	6.72%
C_w (mm^6)	40.8 x 10^9	39.1 x 10^9	40.9 x 10^9	4.40%

Table B.8 HSS Columns-Calculated versus Nominal Cross-Sectional Properties

1	2	3	4	5
Sectional Property	Calculated based on tabulated dimensions	Calculated based on measured dimensions	Tabulated	Percentage difference between tabulated and measured values
A (mm^2)	3,670	3,677	3,270	12.5%
S_x (mm^3)	135 x 10^3	135 x 10^3	152 x 10^3	11.2%
Z_x (mm^3)	202 x 10^3	202 x 10^3	178 x 10^3	-13.5%
I_x (mm^4)	13.1 x 10^6	13.1 x 10^6	11.6 x 10^6	-12.9%
I_y (mm^4)	13.1 x 10^6	13.1 x 10^6	11.6 x 10^6	-12.9%
J (mm^3)	19,620 x 10^3	19,513 x 10^3	18,400 x 10^3	-6.05%
C_w (mm^6)	269 x 10^3	268 x 10^3	228 x 10^3	-17.5%

APPENDIX C

Location of Sensors and Calibration Data

Contents

- Tables C.1, C.2, C.3, and C.4 present calibration data for horizontal transducers, clinometers, vertical LVDTs, and load cells respectively.

- Figures C.1, C.2 and C.3 illustrate sensors locations for Specimens 1, 2, and 3 respectively. Transducers and clinometers horizontal and vertical coordinates for Specimen 1 are provided in Tables C.5 and C.6 respectively. For Specimen 2, transducers and clinometers horizontal and vertical coordinates are provided in Tables C.7 and C.8 respectively. Tables C.9 and C.10 provide transducers and clinometers horizontal and vertical coordinates respectively for Specimen 3.

Table C.1 Calibration Factors for Horizontal Transducers

Transducer No.	Serial No.	Calibration Data	
		mV	mm
0	B1301164B	0	0
		84.5	5
		156.6	10
1	B1301163B	0	0
		84.5	5
		152.9	10
2	K1205019B	0	0
		80.3	5
		151.1	10
3	J1904768A	0	0
		-1022.77	5
		-1849.9	10
4	J1904767A	0	0
		-1070	5
		-1939.7	10
5	J1904766A	0	0
		-1033.15	5
		-1855.6	10
6	J1904763A	0	0
		-863.14	5
		-1819.8	10
7	J1904765A	0	0
		-990.5	5
		-1834.5	10
8	J1904769A	0	0
		-866.69	5
		-1814.8	10
9	J1904770A	0	0
		-936.14	5
		-1746.3	10
10	J1904764A	0	0
		-894.27	5
		-1850.81	10
11	J1904771A	0	0
		928.2	5
		1762	10
12	J1904772A	0	0
		-1060	5
		-1982	10
13	4016	0	0
		384.6	5

		761.2	10
14	4907	0	0
		415.7	5
		733.7	10
		1144.7	15
15	K1205013B	0	0
		69.3	5
		138.9	10
16	K1205020B	0	0
		70.2	5
		138	10

Table C.2 Calibration Factors for Clinometers

Clinometer	Serial No.	Calibration	
		mV	mm
A	50050219	0	0
		153.8	5
		318.3	10
		472.5	15
		631.5	20
B	50110109	0	0
		161.5	5
		318.6	10
		654.1	20
C	50050215	0	0
		167.3	5
		333.6	10
		488.3	15
D	50050216	0	0
		160.5	5
		322.6	10
		474	15
		637.6	20
E	50050217	0	0
		148.6	5
		300.6	10
		458.1	15
		620.5	20
F	50110114	0	0
		170.3	5
		530.2	15
		706.3	20
G	50050218	0	0
		160.5	5
		329.3	10
		471.6	15
		642.2	20

Table C.3 Calibration Factors for Vertical LVDTs

LVDT No.	Serial No.	Calibration	
		mV	mm
1	M920141A313-04	530.8	-25
		0	0
		-538.4	25
2	M920141A313-03	554.6	-25
		0	0
		-566.8	25
3	M920126A313-01	3792	-12.5
		0	0
		-3533.8	12.5
4	M920128B313-02	1615.5	-25
		0	0
		-1790.1	25
5	M920141A313-02	554	-25
		0	0
		-543.9	25
6	M920141A313-05	538.1	-25
		0	0
		-568.3	25

Table C.4 Calibration Factors for Load Cells

Load Cell Location	Serial No.	Calibration	
		mV	Newton
Left Tip	N/A	0	0
		3	178,000
Midspan	N/A	0	0
		3	178,000
Right Tip	N/A	0	0
		3	178,000

Table C.5 Specimen 1-Transducers Horizontal and Vertical Coordinates (mm)

Transducer No.*	Serial No.	Horizontal Coordinate	Vertical Coordinate
0	B1301164B	175	35
1	B1301163B	185	166
2	K1205019B	735	35
3	J1904768A	1515	168
4	J1904767A	1435	45
5	J1904766A	2665	178
6	J1904763A	2575	57
7	J1904765A	3855	171
8	J1904769A	3795	52.5
9	J1904770A	4950	161
10	J1904764A	4865	45
11	J1904771A	6150	161
12	J1904772A	6035	50
13	4016	6800	156
14	4907	6695	40
15	K1205013B	7330	181
16	K1205020B	7325	30

* Based on Transducer Numbers of Figure C.1

Table C.6 Specimen 1-Clinometers Horizontal and Vertical Coordinates (mm)

Clinometer	Serial No.	Horizontal Coordinate	Vertical Coordinate
A	50050219	180	106
B	50110109	735	106
C	50050215	2620	106
D	50050216	3825	106
E	50050217	4908	106
F	50110114	6748	106
G	50050218	7328	106

* Based on Clinometers of Figure C.1

Table C.7 Specimen 2-Transducers Horizontal and Vertical Coordinates (mm)

Transducer No.*	Serial No.	Horizontal Coordinate	Vertical Coordinate
0	B1301164B	195	30
1	B1301163B	195	178
2	K1205019B	795	30
3	J1904768A	1525	188
4	J1904767A	1520	35
5	J1904766A	2675	188
6	J1904763A	2665	30
7	J1904765A	3850	190
8	J1904769A	3845	35
9	J1904770A	5000	188
10	J1904764A	5005	25
11	J1904771A	6095	188
12	J1904772A	6100	25
13	4016	6793	193
14	4907	6795	30
15	K1205013B	7473	193
16	K1205020B	7470	25

* Based on Transducer Numbers of Figure C.2

Table C.8 Specimen 2-Clinometers Horizontal and Vertical Coordinates (mm)

Clinometer	Serial No.	Horizontal Coordinate	Vertical Coordinate
A	50050219	N/A	N/A
B	50110109	N/A	N/A
C	50050215	795	106.4
D	50050216	2670	106.4
E	50050217	3848	106.4
F	50110114	N/A	N/A
G	50050218	N/A	N/A

* Based on Clinometers of Figure C.2

Table C.9 Specimen 3-Transducers Horizontal and Vertical Coordinates (mm)

Transducer No.*	Serial No.	Horizontal Coordinate	Vertical Coordinate
0	B1301164B	200	21.9
1	B1301163B	215	190.7
2	K1205019B	885	21.9
3	J1904768A	1540	190.7
4	J1904767A	1550	21.9
5	J1904766A	2605	190.7
6	J1904763A	2620	21.9
7	J1904765A	3850	190.7
8	J1904769A	3875	21.9
9	J1904770A	4910	190.7
10	J1904764A	4945	21.9
11	J1904771A	6095	190.7
12	J1904772A	6135	21.9
13	4016	6745	190.7
14	4907	6780	21.9
15	K1205013B	7475	190.7
16	K1205020B	7510	21.9

* Based on Transducer Numbers of Figure C.3

Table C.10 Specimen 3-Clinometers Horizontal and Vertical Coordinates (mm)

Clinometer	Serial No.	Horizontal Coordinate	Vertical Coordinate
A	50050219	N/A	N/A
B	50110109	N/A	N/A
C	50050215	N/A	N/A
D	50050216	213	106.3
E	50050217	885	106.3
F	50110114	1545	106.3
G	50050218	7493	106.3

* Based on Clinometers of Figure C.3

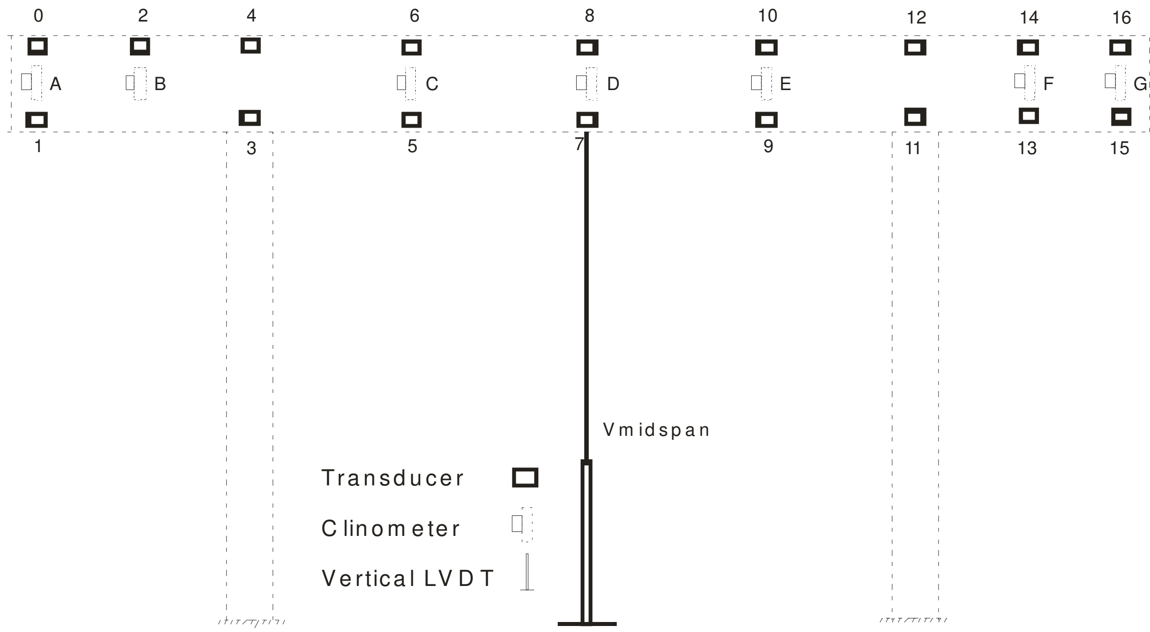

* Refer to Table C.5 for Transducer Locations
* Refer to Table C.6 for Clinometer Locations

Figure C.1-Specimen 1-Measuring Instrumentation Map

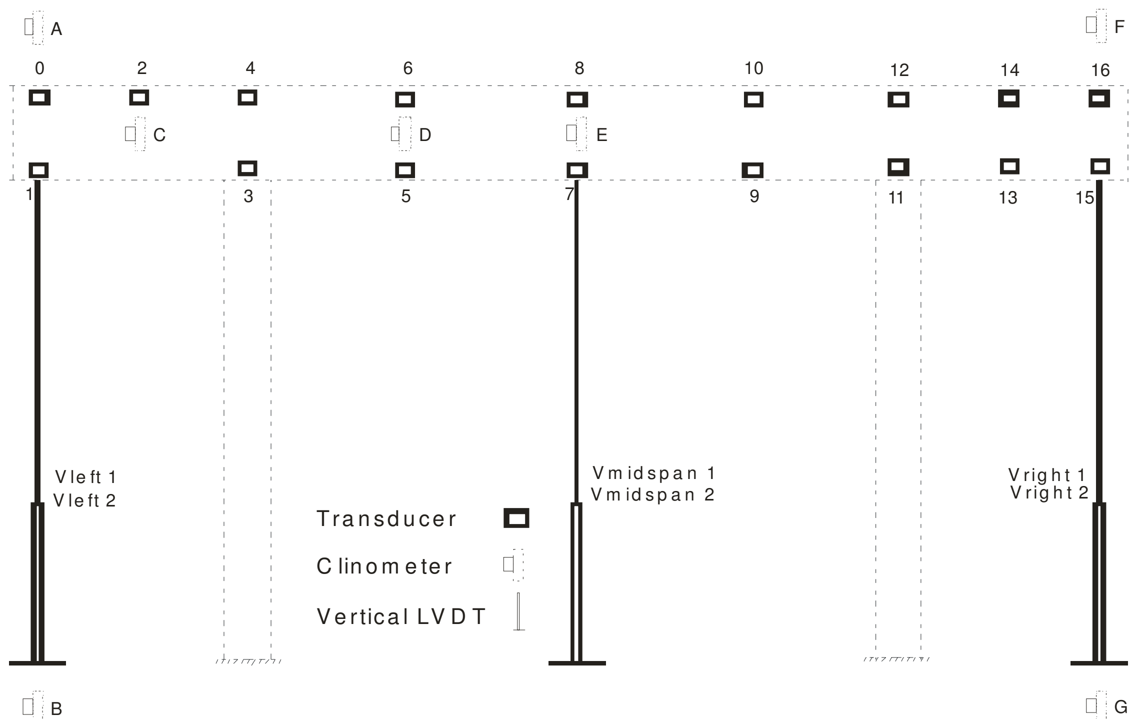

* Refer to Table C.7 for Transducer Locations
* Refer to Table C.8 for Clinometer Locations

Figure C.2-Specimen 2-Measuring Instrumentation Map

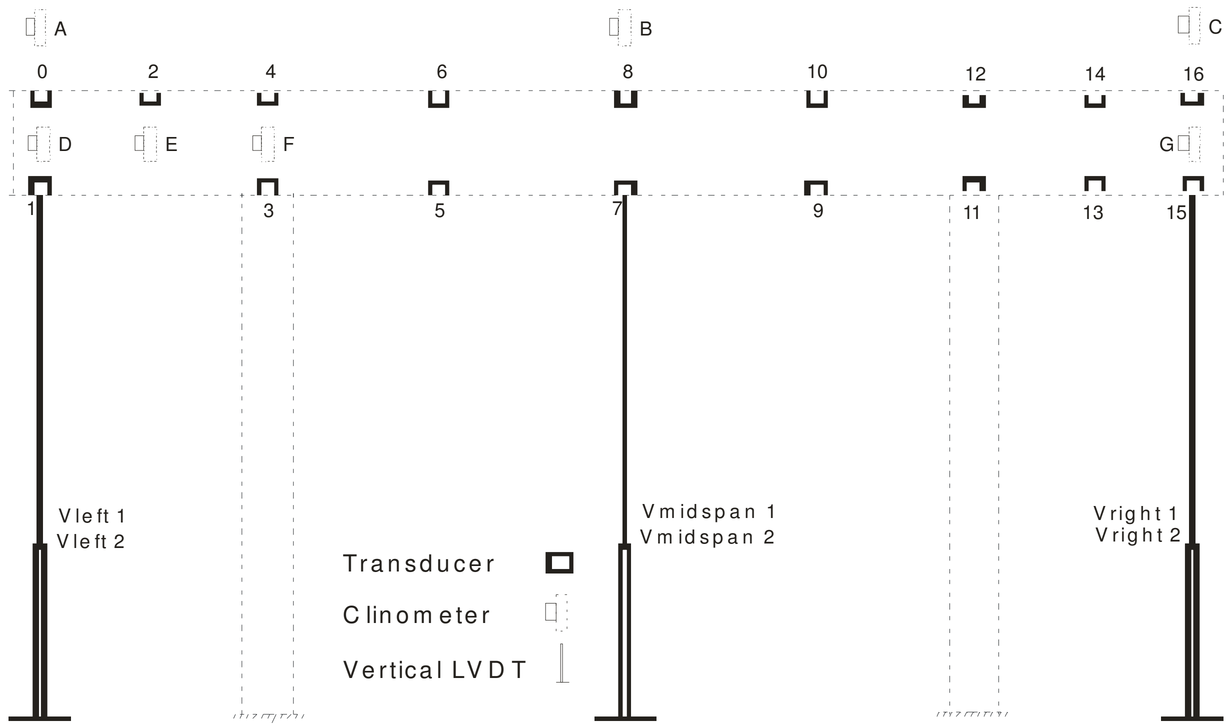

* Refer to Table C.9 for Transducer Locations
* Refer to Table C.10 for Clinometer Locations

Figure C.3-Specimen 3-Measuring Instrumentation Map

APPENDIX D

Experimental Data

Contents

- Tables D.1, D.2, and D.3 present load applied based on load cell readings for Specimens 1, 2, and 3 respectively.

- Horizontal transducers readings for Specimens 1, 2 and 3 are provided in Tables D.4, D.5, and D.6 respectively. Tables D.7, D.8, and D.9 present clinometer readings for Specimens 1, 2 and 3 respectively. For Specimens 1, 2, and 3, vertical LVDTs readings are provided in Tables D.10, D.11, and D.12 respectively.

- Top transducer displacements readings for Specimens 1, 2, and 3 are provided in Tables D.13, D.14, and D.15 respectively. Tables D.16, D.17 and D.18 present bottom transducers displacements readings for Specimens 1, 2, and 3 respectively.

- Specimens 1, 2, and 3 web mid-height lateral displacements readings are provided in Table D.19, D.20, and D.21 respectively.

Table D.1 Specimen 1-Experimental Raw Data for Load Cell Readings (kN)

Step	Mid-span
1	0.0
2	10.0
3	15.2
4	20.2
5	24.8
6	29.9
7	35.0
8	40.1
9	44.6
10	50.1
11	54.4
12	60.1
13	63.1
14	63.5

Table D.2 Specimen 2-Experimental Raw Data for Load Cell Readings (kN)

Step	Average Load	Load Cell Location	
		Left Tip	Right Tip
1	0.0	0.0	0.0
2	5.1	5.4	4.8
3	10.0	9.8	10.2
4	15.1	14.9	15.2
5	20.6	20.3	20.8
6	25.3	25.4	25.2
7	29.4	29.5	29.2
8	35.0	35.0	34.9
9	40.0	39.9	40.1
10	45.7	45.9	45.4
11	47.7	47.9	47.6
12	50.9	50.7	51.0
13	54.3	54.4	54.2
14	47.4	47.3	47.5
15	46.9	46.7	47.1

Table D.3 Specimen 3-Experimental Raw Data for Load Cell Readings (kN)

Step	Average Load	Load Cell Location		
		Left Tip	Mid-span	Right Tip
1	0.0	0.0	0.0	0.0
2	5.5	5.5	5.5	5.4
3	10.4	10.0	10.8	10.3
4	15.3	15.2	15.3	15.2
5	20.2	20.0	20.6	20.1
6	24.7	24.6	24.7	24.7
7	29.5	29.4	29.4	29.7
8	34.7	34.5	34.7	34.8
9	39.6	39.5	39.5	39.7
10	44.4	44.5	44.3	44.3
11	45.6	45.4	45.4	45.9
12	47.2	47.1	47.0	47.3
13	49.6	49.7	49.5	49.7
14	52.3	52.0	52.2	52.6
15	52.5	50.5	52.7	54.5
16	53.3	50.0	54.8	55.1
17	54.3	49.0	55.8	58.0
18	55.1	48.8	56.4	60.0

Table D.4 Specimen 1-Experimental Raw Data for Horizontal Transducer Readings (mm)

Step	Load	Transducer No.									
		0	1	2	3	4	5	6	7	8	9
1	0.0	0.000	0.000	0.000	0.000	0.000	0.000	0.000	0.000	0.000	0.000
2	10.0	-0.104	0.062	-0.104	0.000	-0.003	-0.118	-0.500	-0.004	0.013	-0.001
3	15.2	-0.083	0.248	0.041	-0.002	-0.230	-0.308	-1.259	-0.010	-0.655	-0.131
4	20.2	-0.269	0.434	-0.021	-0.091	-0.443	-0.497	-2.117	-0.224	-1.797	-0.328
5	24.8	0.289	0.599	-0.042	-0.169	-0.708	-0.755	-3.140	-0.528	-3.162	-0.620
6	29.9	0.826	0.888	-0.021	-0.275	-1.125	-1.092	-4.582	-1.022	-5.131	-0.967
7	35.0	0.660	1.136	0.123	-0.426	-1.520	-1.391	-5.823	-1.390	-6.925	-1.298
8	40.1	2.209	1.590	-0.062	-0.682	-2.225	-1.974	-8.180	-2.154	-10.189	-1.982
9	44.6	2.849	2.148	0.144	-0.915	-3.034	-2.605	-10.883	-3.034	-13.995	-2.692
10	50.1	4.005	2.891	0.082	-1.183	-4.073	-3.406	-14.479	-4.072	-19.024	-3.629
11	54.4	5.492	3.738	0.144	-1.622	-5.563	-4.429	-19.223	-5.465	-25.529	-4.801
12	60.1	6.731	4.770	0.185	-2.123	-7.602	-5.713	-25.737	-7.183	-34.676	-6.254
13	63.1	8.073	5.596	0.082	-2.333	-8.330	-6.466	-28.489	-8.652	-38.963	-7.128
14	63.5	8.238	5.617	0.289	-2.335	-8.329	-6.475	-28.492	-8.664	-38.965	-7.141

Step	Load	Transducer No.						
		10	11	12	13	14	15	16
1	0.0	0.000	0.000	0.000	0.000	0.000	0.000	0.000
2	10.0	-0.019	0.003	-0.002	0.009	0.016	0.021	0.041
3	15.2	-0.711	-0.001	-0.150	0.005	-0.004	0.062	0.247
4	20.2	-1.617	-0.020	-0.420	0.017	0.016	0.124	0.454
5	24.8	-2.752	-0.147	-0.719	0.013	0.024	0.330	0.867
6	29.9	-4.315	-0.244	-1.177	0.009	0.024	0.578	1.363
7	35.0	-5.707	-0.331	-1.537	0.005	-0.021	0.785	1.776
8	40.1	-8.184	-0.557	-2.274	0.009	-0.029	1.239	2.684
9	44.6	-11.444	-0.808	-3.075	0.013	-0.021	1.755	3.613
10	50.1	-15.352	-1.067	-4.180	0.009	0.016	2.457	4.935
11	54.4	-20.905	-1.506	-5.665	0.017	-0.057	3.180	6.463
12	60.1	-28.250	-2.034	-7.743	-0.016	-0.249	4.274	8.404
13	63.1	-31.291	-2.264	-8.541	-0.012	-0.209	5.059	9.622
14	63.5	-31.297	-2.256	-8.541	-0.008	-0.233	5.059	9.601

Table D.5 Specimen 2-Experimental Raw Data for Horizontal Transducer Readings (mm)

Step	Average Load	Transducer No.									
		0	1	2	3	4	5	6	7	8	9
1	0.0	0.000	0.000	0.000	0.000	0.000	0.000	0.000	0.000	0.000	0.000
2	5.1	0.039	0.060	0.161	-0.002	-0.005	-0.001	0.000	0.001	0.003	0.004
3	10.0	0.000	0.060	0.202	-0.002	-0.002	0.007	0.032	0.050	0.001	0.004
4	15.1	0.214	0.060	0.404	0.000	0.075	0.370	-0.087	0.526	0.003	0.244
5	20.6	0.233	0.080	0.404	0.005	0.202	0.374	-0.168	0.536	0.003	0.243
6	25.3	0.428	0.060	0.646	0.282	0.332	0.531	-0.196	0.671	0.003	0.255
7	29.4	0.545	0.060	0.767	0.282	0.425	0.644	-0.279	0.768	0.001	0.258
8	35.0	0.875	0.080	0.908	0.286	0.604	0.873	-0.255	0.944	0.001	0.408
9	40.0	1.303	0.338	1.251	0.631	0.801	1.055	-0.340	1.192	0.001	0.459
10	45.7	2.392	0.497	2.058	0.874	1.228	1.445	-0.399	1.535	0.005	0.635
11	47.7	3.404	0.835	2.784	1.195	1.817	1.815	-0.434	1.854	0.003	0.831
12	50.9	5.271	0.955	4.075	1.208	2.369	2.023	-0.569	2.010	0.003	0.852
13	54.3	10.366	1.472	7.444	1.553	4.033	2.696	-0.803	2.538	0.296	1.159
14	47.4	54.555	10.958	37.703	3.161	18.624	2.386	6.193	0.785	-0.708	-4.302
15	46.9	55.586	11.217	39.216	3.318	19.456	3.526	6.907	2.246	0.487	-1.718
Step	Average Load	Transducer No.									
		10	11	12	13	14	15	16			
1	0.0	0.000	0.000	0.000	0.000	0.000	0.000	0.000			
2	5.1	0.002	0.002	0.002	0.004	0.000	-0.044	-0.044			
3	10.0	0.004	0.007	0.003	0.008	-0.004	0.000	-0.353			
4	15.1	0.300	0.529	0.449	0.352	0.203	0.088	-0.353			
5	20.6	0.302	0.528	0.449	0.357	0.203	0.110	-0.353			
6	25.3	0.299	0.529	0.446	0.352	0.199	0.066	-0.376			
7	29.4	0.297	0.531	0.448	0.352	0.203	0.066	-0.486			
8	35.0	0.299	0.535	0.452	0.352	0.203	0.044	-0.707			
9	40.0	0.309	0.535	0.448	0.352	0.199	0.000	-0.906			
10	45.7	0.310	0.533	0.449	0.352	0.203	-0.242	-1.304			
11	47.7	0.587	0.559	0.451	0.352	0.203	-0.286	-1.238			
12	50.9	0.589	0.561	0.449	0.357	-0.057	-0.440	-1.481			
13	54.3	0.696	0.559	0.449	0.352	-0.552	-0.813	-2.277			
14	47.4	-8.316	-5.131	-20.724	-7.169	-41.476	-11.580	-66.852			
15	46.9	-6.061	-1.504	-17.565	-3.128	-37.890	-6.702	-61.876			

Table D.6 Specimen 3-Experimental Raw Data for Horizontal Transducer Readings (mm)

Step	Average Load	Transducer No.									
		0	1	2	3	4	5	6	7	8	9
1	0.0	0.000	0.000	0.000	0.000	0.000	0.000	0.000	0.000	0.000	0.000
2	5.5	0.100	0.052	0.121	-0.001	0.002	-0.001	0.000	-0.003	0.000	0.000
3	10.4	0.537	0.052	0.444	0.000	0.006	0.000	0.002	-0.005	0.005	0.000
4	15.3	0.876	0.072	0.706	-0.001	0.184	-0.001	0.005	-0.003	0.005	-0.001
5	20.2	1.313	0.188	0.988	0.004	0.331	-0.001	0.070	-0.005	0.010	0.000
6	24.7	1.770	0.363	1.372	0.017	0.511	0.002	0.189	-0.003	0.015	0.009
7	29.5	2.626	0.461	1.755	0.058	0.635	0.002	0.214	-0.005	0.146	0.065
8	34.7	3.183	0.636	2.118	0.118	0.892	0.008	0.335	-0.003	0.161	0.065
9	39.6	4.376	0.908	2.844	0.249	1.284	0.186	0.561	-0.007	0.267	0.205
10	44.4	6.225	1.180	4.014	0.406	1.854	0.372	0.927	-0.005	0.403	0.222
11	45.6	6.544	1.200	4.216	0.418	1.962	0.373	1.002	-0.005	0.407	0.220
12	47.2	7.936	1.277	5.083	0.605	2.335	0.373	1.185	-0.003	0.526	0.264
13	49.6	11.018	1.511	7.000	0.858	3.450	0.812	1.684	-0.003	0.750	0.334
14	52.3	18.178	1.958	11.559	1.767	5.863	1.223	2.810	-0.002	1.285	0.517
15	52.5	41.388	4.448	26.245	3.808	13.263	2.325	6.849	0.983	2.641	1.389
16	53.3	44.033	5.109	28.121	3.933	14.336	2.321	7.589	1.383	2.789	1.389
17	54.3	46.181	5.517	29.674	4.068	15.153	2.321	8.186	1.761	2.927	1.401
18	55.1	46.777	5.692	30.118	4.077	15.468	2.323	8.399	1.832	2.928	1.403

Step	Average Load	Transducer No.						
		10	11	12	13	14	15	16
1	0.0	0.000	0.000	0.000	0.000	0.000	0.000	0.000
2	5.5	-0.002	0.000	0.003	0.002	0.004	0.022	0.067
3	10.4	0.000	0.004	0.002	0.002	0.126	0.417	0.642
4	15.3	-0.002	0.008	0.020	0.007	0.130	0.505	0.819
5	20.2	-0.002	0.068	0.108	0.113	0.381	0.813	1.150
6	24.7	-0.002	0.080	0.139	0.113	0.381	0.923	1.394
7	29.5	-0.002	0.184	0.215	0.118	0.661	1.054	1.703
8	34.7	0.000	0.188	0.214	0.116	0.661	1.032	1.725
9	39.6	0.002	0.196	0.366	0.319	0.661	1.142	1.924
10	44.4	0.000	0.200	0.378	0.317	0.901	1.186	2.145
11	45.6	0.002	0.200	0.375	0.317	0.893	1.164	2.145
12	47.2	0.003	0.200	0.386	0.320	0.897	1.208	2.234

13	49.6	0.007	0.196	0.388	0.319	0.897	1.186	2.234
14	52.3	0.071	0.208	0.560	0.320	1.140	1.252	2.566
15	52.5	1.108	0.405	0.800	0.490	1.140	0.769	2.145
16	53.3	1.414	0.405	0.829	0.487	1.144	0.747	2.145
17	54.3	1.676	0.405	0.983	0.485	1.144	0.879	2.389
18	55.1	1.729	0.405	1.004	0.488	1.148	0.857	2.389

Table D.7 Specimen 1-Experimental Raw Data for Clinometer Readings (degrees)

Step	Load	Clinometer						
		A	B	C	D	E	F	G
1	0.0	0.000	0.000	0.000	0.000	0.000	0.000	0.000
2	10.0	0.019	0.106	-0.067	-0.319	-0.251	0.020	0.020
3	15.2	0.087	0.039	-0.328	-0.849	-0.493	0.067	0.087
4	20.2	0.116	0.116	-0.676	-1.467	-0.908	0.049	0.126
5	24.8	0.212	0.116	-1.081	-2.027	-1.303	0.058	0.213
6	29.9	0.270	0.039	-1.660	-2.877	-1.844	0.019	0.280
7	35.0	0.367	0.019	-2.220	-3.562	-2.356	0.029	0.367
8	40.1	0.502	0.029	-3.359	-5.049	-3.340	0.020	0.541
9	44.6	0.647	0.029	-4.460	-6.777	-4.470	0.010	0.705
10	50.1	0.859	0.058	-6.091	-9.122	-6.053	0.010	0.956
11	54.4	1.120	0.010	-8.167	-12.211	-8.099	0.068	1.236
12	60.1	1.458	0.029	-10.976	-16.642	-11.101	0.232	1.651
13	63.1	1.583	0.058	-12.009	-18.418	-12.173	0.309	1.815
14	63.5	1.583	0.048	-12.095	-18.235	-12.115	0.222	1.815

Table D.8 Specimen 2-Experimental Raw Data for Clinometer Readings (degrees)

Step	Average Load	Clinometer						
		A	B	C	D	E	F	G
1	0.0	0.000	0.000	0.000	0.000	0.000	0.000	0.000
2	5.1	-0.145	0.018	-0.028	0.029	0.009	-0.043	0.134
3	10.0	0.318	0.028	-0.047	0.029	0.009	-0.043	-0.277
4	15.1	0.000	0.028	-0.103	0.029	0.029	-0.060	0.029
5	20.6	-0.155	0.037	-0.103	0.058	0.049	-0.060	0.172
6	25.3	-0.319	0.018	-0.131	0.067	0.068	-0.069	0.335
7	29.4	-0.222	0.037	-0.159	0.096	0.078	-0.060	0.220
8	35.0	-0.338	-0.047	-0.262	0.086	0.098	0.008	0.335
9	40.0	-0.396	-0.028	-0.327	0.115	0.147	0.008	0.392
10	45.7	-0.444	-0.159	-0.561	0.134	0.196	0.103	0.459
11	47.7	-0.608	-0.047	-0.767	0.144	0.206	0.026	0.583
12	50.9	-0.550	-0.206	-1.197	0.154	0.246	0.138	0.554
13	54.3	-0.512	-0.206	-2.404	0.106	0.275	0.146	0.507
14	47.4	-0.068	0.056	-12.233	-0.893	1.161	0.275	0.354
15	46.9	0.000	-0.523	-13.056	-1.306	0.285	0.318	0.459

Table D.9 Specimen 3-Experimental Raw Data for Clinometer Readings (degrees)

Step	Average Load	Clinometer						
		A	B	C	D	E	F	G
1	0.0	0.000	0.000	0.000	0.000	0.000	0.000	0.000
2	5.5	-0.001	-0.004	0.000	-0.002	-0.001	-0.002	0.000
3	10.4	0.000	-0.006	-0.001	-0.002	-0.002	-0.008	-0.001
4	15.3	-0.001	-0.007	-0.002	-0.005	-0.002	-0.004	-0.001
5	20.2	-0.001	-0.009	-0.004	-0.006	-0.003	-0.008	-0.002
6	24.7	-0.001	-0.011	-0.005	-0.009	-0.005	-0.006	-0.003
7	29.5	-0.001	-0.014	-0.006	-0.011	-0.006	-0.006	-0.004
8	34.7	-0.001	-0.015	-0.006	-0.015	-0.009	-0.007	-0.004
9	39.6	-0.001	-0.016	-0.005	-0.020	-0.012	-0.008	-0.005
10	44.4	-0.003	-0.017	-0.007	-0.030	-0.018	-0.016	-0.006
11	45.6	-0.004	-0.018	-0.007	-0.033	-0.019	-0.013	-0.007
12	47.2	-0.002	-0.018	-0.008	-0.040	-0.024	-0.019	-0.007
13	49.6	-0.004	-0.018	-0.007	-0.059	-0.035	-0.020	-0.007
14	52.3	-0.005	-0.019	-0.009	-0.103	-0.061	-0.036	-0.009
15	52.5	-0.005	-0.019	-0.008	-0.237	-0.145	-0.081	-0.008
16	53.3	-0.005	-0.018	-0.008	-0.251	-0.155	-0.085	-0.008
17	54.3	-0.006	-0.019	-0.009	-0.263	-0.163	-0.087	-0.010
18	55.1	-0.007	-0.019	-0.009	-0.266	-0.166	-0.086	-0.010

Table D.10 Specimen 1-Experimental Raw Data for Vertical LVDT Readings (mm)

Step	Load	Midspan
1	0.0	0.0
2	10.0	2.3
3	15.2	3.5
4	20.2	4.6
5	24.8	5.7
6	29.9	6.9
7	35.0	8.1
8	40.1	9.3
9	44.6	10.5
10	50.1	11.9
11	54.4	13.1
12	60.1	14.8
13	63.1	17.2
14	63.5	18.5

Table D.11 Specimen 2-Experimental Raw Data for Vertical LVDT Readings (mm)

Step	Average Load	Left Tip		Mid-span		Right Tip	
		1	2	1	2	1	2
1	0.0	0.0	0.0	0.0	0.0	0.0	0.0
2	5.1	3.1	3.0	-1.5	-1.7	2.8	2.8
3	10.0	5.9	5.6	-3.1	-3.4	5.9	6.0
4	15.1	8.9	8.5	-5.0	-5.2	9.2	9.3
5	20.6	12.3	11.7	-6.9	-7.2	12.7	12.8
6	25.3	15.3	14.6	-8.5	-8.9	15.4	15.5
7	29.4	18.0	17.1	-10.1	-10.4	18.0	18.2
8	35.0	21.4	20.3	-12.2	-12.5	21.5	21.8
9	40.0	24.5	23.2	-14.0	-14.4	24.6	25.1
10	45.7	28.4	26.9	-15.8	-16.7	28.1	28.7
11	47.7	29.9	28.2	-16.3	-17.6	29.8	30.5
12	50.9	31.8	30.0	-16.7	-18.8	31.7	32.5
13	54.3	34.5	32.4	-17.2	-20.3	34.3	35.1
14	47.4	30.1	28.0	-16.9	-18.9	30.1	30.2
15	46.9	29.9	27.9	-16.8	-18.8	30.3	30.5

Table D.12 Specimen 3-Experimental Raw Data for Vertical LVDT Readings (mm)

Step	Average Load	Left Tip		Mid-span		Right Tip	
		1	2	1	2	1	2
1	0.0	0.0	0.0	0.0	0.0	0.0	0.0
2	5.5	2.2	2.2	-0.5	-0.5	2.1	2.2
3	10.4	3.9	3.8	-0.8	-0.8	4.0	4.1
4	15.3	6.3	6.1	-1.8	-1.5	6.3	6.4
5	20.2	8.1	7.8	-1.9	-1.9	8.2	8.4
6	24.7	10.2	9.7	-2.5	-2.4	10.3	10.4
7	29.5	12.2	11.7	-3.3	-3.0	12.4	12.6
8	34.7	14.4	13.7	-3.7	-3.4	14.6	14.8
9	39.6	16.5	15.8	-4.2	-4.0	16.7	16.9
10	44.4	18.6	17.7	-4.7	-4.5	18.8	19.0
11	45.6	18.9	18.1	-4.7	-4.6	19.4	19.7
12	47.2	19.6	18.8	-4.8	-4.8	20.0	20.4
13	49.6	20.6	19.7	-5.0	-5.0	21.1	21.4
14	52.3	21.3	20.5	-5.2	-5.3	22.4	22.7
15	52.5	19.6	19.7	-5.4	-5.5	23.3	23.7
16	53.3	18.9	19.1	-5.1	-4.9	23.3	23.6
17	54.3	18.6	18.9	-5.1	-5.1	24.5	25.0
18	55.1	18.5	18.9	-5.1	-5.2	25.4	25.9

Table D.13 Specimen 1-Top Transducer Displacements (mm) based on Transducer Readings at various Loading Levels (kN)

Step	Load	Transducer No.								
		0	2	4	6	8	10	12	14	16
1	0.0	0.0	0.0	0.0	0.0	0.0	0.0	0.0	0.0	0.0
2	10.0	-0.1	-0.1	0.0	-0.5	0.0	0.0	0.0	0.0	0.0
3	15.2	-0.1	0.0	-0.2	-1.3	-0.7	-0.7	-0.2	0.0	0.2
4	20.2	-0.3	0.0	-0.4	-2.1	-1.8	-1.6	-0.4	0.0	0.5
5	24.8	0.3	0.0	-0.7	-3.1	-3.2	-2.8	-0.7	0.0	0.9
6	29.9	0.8	0.0	-1.1	-4.6	-5.1	-4.3	-1.2	0.0	1.4
7	35.0	0.7	0.1	-1.5	-5.8	-6.9	-5.7	-1.5	0.0	1.8
8	40.1	2.2	-0.1	-2.2	-8.2	-10.2	-8.2	-2.3	0.0	2.7
9	44.6	2.8	0.1	-3.0	-10.9	-14.0	-11.4	-3.1	0.0	3.6
10	50.1	4.0	0.1	-4.1	-14.5	-19.0	-15.4	-4.2	0.0	4.9
11	54.4	5.5	0.1	-5.6	-19.2	-25.5	-20.9	-5.7	-0.1	6.5
12	60.1	6.7	0.2	-7.6	-25.7	-34.7	-28.3	-7.7	-0.2	8.4
13	63.1	8.1	0.1	-8.3	-28.5	-39.0	-31.3	-8.5	-0.2	9.6
14	63.5	8.2	0.3	-8.3	-28.5	-39.0	-31.3	-8.5	-0.2	9.6

Table D.14 Specimen 2-Top Transducer Displacements (mm) based on Transducer Readings at various Loading Levels (kN)

Step	Average Load	Transducer No.								
		0	2	4	6	8	10	12	14	16
1	0.0	0.0	0.0	0.0	0.0	0.0	0.0	0.0	0.0	0.0
2	5.1	0.0	0.2	0.0	0.0	0.0	0.0	0.0	0.0	0.0
3	10.0	0.0	0.2	0.0	0.0	0.0	0.0	0.0	0.0	-0.4
4	15.1	0.2	0.4	0.1	-0.1	0.0	0.3	0.4	0.2	-0.4
5	20.6	0.2	0.4	0.2	-0.2	0.0	0.3	0.4	0.2	-0.4
6	25.3	0.4	0.6	0.3	-0.2	0.0	0.3	0.4	0.2	-0.4
7	29.4	0.5	0.8	0.4	-0.3	0.0	0.3	0.4	0.2	-0.5
8	35.0	0.9	0.9	0.6	-0.3	0.0	0.3	0.5	0.2	-0.7
9	40.0	1.3	1.3	0.8	-0.3	0.0	0.3	0.4	0.2	-0.9
10	45.7	2.4	2.1	1.2	-0.4	0.0	0.3	0.4	0.2	-1.3
11	47.7	3.4	2.8	1.8	-0.4	0.0	0.6	0.5	0.2	-1.2
12	50.9	5.3	4.1	2.4	-0.6	0.0	0.6	0.4	-0.1	-1.5
13	54.3	10.4	7.4	4.0	-0.8	0.3	0.7	0.4	-0.6	-2.3
14	47.4	54.6	37.7	18.6	6.2	-0.7	-8.3	-20.7	-41.5	-66.9
15	46.9	55.6	39.2	19.5	6.9	0.5	-6.1	-17.6	-37.9	-61.9

Table D.15 Specimen 3-Top Transducer Displacements (mm) based on Transducer Readings at various Loading Levels (kN)

Step	Average Load	Transducer No.								
		0	2	4	6	8	10	12	14	16
1	0.0	0.0	0.0	0.0	0.0	0.0	0.0	0.0	0.0	0.0
2	5.5	0.1	0.1	0.0	0.0	0.0	0.0	0.0	0.0	0.1
3	10.4	0.5	0.4	0.0	0.0	0.0	0.0	0.0	0.1	0.6
4	15.3	0.9	0.7	0.2	0.0	0.0	0.0	0.0	0.1	0.8
5	20.2	1.3	1.0	0.3	0.1	0.0	0.0	0.1	0.4	1.2
6	24.7	1.8	1.4	0.5	0.2	0.0	0.0	0.1	0.4	1.4
7	29.5	2.6	1.8	0.6	0.2	0.1	0.0	0.2	0.7	1.7
8	34.7	3.2	2.1	0.9	0.3	0.2	0.0	0.2	0.7	1.7
9	39.6	4.4	2.8	1.3	0.6	0.3	0.0	0.4	0.7	1.9
10	44.4	6.2	4.0	1.9	0.9	0.4	0.0	0.4	0.9	2.1
11	45.6	6.5	4.2	2.0	1.0	0.4	0.0	0.4	0.9	2.1
12	47.2	7.9	5.1	2.3	1.2	0.5	0.0	0.4	0.9	2.2
13	49.6	11.0	7.0	3.5	1.7	0.8	0.0	0.4	0.9	2.2
14	52.3	18.2	11.6	5.9	2.8	1.3	0.1	0.6	1.1	2.6
15	52.5	41.4	26.2	13.3	6.8	2.6	1.1	0.8	1.1	2.1
16	53.3	44.0	28.1	14.3	7.6	2.8	1.4	0.8	1.1	2.1
17	54.3	46.2	29.7	15.2	8.2	2.9	1.7	1.0	1.1	2.4
18	55.1	46.8	30.1	15.5	8.4	2.9	1.7	1.0	1.1	2.4

Table D.16 Specimen 1-Bottom Transducer Displacements (mm) based on Transducer Readings at various Loading Levels (kN)

Step	Load	Transducer No.							
		1	3	5	7	9	11	13	15
1	0.0	0.0	0.0	0.0	0.0	0.0	0.0	0.0	0.0
2	10.0	0.1	0.0	-0.1	0.0	0.0	0.0	0.0	0.0
3	15.2	0.2	0.0	-0.3	0.0	-0.1	0.0	0.0	0.1
4	20.2	0.4	-0.1	-0.5	-0.2	-0.3	0.0	0.0	0.1
5	24.8	0.6	-0.2	-0.8	-0.5	-0.6	-0.1	0.0	0.3
6	29.9	0.9	-0.3	-1.1	-1.0	-1.0	-0.2	0.0	0.6
7	35.0	1.1	-0.4	-1.4	-1.4	-1.3	-0.3	0.0	0.8
8	40.1	1.6	-0.7	-2.0	-2.2	-2.0	-0.6	0.0	1.2
9	44.6	2.1	-0.9	-2.6	-3.0	-2.7	-0.8	0.0	1.8
10	50.1	2.9	-1.2	-3.4	-4.1	-3.6	-1.1	0.0	2.5
11	54.4	3.7	-1.6	-4.4	-5.5	-4.8	-1.5	0.0	3.2
12	60.1	4.8	-2.1	-5.7	-7.2	-6.3	-2.0	0.0	4.3
13	63.1	5.6	-2.3	-6.5	-8.7	-7.1	-2.3	0.0	5.1
14	63.5	5.6	-2.3	-6.5	-8.7	-7.1	-2.3	0.0	5.1

Table D.17 Specimen 2-Bottom Transducer Displacements (mm) based on Transducer Readings at various Loading Levels (kN)

Step	Average Load	Transducer No.							
		1	3	5	7	9	11	13	15
1	0.0	0.0	0.0	0.0	0.0	0.0	0.0	0.0	0.0
2	5.1	0.1	0.0	0.0	0.0	0.0	0.0	0.0	0.0
3	10.0	0.1	0.0	0.0	0.1	0.0	0.0	0.0	0.0
4	15.1	0.1	0.0	0.4	0.5	0.2	0.5	0.4	0.1
5	20.6	0.1	0.0	0.4	0.5	0.2	0.5	0.4	0.1
6	25.3	0.1	0.3	0.5	0.7	0.3	0.5	0.4	0.1
7	29.4	0.1	0.3	0.6	0.8	0.3	0.5	0.4	0.1
8	35.0	0.1	0.3	0.9	0.9	0.4	0.5	0.4	0.0
9	40.0	0.3	0.6	1.1	1.2	0.5	0.5	0.4	0.0
10	45.7	0.5	0.9	1.4	1.5	0.6	0.5	0.4	-0.2
11	47.7	0.8	1.2	1.8	1.9	0.8	0.6	0.4	-0.3
12	50.9	1.0	1.2	2.0	2.0	0.9	0.6	0.4	-0.4
13	54.3	1.5	1.6	2.7	2.5	1.2	0.6	0.4	-0.8
14	47.4	11.0	3.2	2.4	0.8	-4.3	-5.1	-7.2	-11.6
15	46.9	11.2	3.3	3.5	2.2	-1.7	-1.5	-3.1	-6.7

Table D.18 Specimen 3-Bottom Transducer Displacements (mm) based on Transducer Readings at various Loading Levels (kN)

Step	Average Load	Transducer No.							
		1	3	5	7	9	11	13	15
1	0.0	0.0	0.0	0.0	0.0	0.0	0.0	0.0	0.0
2	5.5	0.1	0.0	0.0	0.0	0.0	0.0	0.0	0.0
3	10.4	0.1	0.0	0.0	0.0	0.0	0.0	0.0	0.4
4	15.3	0.1	0.0	0.0	0.0	0.0	0.0	0.0	0.5
5	20.2	0.2	0.0	0.0	0.0	0.0	0.1	0.1	0.8
6	24.7	0.4	0.0	0.0	0.0	0.0	0.1	0.1	0.9
7	29.5	0.5	0.1	0.0	0.0	0.1	0.2	0.1	1.1
8	34.7	0.6	0.1	0.0	0.0	0.1	0.2	0.1	1.0
9	39.6	0.9	0.2	0.2	0.0	0.2	0.2	0.3	1.1
10	44.4	1.2	0.4	0.4	0.0	0.2	0.2	0.3	1.2
11	45.6	1.2	0.4	0.4	0.0	0.2	0.2	0.3	1.2
12	47.2	1.3	0.6	0.4	0.0	0.3	0.2	0.3	1.2
13	49.6	1.5	0.9	0.8	0.0	0.3	0.2	0.3	1.2
14	52.3	2.0	1.8	1.2	0.0	0.5	0.2	0.3	1.3
15	52.5	4.4	3.8	2.3	1.0	1.4	0.4	0.5	0.8
16	53.3	5.1	3.9	2.3	1.4	1.4	0.4	0.5	0.7
17	54.3	5.5	4.1	2.3	1.8	1.4	0.4	0.5	0.9
18	55.1	5.7	4.1	2.3	1.8	1.4	0.4	0.5	0.9

Table D.19 Specimen 1-Web Mid-Height Lateral Displacements (mm) based on Transducer Readings at various Loading Levels (kN)

Step	Average Load	0,1	3,4	5,6	7,8	9,10	11,12	13,14	15,16
1	0.0	0.0	0.0	0.0	0.0	0.0	0.0	0.0	0.0
2	10.0	0.0	0.0	-0.3	0.0	0.0	0.0	0.0	0.0
3	15.2	0.1	-0.1	-0.7	-0.3	-0.4	-0.1	0.0	0.1
4	20.2	0.1	-0.3	-1.1	-0.9	-1.0	-0.2	0.0	0.2
5	24.8	0.4	-0.4	-1.7	-1.7	-1.7	-0.4	0.0	0.5
6	29.9	0.9	-0.7	-2.5	-2.9	-2.7	-0.7	0.0	0.9
7	35.0	0.9	-1.0	-3.2	-3.9	-3.6	-3.6	0.0	1.1
8	40.1	1.9	-1.4	-4.5	-5.7	-5.2	-5.2	0.0	1.8
9	44.6	2.5	-2.0	-5.9	-7.9	-7.3	-7.3	0.0	2.4
10	50.1	3.5	-2.6	-7.8	-10.8	-9.7	-9.8	0.0	3.4
11	54.4	4.7	-3.6	-10.3	-14.4	-13.2	-13.3	0.0	4.4
12	60.1	5.8	-4.8	-13.7	-19.5	-17.7	-18.0	-0.1	5.8
13	63.1	6.9	-5.3	-15.3	-22.2	-19.7	-5.4	-0.1	7.3
14	63.5	7.0	-5.3	-15.3	-22.2	-19.7	-5.4	-0.1	7.3

Table D.20 Specimen 2-Web Mid-Height Lateral Displacements (mm) based on Transducer Readings at various Loading Levels (kN)

Step	Average Load	0,1	3,4	5,6	7,8	9,10	11,12	13,14	15,16
1	0.0	0.0	0.0	0.0	0.0	0.0	0.0	0.0	0.0
2	5.1	0.0	0.0	0.0	0.0	0.0	0.0	0.0	0.0
3	10.0	0.0	0.0	0.0	0.0	0.0	0.0	0.0	-0.1
4	15.1	0.1	0.0	0.1	0.3	0.3	0.5	0.3	-0.1
5	20.6	0.2	0.1	0.1	0.3	0.3	0.5	0.3	-0.1
6	25.3	0.3	0.3	0.2	0.4	0.3	0.5	0.3	-0.1
7	29.4	0.3	0.3	0.2	0.4	0.3	0.4	0.3	-0.2
8	35.0	0.5	0.4	0.3	0.5	0.4	0.4	0.3	-0.3
9	40.0	0.8	0.7	0.4	0.6	0.4	0.4	0.3	-0.4
10	45.7	1.5	1.0	0.6	0.8	0.5	0.4	0.3	-0.7
11	47.7	2.2	1.5	0.7	1.0	0.7	0.5	0.3	-0.7
12	50.9	3.2	1.8	0.8	1.1	0.7	0.5	0.2	-0.9
13	54.3	6.1	2.7	1.0	1.5	0.9	0.5	-0.1	-1.5
14	47.4	33.5	10.4	4.2	0.1	-6.3	-12.9	-23.3	-38.8
15	46.9	34.2	10.9	5.2	1.4	-3.9	-9.5	-19.4	-33.9

Table D.21 Specimen 3-Web Mid-Height Lateral Displacements (mm) based on Transducer Readings at various Loading Levels (kN)

Step	Average Load	0,1	3,4	5,6	7,8	9,10	11,12	13,14	15,16
1	0.0	0.0	0.0	0.0	0.0	0.0	0.0	0.0	0.0
2	5.5	0.1	0.0	0.0	0.0	0.0	0.0	0.0	0.0
3	10.4	0.3	0.0	0.0	0.0	0.0	0.0	0.1	0.5
4	15.3	0.5	0.1	0.0	0.0	0.0	0.0	0.1	0.6
5	20.2	0.8	0.2	0.0	0.0	0.0	0.1	0.2	1.0
6	24.7	1.1	0.3	0.1	0.0	0.0	0.1	0.2	1.1
7	29.5	1.5	0.3	0.1	0.1	0.0	0.1	0.4	1.3
8	34.7	1.9	0.5	0.2	0.1	0.0	0.1	0.4	1.3
9	39.6	2.6	0.8	0.4	0.1	0.1	0.2	0.5	1.5
10	44.4	3.7	1.1	0.6	0.2	0.1	0.2	0.6	1.6
11	45.6	3.9	1.2	0.7	0.2	0.1	0.2	0.6	1.6
12	47.2	4.6	1.5	0.8	0.3	0.1	0.2	0.6	1.6
13	49.6	6.3	2.2	1.2	0.4	0.2	0.3	0.6	1.7
14	52.3	10.1	3.8	2.0	0.6	0.3	0.4	0.7	1.9
15	52.5	22.9	8.5	4.6	1.8	1.2	0.6	0.8	1.5
16	53.3	24.6	9.1	5.0	2.1	1.4	0.6	0.8	1.4
17	54.3	25.8	9.6	5.3	2.3	1.5	0.7	0.8	1.4
18	55.1	26.2	9.8	5.4	2.4	1.6	0.7	0.8	1.5

APPENDIX E

Experimental Results

Contents

- Table E.1 presents applied load at mid-span versus mid-span vertical and lateral displacements for Specimen 1. For Specimen 2 and 3, applied load versus vertical and lateral displacements are provided in Tables E.2 and E.3 respectively.

Table E.1 Specimen 1-Mid-span Load (kN) versus Mid-span Vertical and Lateral Displacements (mm)

Step	Load	Vertical Displacement	Lateral Displacement*
1	0.0	0.0	0.00
2	10.0	2.3	-0.03
3	15.2	3.5	0.07
4	20.2	4.6	0.06
5	24.8	5.7	0.43
6	29.9	6.9	0.85
7	35.0	8.1	0.88
8	40.1	9.3	1.92
9	44.6	10.5	2.53
10	50.1	11.9	3.49
11	54.4	13.1	4.68
12	60.1	14.8	5.83
13	63.1	17.2	6.93
14	63.5	18.5	7.03

* At Web Mid-Height

Table E.2 Specimen 2-Load (kN) versus Vertical and Lateral Displacements (mm)

Step	Load		Vertical Displacement		Lateral Displacement*	
	Left Tip	Right Tip	Left Tip	Right Tip	Left Tip	Right Tip
1	0.0	0.0	0.0	0.0	0.00	0.0
2	5.4	4.8	3.1	2.8	0.05	0.0
3	9.8	10.2	5.9	5.9	0.03	-0.1
4	14.9	15.2	8.9	9.2	0.14	-0.1
5	20.3	20.8	12.3	12.7	0.16	-0.1
6	25.4	25.2	15.3	15.4	0.25	-0.1
7	29.5	29.2	18.0	18.0	0.31	-0.2
8	35.0	34.9	21.4	21.5	0.49	-0.3
9	39.9	40.1	24.5	24.6	0.84	-0.4
10	45.9	45.4	28.4	28.1	1.48	-0.7
11	47.9	47.6	29.9	29.8	2.16	-0.7
12	50.7	51.0	31.8	31.7	3.19	-0.9
13	54.4	54.2	34.5	34.3	6.07	-1.5
14	47.3	47.5	30.1	30.1	33.49	-38.8
15	46.7	47.1	29.9	30.3	34.15	-33.9

* At Web Mid-Height

Table E.3 Specimen 3-Load (kN) versus Vertical and Lateral Displacements (mm)

Step	Load			Vertical Displacement			Lateral Displacement*		
	Left Tip	Mid-span	Right Tip	Left Tip	Mid-span	Right Tip	Left Tip	Mid-span	Right Tip
1	0.0	0.0	0.0	0.0	0.0	0.0	0.00	0.00	0.00
2	5.5	5.5	5.4	2.2	0.5	2.1	0.08	0.00	0.04
3	10.0	10.8	10.3	3.8	0.8	4.0	0.29	0.00	0.53
4	15.3	15.3	15.3	6.1	1.5	6.3	0.47	0.00	0.66
5	20.0	20.5	20.1	7.8	1.9	8.2	0.75	0.00	0.98
6	24.7	24.7	24.7	9.7	2.4	10.3	1.07	0.01	1.16
7	29.5	29.3	29.7	11.7	3.0	12.4	1.54	0.07	1.38
8	34.5	34.7	34.8	13.7	3.4	14.6	1.91	0.08	1.38
9	39.5	39.5	39.8	15.8	4.0	16.7	2.64	0.13	1.53
10	44.5	44.2	44.3	17.7	4.5	18.8	3.70	0.20	1.67
11	45.5	45.4	45.9	18.1	4.6	19.4	3.87	0.20	1.65
12	47.2	47.0	47.3	18.8	4.8	20.0	4.61	0.26	1.72
13	49.7	49.4	49.7	19.7	5.0	21.1	6.26	0.37	1.71
14	52.1	52.2	52.6	20.5	5.3	22.4	10.07	0.64	1.91
15	50.5	52.7	54.5	19.7	5.5	23.3	22.92	1.81	1.46
16	50.0	54.8	55.2	19.1	4.9	23.3	24.57	2.09	1.45
17	49.1	55.7	58.0	18.9	5.1	24.5	25.85	2.34	1.63
18	48.8	56.4	60.0	18.9	5.2	25.4	26.23	2.38	1.62

* At Web Mid-Height

References

American Institute of Steel Construction (AISC) (2003) “Design Guideline for Continuous Beams Supporting Steel Joist Roof Structures” p. 23-1 - 23-44.

American Iron and Steel Institute (AISI) (1986) “Specification for the Design of Cold-Formed Steel Structural Members” Cold-formed steel design Manual, August 1986 with December 1989 Addendum.

American Iron and Steel Institute (AISI) (1996) “Specification for the Design of Cold-Formed Steel Structural Members” Washington, D.C.

American Iron and Steel Institute (AISI) (2001) “North American Specification for the Design of Cold-Formed Steel Structural Members” Washington, D.C.

American Iron and Steel Institute (AISI) (2004) “Supplement 2004 to the North American Specification for the Design of Cold-Formed Steel Structural Members, 2001 Edition, Appendix 1, Design of Cold-Formed Steel Structural Members Using Direct Strength Method” Washington, D.C.

American Society for Testing and Materials (ASTM) E8 (2009) “Standard Test Methods for Tension Testing of Metallic Materials” Pennsylvania, USA.

Brown, P. T., and Trahair, N. S. (1968) “Finite Integral Solution of Differential Equations” Civil Engineering Transactions, Institution of Engineers, Australia, CE10(2), p.193-196.

Canadian Institute of Steel Construction (CISC), (1989) “Roof framing with cantilever (Gerber) girders and open web steel joists” Willowdale, Ontario, Canada.

Canadian Standards Association (CSA) (1994) “Cold-Formed Steel Structural Members” S136-94, Ontario, Canada.

Chajes, A. (1974) “Principles of Structural Stability Theory” Prentice-Hall Inc., Englewood Cliffs, New Jersey.

Comite European de Normalisation (CEN) (2002) “Eurocode 3: Design of Steel Structure” European Standard EN1993-1-3., CEN, Brussels, Belgium.

CAN CSA S16-09 (2009) “Limit States Design of Steel Structures,” Canadian Standards Association, Rexdale, Ontario.

Dabbas, A. (2002) “Lateral Stability of Partially Restrained Cantilever” MASc dissertation, Ottawa, ON, Canada: Department of Civil Engineering, University of Ottawa.

Erkmen, R. E. (2006) “Finite Element Formulations for Thin-Walled Members” PhD dissertation, Ottawa, ON, Canada: Department of Civil Engineering, University of Ottawa.

Essa, H. S. and Kennedy, D. J. L. (1993) “Distorsional Buckling of Steel Beams” University of Alberta, Department of Civil Engineering, Structural Engineering Report No. 185.

Essa, H. S. and Kennedy, D. J. L. (1994) “Design of Cantilever Steel Beams: Refined Approach” Journal of Structural Engineering, 120(9), p. 2623-2636.

Essa, H. S. and Kennedy, D. J. L. (1995) “Design of Steel Beam in Cantilever-Suspended-Span Construction” Journal of Structural Engineering, 120(11), p. 1667-1673.

Galambos, T. V., and Ketter, R. L. (1959) "Column under Combined Bending and Thrust" *ASCE, J. Eng. Mech. Div.*, 85, 25-38.

Ghersi, A., Landolfo, R., and Mazzolani F. M. (1994) “Buckling Modes of Double-channel Cold-Formed Beams” Thin-Walled Structures, 19(2-4), p 353-366.

Helwig, T. A. and Yura, J. A. (1995) “Bracing for Stability” sponsored by Structural Stability Research Council and American Institute of Steel Construction.

Kirby, P. A. and Nethercot, D. A. (1978) “Design for Structural Stability” Constrado Nomographs, Granada Publishing, London.

Kubo, M. and Fukumoto, Y. (1988) “Lateral-torsional buckling of thin-walled I-beams” Journal of Structural Engineering, ASCE, 114(4), p 841-855.

Liu, Y. and Gannon, L. (2009) “Experimental Behavior and Strength of Steel Beams Strengthened while Under Load”, Journal of Constructional Steel Research, 65(6), p 1346-1354.

Menken, C. M., Schreppers, G. M. A., Groot, W. J., and Petterson, R. (1997) Analyzing Buckling Mode Interactions in Elastic Structures Using an Asymptotic Approach; Theory and Experiments”, Computers and Structures, 64(1-4), p 473-480.

Mottram, J.T. (1992) “Lateral-torsional buckling of thin walled composite I-beams by the finite difference method” Composites Engineering, 2(2), p. 191-104.

Mottram, J.T. (1992) “Lateral-torsional buckling of a pultruded I-beam” Composites, 23(2), p 81-92.

Nowzartash, F. and Mohareb, M. (2011) “Predicting Residual Stresses in Wide Flange Sections”, Submitted to CSCE Annual Conference.

Razzaq, Z., Prabhakaran, R., and Sirjani, M. M. (1995) “Load and Resistance Factor Design (LRFD) Approach for Reinforced-Plastic Channel Beam Buckling”, Composites Part B, 27B, p 361-369.

Rongoe, J. (1996) “Design Guidelines for Continuous Beams Supporting Steel Joist Roof Structures” National Steel Construction Conference Proceedings, Phoenix, 23.1-23.44, American Institute of Steel Construction (AISC), Chicago, IL.

Structural Analysis Program (SAP), (2000), SAP2000 Nonlinear 8.1.1, Computers and Structures Inc., Berkley, California.

Standards Australia and the Australian Institute of Steel Construction (AS/NZS) (1996) AS/NZS 4600, 1996 Cold-Formed Steel Structures.

SIMULIA, (2007), ABAQUS Analysis User’s Manual, Dassault Systemes. [cited; Available from: http://www.simulia.com/products/abaqus fea.html]

Timoshenko, S. P. and Gere, J.M. (1961) “Theory of Elastic Stability” 2nd edition, McGraw-Hill, NY, USA.

Roberts, T. M., H. M. Masri (2003) “Section Properties and Buckling Behavior of Pultruded FRP Profiles” Journal of Reinforced Plastics and Composites Structures, 22(14), p. 1305-1317.

Vacharajittiphan, P., and Trahair, N. S. (1973) “Elastic Lateral Buckling of Portal Frames” Journal of Structural Division, ASCE, 99(5), p 821-835.

Wu, L. (2010) “Finite Element Formulations for Lateral Torsional Buckling of Shear Deformable Planar Frames” PhD dissertation, Ottawa, ON, Canada: Department of Civil Engineering, University of Ottawa, 2010.

Yu, C. and Schafer, B. W. (2006) “Distortional Buckling Test on Cold-Formed Steel Beams”, Journal of Structural Engineering, 132(4), p 19-45.

Zinoviev, I. and Mohareb, M. (2004) “Analysis and design of laterally unsupported portal frames for out-of-plane stability” Canadian Journal of Civil Engineering, 13(3), p.440-452.